

Thesis: Expanded roles of IAP inhibitors and the caspase pathway in damaged and regenerating imaginal wing disc tissue.

Cristina D'Ancona

I would like to thank my advisors and committee, Adrian Halme, Ray Keller, Jay Hirsh, Sarah Siegrist, Michelle Bland, and Alan Bergland for their support. I also would like to thank my family, and my loving fiance, Stefan Terry.

Table of Contents

Acknowledgements	1
List of Figures	3
Abbreviations	5
Chapter 1	
Introduction	6
Regeneration	6
Theories of Why Regenerative Ability is Limited	10
Regeneration in <i>Drosophila</i>	15
Cell Death in Regeneration and Cancer	27
Growth Inhibition in <i>Drosophila</i>	28
Summary	32
Chapter 2	
Abstract	34
Introduction	35
Results	36
Discussion	64
Materials and Methods	69
Chapter 3	
Abstract	71
Introduction	72
Results	73
Discussion	89
Methods	96
Chapter 4	
Summary	100
Conclusions	110
Citations	113

List of Figures

Chapter 1	
Figure 1. Wing disc development	16
Figure 2. JNK pathway phosphorylation steps.	19
Figure 3. Dilp8 expression increases in <i>eiger</i> expressing tissue	20
Figure 4. <i>wingless</i> is necessary for regeneration after X-irradiation.	21
Figure 5. Brv118 transcriptional activity increases in <i>eiger</i> expressing tissues	22
Figure 6. Regeneration is restricted during development	23
Figure 7. Caspase cell death (apoptosis) pathway.	26
Chapter 2	
Figure 1. IAP inhibitors limit regeneration checkpoint activation	37
Figure 2. Increased cell death and loss of viability in tissues constitutively expressing <i>eiger</i>	38
Figure 3. RGH depletion produces excessive regenerative activity	41
Supplemental Figure 1. Normalized Ave. Fluorescent Intensity/ROI of BRV118 GFP and Wg is higher in <i>eiger</i> and <i>RGH^{μRNA}</i> co-expressing discs. Normalized Area of Fluorescence is higher in <i>eiger</i> and <i>RGH^{μRNA}</i> co-expressing discs.	43
Figure 4. IAP inhibitors prevent neoplasia in <i>eiger</i> ablated regenerating tissues	49
Supplemental Figure 2. The pouch of <i>eiger</i> and <i>eiger</i> RGH discs is abnormal	50
Figure 5. IAP inhibitors prevent neoplasia in regenerating X-irradiated tissues	52
Supplemental Figure 3. The pouch of X-irradiated RGH discs is abnormal, unlike control	53
Figure 6. JNK activity is necessary and sufficient for neoplasia in RGH depleted background	55
Supplemental Figure 4. <i>eiger</i> and RGH microRNA co-expressing discs have greater area of AP-1 GFP activity and a higher average AP-1 GFP activity	57
Figure 7. Regeneration through Wingless is necessary for the neoplastic phenotype.	58
Figure 8. Inhibition of IAP inhibitors via other caspase pathway members produces neoplasia.	61
Figure 9. Model: Cell death prevents neoplasia caused by JNK and Wg regenerative activity.	67

Chapter 3	
Figure 1 Beadex, Apterous, or Nubbin promoter driven <i>reaper</i> expression causes larval growth inhibition	75
Figure 2. Temporally-limited reaper expression is sufficient to limit larval growth.	77
Figure 3. <i>RGH</i> expression in imaginal wing discs produces a decrease in pupal weight	79
Figure 4. Reaper expression in imaginal wing discs produces checkpoint delay, with the smallest larvae delaying longest.	81
Figure 5. Other methods of causing injury or delay do not recapitulate the growth inhibition phenotype.	83
Figure 6. Diap1 inhibitor co-expression partially rescues larval size.	87
Figure 7. Metabolic observations indicate there may be an altered metabolism	88

List of Abbreviations

Activator Protein-1- AP-1	Green Fluorescent Protein-GFP
Alternate reading frame- ARF	G-protein coupled receptor-Lgr3
5' AMP-activated protein kinase-AMPK	Head Involution Defect- Hid
Apterosus-Ap	Hypoxia Inducible Factor 1 Subunit
Atypical protein kinase c- aPKC	Alpha-HIF1 alpha
avian myelocytomatosis viral oncogene homolog-Myc	Hours After Egg Deposition-HAED
Baculovirus Inhibitor of apoptosis protein	Insulin-like growth factor 1 -IGF-1
Repeat Domain- BIR domain	Insulin Producing Cell-IPC
B-cell lymphoma 2-Bcl-2	Jun N-terminal-kinase-JNK
B-cell lymphoma extra large-Bcl-x	mitogen-activated protein kinase -MAPK
Beadex-Bx	Nubbin-nub
β -galactosidase -LacZ	Phosphatidylinositol-4,5-bisphosphate
Bromodeoxyuridine	3-kinase -PI3K
5-bromo-2'-deoxyuridine-BrdU	Phosphatidylinositol
C-X-C chemokine receptor type 4-CXCR4	(3,4,5)-trisphosphate-pip3
cyclin-dependent kinase inhibitor	Pleckstrin Homology Domain-PH
2A-p16INK4a	Prothoracic Gland- PG
cysteine-aspartic proteases- caspase	Prothoracicotropic Hormone-PTTH
Death-associated APAF1-related	Phosphatase and tensin homolog-Pten
killer-Dark	Progesterone receptor isoform B- pRB
Death regulator Nedd2-like caspase-	Puckered- puc
Dronc	Reaper, Grim, and Hid- RGH
Death related ICE-like caspase- DrICE	Reaper- Rpr
Decapentaplegic-DPP	Reactive Oxygen Species-ROS
Decapping protein 1- Dcp1	Ribonucleic Acid-RNA
Dominant Negative-DN	Rotund-Rn
<i>Drosophila</i> Inhibitor of Apoptosis- DIAP	Scribbled-scrib
<i>Drosophila</i> Insulin like peptide-Dilp	stromal-cell-derived factor-1-SDF1
Ecdysone-inducible gene L2-Impl2	small interfering Ribonucleic Acid- siRNA
Extracellular Matrix-ECM	Target of rapamycin-Tor
eda-like cell death trigger-eiger-egr	Transforming Growth Factor Beta-TGF beta
extracellular signal-regulated	Tumor Necrosis Factor- TNF
kinases-ERK	TNF receptor associated factor 6- TRAF-6
filamentous F-actin- F-actin	Upstream Activation Sequence-UAS
Forkhead box-Foxo	Wingless- Wg
	X-Linked Inhibitor Of Apoptosis-XIAP

Chapter 1: Introduction

Caspase-mediated cell death is critical for development and stress responses¹ but my data indicates caspase-mediated cell death—referred to from here out as apoptosis—may also have other roles. During regeneration after damage, apoptosis is necessary to clear injured tissues and make way for new growth². My thesis research explores the role of apoptosis and pro-apoptotic proteins Reaper, Grim, and Hid (RGH) during damage and regeneration. RGH proteins bind Inhibitors of Apoptosis Proteins (IAPs) and induce IAP auto-ubiquitination/degradation to promote programmed cell death^{3,4}. Chapter 2 describes experiments demonstrating that apoptosis is necessary to prevent overgrowth and tumorigenesis in regenerating tissues. Chapter 3 describes experiments showing that IAP inhibitor expression in the wing imaginal disc produces non-autonomous larval growth inhibition. Thus, the experiments in this thesis describe two new roles for apoptosis and IAP-inhibitor proteins following damage and during regeneration beyond the clearance of injured cells: limiting regeneration and causing non-autonomous larval and pupal growth inhibition.

Regeneration

Types of regeneration

Regeneration is a coordinated restoration of damaged cells, tissues, or organs that simultaneously integrates the new tissue with pre-existing structures⁵, which restores form and function (morphostasis). In 1901, Thomas Hunt Morgan described two distinct regenerative processes: morphallaxis and epimorphosis⁶. Morphallaxis describes examples of regeneration where the regenerated tissue remodels existing material without new cellular proliferation, such as in the head and foot of the hydra. Epimorphosis describes examples where the regeneration results from cellular proliferation and the growth of new tissue, such as in limb regeneration in salamanders.

These two categories of regeneration can both act in concert during regeneration. Planarians utilize both epimorphosis and morphallaxis, which both contribute to the regenerative process⁷. Cutting the head or trunk of planarians causes the separated tissue to regenerate with epimorphic regeneration via blastema formation and cell proliferation to create new tissue. Also, in this same injured tissue, pre-existing tissues are remodeled to restore symmetry in planaria (morphallaxis). Due to observations in planaria where the blastemal stem cells stop proliferating, become distal to induce cell intercalation, and differentiate into the needed cells depending on their new position^{8,9}, some argue that the categories of epimorphosis and morphallaxis are not reflective of our current understanding of regeneration^{8,9}. Instead, it is argued that the categories should be replaced with a more unified model, where regeneration involves two steps: distalization, where the exposed wound region first produces the most distal tissues, and intercalary regeneration, where proximal tissues reorganize and regenerate the missing intercalary tissues^{8,9}. Not every animal can regenerate as effectively as salamanders, hydra, and planarians, and the extensive limb or body axis regeneration described above is rare.

Regenerative capacity is variable across evolution

The ability to regenerate is variable across both evolution and between tissues in an individual animal. For example, hydra can regenerate an entire polyp from a pellet of centrifuged cells whereas adult mammalian regeneration is limited to only specific tissues or organs including skeletal muscle, bone, peripheral nerve, urinary bladder, and liver¹⁰⁻¹⁸. In fact, the ability of adult animals to regenerate large sections of primary or secondary body axes is only found in six phyla (Porifera, Cnidaria, Mollusca, Annelida, Nemertea, Vertebrata)^{19, 206}. Despite this incredible variability in primary or secondary axes regeneration there are few cases where closely related phyla exhibit comparatively different regenerative potential and almost all phyla (except Nematoda) can scarlessly regenerate to some extent on a tissue or organ level^{20,21}, suggesting regenerative capability is unlikely to have

independently arisen many times. Thus, I focus not on the variability of regenerative ability between phyla but on the underlying mechanisms that affect regenerative variability within an organism.

Regeneration is suppressed during development of many tissues

Although regenerative capacity occurs sporadically across evolution there is a clear trend across taxa that regenerative ability is higher in early development and declines with age. For example, mammalian fetuses can regenerate skin scarlessly, but this ability to produce scarless skin regeneration is lost soon after birth²²⁻²⁷. Even in highly regenerative species such as fish, newts, or planaria, the degree or speed of regeneration can decline with age. For instance, axolotls produce slower re-epithelialization of flank wounds as mature metamorphs²⁸. Thus, a more mature state seems to correlate with less capacity for regeneration.

One potential reason for the loss of regenerative potential is that in adult skin tissue regeneration, the need for fast wound healing in an unclean environment may necessitate more drastic cytokine and inflammatory cascades to prevent infection and future wound breakdown, and thus prevent full regeneration of tissue, although it unknown what exact factor prevents scarless regeneration²⁹. This response in adult tissue is drastically different from scarless fetal wound healing which is characterized by a decreased inflammatory response, rapid up-regulation of cell growth and proliferation genes, high matrix metalloproteinase expression and activity to favor extracellular matrix turnover, and an increase in skin progenitor cells³⁰. The decrease in inflammatory activity seems to prevent the layering of collagen and fibrin that results in scarring, but the exact mechanism for decreased inflammatory response in fetuses is unknown. Overall, fetal immune response is weaker than adult immune response in the case of infection.²⁰⁷ The ability to heal scarlessly is intrinsic to fetal skin and not dependent on the sterile intrauterine environment^{30,31}. Thus, the need in adult organisms for fast wound healing may prevent full restoration of tissue due to the immune response and subsequent

scarring, but the properties that prevent this inflammatory response in fetal tissue are unknown.

Another theory for loss of regenerative capacity is that compared to urodeles, mammals, and avians either lack crucial regeneration genes or suppress them in later stages of development. For example, in urodeles, the blastemal cell surface protein Prod1 is expressed throughout the organism's lifespan and is critical for limb regrowth but does not have a homolog or any protein that performs similar functions in other vertebrates³². Another example that demonstrates the difference in mammalian and urodele regeneration is that newt myotube nuclei in muscles can re-enter the cell cycle in response to Fetal Bovine Serum that inactivates pRB, whereas mammalian myotube nuclei cannot re-enter the cell cycle³³. pRB is a cell cycle checkpoint protein that prevents proliferation of primary myoblasts in its phosphorylated and inactive form during muscle development but blocks the cell cycle when activated after myoblasts mature into myotubules. Fetal Bovine Serum that contains kinases to phosphorylate pRB permits myoblasts to proliferate in newts but not in mammals³⁴. Knockdown by siRNA or deletion of pRB^{35,36}, did not result in myotube nuclei re-entering the cell cycle. Ultimately, Pajcini et al. (2010) found that in addition to *pRB*, the cell cycle checkpoint gene and tumor suppressor *ARF* must also be inactivated for mammalian myotube nuclei to enter the cell cycle in mice and dedifferentiate³⁶. *ARF* is not found in urodeles, suggesting that vertebrates have additional methods to suppress regenerative gene pathways later in development.

Another explanation for the loss of regenerative capacity is that mammalian proliferative cells decrease their proliferation and activity with age. During development, stem cells proliferate to form tissues, but stem cell division slows postnatally³⁷. For example, neuronal cells see decreased DNA synthesis as marked by BrdU³⁸ which may indicate a decrease in proliferation. Adult stem cells eventually lose their proliferative capacity due to lower levels of telomerase and the inevitable shortening of their telomeres after so many replicative cycles³⁹. Once a cell's

telomeres reach critically short length of 4-6 kb, the cell enters permanent growth arrest called senescence⁴⁰. The activity of proliferative stem cells decreases with age. For example, Notch signaling is required for stem cell maintenance, but with age in mice this signaling decreases and results in a decrease in the number of skeletal muscle stem cells^{41,42}. Thus, the proliferative ability and activity of stem cells reduces with age, which decreases regenerative capacity in the adult organism.

The loss of regenerative capacity in aging may be reflected in the loss of systemic signals that promote regeneration. Serum from young mice whose circulatory system was shared with old mice enhanced regeneration via the restoration of Notch signaling in satellite cells of old individuals⁴¹. Joining young mice surgically to older ones promoted remyelination of axons and rejuvenation of aged oligodendrocyte precursor cells in the latter⁴³. These studies show that regeneration depends on age and partly depends on the systemic effects of blood and serum factors on the ability for individual tissues to heal.

Despite the obvious benefits of regeneration, evolution has not maintained regenerative capacity uniformly across all species or stages of development. Are there costs to the organism associated with maintaining regenerative capacity?

Theories of why regenerative ability is limited

Energetic cost of regeneration

There is an energetic cost to allocating resources to regenerating tissues. Sometimes this cost is up to half of the organism's total energy, measured in lipids and joules per milligram of the dry weight of lizards that had undergone tail-regeneration⁴⁶. The energetically costly process of regeneration can also affect an organism's fecundity. In vertebrates, juvenile Eastern fence lizards, bunchgrass lizards, and side-blotched lizards grow more slowly if they are regenerating their tail^{46,47}. This slow growth delays the lizard's maturity^{46,47}. Regeneration in bunchgrass and side-blotched lizards, plethodontid salamanders, Texas banded

geckos, and Australian skinks⁴⁷⁻⁵¹ also caused a decrease in fecundity, due to failure to participate in a mating cycle or by producing less offspring.

Another theory of why regenerative capacity might be limited in mammals is that the regenerative process takes too much time, particularly given the size of many tissues. In humans, it takes fifteen years to create a mature adult arm and it simply may not be feasible to take another fifteen years to regrow a mature tissue^{44,45}. Thus, limb regrowth, as one example of regeneration, may be energetically too costly, may have negative repercussions on maturation or fecundity, or may not be feasible due to the time to regenerate the tissue in larger vertebrates.

Risk of tumorigenesis

Regenerative capacity may also be limited in mammals because regenerative processes may make an organism more susceptible to tumorigenesis. Tumorous tissue is histologically abnormal and is characterized by cells that have an altered physiology that permits malignant growth. The salient features of these cells include being insensitive to anti-growth signals, evasion of apoptosis, sustained angiogenesis, limitless replicative potential, self sufficiency in growth signals, and gaining properties of tissue invasion and metastasis¹⁴⁰. Normally, regenerative activity does not lead to tumorigenesis, and in fact, regulated regeneration decreases the chance of cancer. For example, regenerating dorsal newt irises are more resistant than non-regenerating tissue to forming tumors when treated with a carcinogenic nickel subsulfide solution⁵². Likewise, regenerating newt limbs do not form tumors when exposed to carcinogens whereas non-regenerating tissues do^{53,54}. However, there are similarities between regenerative wound healing and tumorigenesis particularly when regenerative pathways are misregulated

Similarities between wound healing/regeneration and tumorigenesis

In humans, an important part of regeneration is adult wound healing. Adult wound healing is a response characterized by fibroblast proliferation, hemostasis, inflammation, tissue formation, and tissue remodeling/resolution, that results in an

incomplete regeneration of the original tissue and scarring^{30,55}. The process of adult wound healing creates layers of collagen and fibrin. These layers form granulation tissue and mature to form a scar⁵⁵. In 1986, Dvorak⁵⁶ described tumors as wounds that never heal by comparing healing wounds' granulation tissue to the stroma of tumors. In vivo, tumor stroma is composed of new blood vessels, inflammatory cells like lymphocytes and macrophages, a fibrin-gel matrix, and connective ECM tissue such as fibronectin, collagen, and fibroblasts. Maturation of tumor stroma depends on angiogenesis of new blood vessels and the transformation of the fibrin–fibronectin gel into a vascular and collagenous matrix⁵⁶. The collagenous matrix that makes up a tumor is made of the same components that form collagen matrix formed from inflammatory wound healing.

Similarities exist in the way that wounds heal and tumors form. For example, after tissue damage, blood clots, which consist of crosslinked fibrin and plasma fibronectin, provide a barrier against bacteria and prevent water loss during wound healing. Tumors make these fibrin and fibronectin networks by secreting vascular permeability factors that permit vessels to be permeable to plasma proteins that will form fibrin/plasma fibronectin gels. These fibrin and fibronectin assemblies appear for only a few days following injury but persist in tumors^{56,57}.

Second, in both wound healing and tumor environments inflammatory cells are increased. For example, in normal wounds M1 macrophages produce ROS and inflammatory cytokines that prevent infection. In tumors, tumor-derived cytokines induce macrophages to differentiate into M2 macrophages which stimulate angiogenesis and extracellular matrix breakdown that promote more tumorigenesis and metastasis^{57,58}.

Third, there are genes necessary for wound healing that also promote growth in tumors. One example is the chemokine stromal-cell-derived factor-1 (SDF1), which is a mitogen for the keratinocytes expressed in endothelial cells of wounded skin during wound re-epithelialization. However, carcinoma cells also express SDF1 receptor CXCR4, so SDF1 also promotes their proliferation^{57,59}. Taken together,

these facts demonstrate similarities between wound healing and tumor formation, including granular tissue that contains fibrin, fibronectin, and collagen, an inflammatory environment, and genes that are activated during wound healing and to promote tumor growth. Thus, some factors associated with regenerative activity also enhance tumor formation.

Chronic damage and repair are associated with tumorigenesis

One classic experiment that demonstrates the risk of healing tissue being at risk for tumorigenesis is where chickens injected with Rous Sarcoma Virus (a retrovirus that causes tumor growth in chickens) could be induced to produce tumors not only at the site of injection but also at areas that were wounded post infection. However, if inflammatory cytokines, enzymes, receptors, and adhesion molecules were inhibited by glucocorticoids, tumors no longer developed at the new wound sites, indicating that inflammatory signals arising from tissue damage could serve as a trigger for Rous Sarcoma Virus infection tumorigenesis⁶⁰. Thus, there is a risk where inflammation can make tissues more susceptible to tumorigenesis.

Cases with chronic damage and inflammation also pose a cancer risk. Chronic injury, such as chronic viral hepatitis, gastric inflammation, inflammatory bowel disease, or from skin blistering disease, can often result in malignant tumor formation⁵⁷. Patients with immunosuppression or who undergo chemotherapy can develop painful non-healing ulcers, whose excessive repair mechanisms causes hypertrophic scars and keloids that often undergo malignant transformation and develop cancerous fibrotic tissue. Therefore, the connection between wound repair during cases of chronic damage and tumorigenesis is at least correlative. In Chapter 2, we show that in some cases tissues undergoing regeneration in response to constitutive *eiger* (*egr*) damage also exhibit signs of neoplasia with loss of IAP inhibitors.

Adult tissues have an increase in the number of genes that act as tumor suppressors that prevent regeneration, possibly to prevent tumorigenesis

Another reason that regenerative ability may not be maintained across phyla is that with age, regenerative mechanisms such as re-entry into the cell cycle are less available due to an increase in number of tumor suppressors. As mentioned previously, in some cases mammals have an increased number of tumor suppressors that prevent re-entry into the cell cycle and de-differentiation compared to urodeles, such as *ARF*³⁶. Also, some genes that act as tumor suppressors in adult vertebrates such as *p53*, *RB1*, *PTEN*, and *p16INK4a*, do not appear to act as tumor suppressors in adult *Drosophila* and *C. elegans*⁶¹. One theory for the increase in tumor suppressors that act into adulthood in vertebrates is that longer lifespan increases the amount of tissue cycling and proliferation which if not carefully regulated can lead to hyperproliferation and tumorigenesis⁶¹. In fact, in *Drosophila*, cancer is normally quite uncommon possibly due to their short lifespan leading to less tissue cycling and proliferation⁶¹. Thus, the risk of hyperproliferation and tumorigenesis may limit regenerative activity.

Hormonal dysregulation during regeneration can lead to cancer

Finally, hormonal regulation of regeneration may prevent tumorigenesis. Male deer regenerate antler tissue during their seasonal shedding and regrowth. Castration of fallow deer during antler-regrowth, results in dysmorphic overgrowth of the antler tissue characterized by histological immaturity and, eventually, cystic structures that are comparable to osteomas⁶². This hormonal regulation may not be critical during development but may limit regenerative activity as organisms age. In humans, levels of the sex steroid testosterone decrease with age, so it is possible that this decrease in sex steroids could lead to a risk of misregulated regeneration in later life in humans⁶³.

Is tumorigenic potential a cost of regenerative activity?

There are many similarities between the wound healing and tumor environments, including an increase of fibrin matrix and collagen, of inflammatory cells, and activation of genes promoting wound healing but also tumor growth. Wound sites are more at risk of tumorigenesis than unwounded sites after infection with tumorigenic Rous Sarcoma virus⁶⁰. In cases of chronic injury, such as chronic viral hepatitis, neoplasias have a risk of forming⁵⁷. Longer lived organisms may have evolved more tumor suppressors, which lowers risk of cancer but may compromise regeneration. On the other hand, regenerative capacity poses increased risk of cancer in cases of misregulation of other systems, as shown in the case of overgrowth during antler regeneration in hormonally compromised deer. Altogether, the evidence shows that some risk is associated with regenerative activity, or the associated inflammation, that can lead to neoplasia if oncogenes or tumor suppressors are misregulated. The research presented here shows an additional risk of tumorigenesis following damage from X-irradiation or *egr*-ablation, if the tumor suppressor activity of the caspase cell death pathway is inhibited.

Regeneration in *Drosophila*

Wing Imaginal disc development

Adult *Drosophila* size is determined by growth during larval development. During larval development, diploid tissues called imaginal discs grow via mitosis as precursors to adult organs^{64,65}. The wing imaginal disc is an epithelial sac that evaginates post pupation to form the wing. The tissue grows from 20 cells to 75,000 cells by third instar⁶⁶. The wing imaginal disc is composed of sections that will form the adult dorsal thorax, the hinge tissue that connects the fly's thorax to the wing, and the wing blade. In the developing wing disc, the portion that forms the wing is called the wing pouch, and the cells in the pouch are single sheets of pseudostratified epithelia. In the center of the pouch a margin, or axis that the

pouch will fold along, forms the dorsal and ventral halves of the wing, which eventually evaginate and fold onto each other to form the wing blade (Fig. 1).

The wing blade fate is determined by a series of early markers, with the anterior-posterior axis of the wing pouch patterned by Hedgehog and Decapapelegic and the dorsal-ventral axis of the pouch governed by a Wingless gradient^{66,67}. During metamorphosis, hormonal signaling leads the disc to differentiate into the adult wing⁶⁸.

Figure 1.

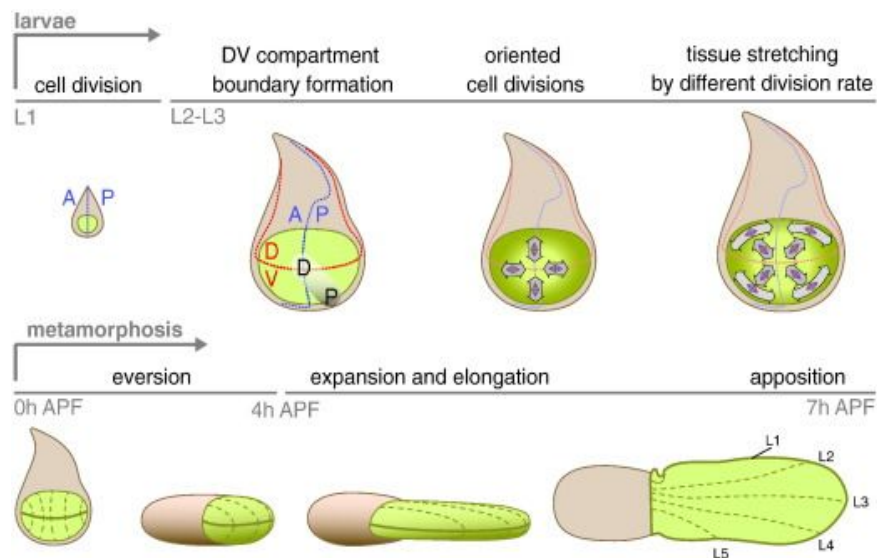


Figure 1. Wing disc development During L1 stage, the imaginal wing disc undergoes cell division. During the L2/L3 phase, the Dorsal and Ventral compartment boundaries of the pouch are formed, and cells continue to divide. During metamorphosis, the tissue of the wing pouch begins to evaginate, and the wing blade will eventually be formed by the expanded pouch, whose Dorsal and ventral layers form the top and bottom of the wing. Image from Diaz de la Loza and Thompson 2017

Different models for producing damage—regeneration in imaginal discs

There are several models currently used to create damage in *Drosophila*. Early studies of regeneration in imaginal discs used ex vivo techniques, where imaginal discs were dissected from a larvae, surgically damaged, and then the cut

fragments were transplanted into the abdomen of adult hosts, which is an environment that promotes regeneration of the discs^{69,70}. These studies showed that under the right conditions, a disc fragment or injured disc can regenerate the remainder of the disc⁷¹. However these studies are technical, and it is difficult to replicate damage to the same precise area with each damaging surgery.

To produce uniform and easily replicable damage in situ, the Gal4/UAS system can be used to express pro-apoptotic genes *rpr* and *egr* constitutively^{72,73}. Instead of expressing ablation genes constitutively, one can temporally limit the Gal4 driver with Gal80 temperature sensitive control of Gal4 to see if less gene expression leads to a less dramatic ablation phenotype. Ablation damage caused by *egr* or *rpr* as well as from surgical damage both increase expression of *myc*, *wg*, and *JNK*⁷². Ablation damage is useful in targeting specific tissues using the UAS/Gal4 system and to give control for the duration of the damage. In addition to the replicable damage, with the Gal4/UAS system one can cause ablation damage with *egr* or *rpr* in any Gal4 driver pattern. Thus, this technique consistently produces replicable damage making it a valuable research tool.

Finally, X-irradiation is another frequently used technique that can be used to damage entire *Drosophila* larvae in a temporally restricted manner, although it is not tissue specific⁷⁴⁻⁷⁶. X-irradiation causes cell death in diploid cells of imaginal discs^{77,78}. Like conditional Gal4/UAS driven ablation, X-irradiation damage is useful because it creates temporally limited damage. Critically, X-irradiation requires no additional genetic elements and does not rely on times when a Gal4 driver gene is expressed during development. X-irradiation damage promotes p53 to increase transcription of *rpr* and *hid* to cause apoptosis. All three methods cause JNK pathway activation in dying and neighboring cells. This JNK activity causes apoptosis and regeneration. Thus, we can use all three systems to cause damage in our model if we wish to observe the effects of JNK pathway dependent regeneration.

During wound healing, *Drosophila* columnar and squamous epithelia that characterize the disc establish temporary heterotypic contacts, the wound edges contract, the surface area is reduced, epithelia is redirected to wound edges, and actin extensions seal the wound⁷⁹⁻⁸¹. This process requires Grainyhead, a transcription factor, and its target gene *stitcher*, which upregulate ERK signaling⁸². However, this wound healing takes time and disturbs the normal growth of the injured tissue.

Signaling pathways involved in imaginal disc regeneration

The Jun N-terminal Kinase (JNK) pathway is a highly conserved eukaryotic stress signaling pathway that is activated after injury⁸³ and is critical for imaginal disc regeneration. In *Drosophila* injury or cellular stress causes TNF/eiger ligand to be secreted from the fat body to bind to its receptor Grindelwald in insulin producing cells (IPCs) in the brain and start the JNK pathway phosphorylation cascade^{99,18}. A series of phosphorylation steps eventually triggers phosphorylation of *Drosophila* JNK (Fig. 2). JNK phosphorylates *Drosophila* Jun (dJun), which then binds to *Drosophila* Fos (dFos) and homo or heterodimerizes to form activator protein-1 (AP-1), which can act as a transcription factor to increase cell death or proliferation^{83,84}.

Figure 2.

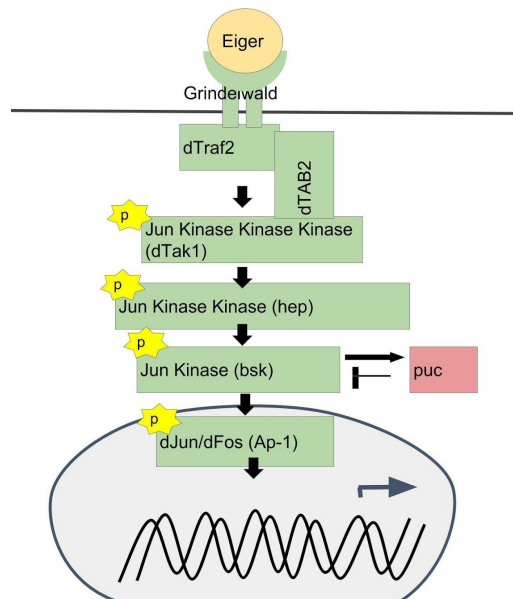


Figure 2. JNK pathway phosphorylation steps. Image from Cristina D’Ancona

JNK signaling promotes expression of apoptotic genes in *Drosophila*. In the imaginal wing disc when DPP is misregulated, JNK signaling through JNK pathway member hemipterous causes cell death⁸⁵. JNK pathway signaling promotes transcription of *rpr* and *grim* in the eye imaginal disc⁸⁶, but in both these cases it is unknown if AP-1 activity is necessary for the cell death.

Ras signaling also promotes growth through JNK activity after dead cell clearance^{81,87-89}. Thus, JNK signaling is necessary for the regenerative process. In Chapter 2, we observe that *egr*-ablated tissues have higher levels of AP-1 transcriptional activity (measured with fluorescence of a transcriptional GFP reporter) than control tissues. Thus, AP-1 signaling increases in regenerating tissues.

The segment polarity gene *wingless* (*wg*) is the fly homologue of *Wnt* that encodes a ligand whose signaling can lead to transdetermination⁹⁰. In the wing discs, cells at the dorsal-ventral boundary secrete *Wg*, which diffuses to activate

segment polarity genes *achaete* and *scute* at high thresholds and *vg* and *Dll* in a more graded manner. It is known previously that *Wg* is also a regulator of regeneration and is upregulated after damage (Fig. 3)⁷².

Figure 3.

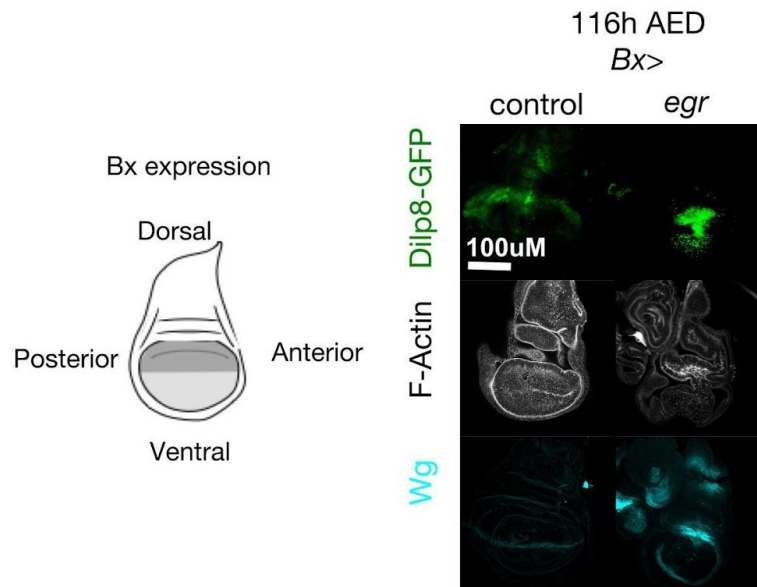


Figure 3. Dilp8 expression increases in *eiger* expressing tissue

In *Drosophila* one can express genes using the Gal4/UAS system. We use Beadex (Bx) as the gene that drives expression of Gal4. Gal4 protein activates UAS and the target of UAS, our gene of interest. Beadex expression is in the pouch of the imaginal disc (marked in dark and light grey in the cartoon). *Bx>egr* expression causes ablation damage that leads to an increase in Dilp8 expression (green) and increase in the area of regeneration marker *Wg* (cyan) compared to control discs (*Bx>LacZ*). (Data from Chapter 2 Figure 2). F-actin stain, shows the overall shape of the disc (gray). The green, gray, and cyan images are of a single control and single *eiger* expressing disc. Scale bar represents 100µM. Image from Danielle DeCrema

Smith-Bolton (2009) showed that *wg* and *myc* gene expression are increased during *egr* or *rpr* tissue damage after ablation of the wing discs⁷². *Wg* alleviates Notch inhibition of *myc* expression and thus promotes Myc activity in the *Drosophila* wing disc⁹¹. Myc induces growth by increasing cellular mass and cell size in *Drosophila*⁹². Mature *Drosophila* larvae lose the ability to regenerate after *eiger* damage even if *wg* or *myc* are expressed⁷².

Subsequent studies have shown that the *wg* Regenerative response element/BRV118 (an enhancer region downstream from the *wg* coding sequence), which is deleted in the 2416 base-pair *wg[1]* deletion, is critical for regeneration post irradiation or *egr*-ablation damage¹³⁵. For example, homozygous *wg[1]* mutant eye imaginal discs fail to regenerate following X-irradiation (Fig. 4). However it remains to be seen if the *wg* and *myc* expression are necessary for regeneration in imagina discs besides the wing and eye, and well as with surgical ablation damage models.

Figure 4.

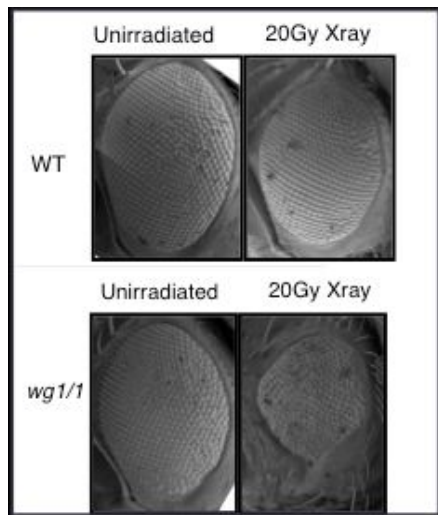


Figure 4. *wingless* is necessary for regeneration after X-irradiation. Inhibition of the wingless regenerative region with mutation *wg[1]/1* prevents healing of the *Drosophila* eye after irradiation with 20 Grays of X-irradiation compared to wild type eyes (WT) (Adrian Halme unpublished).

Figure 5.

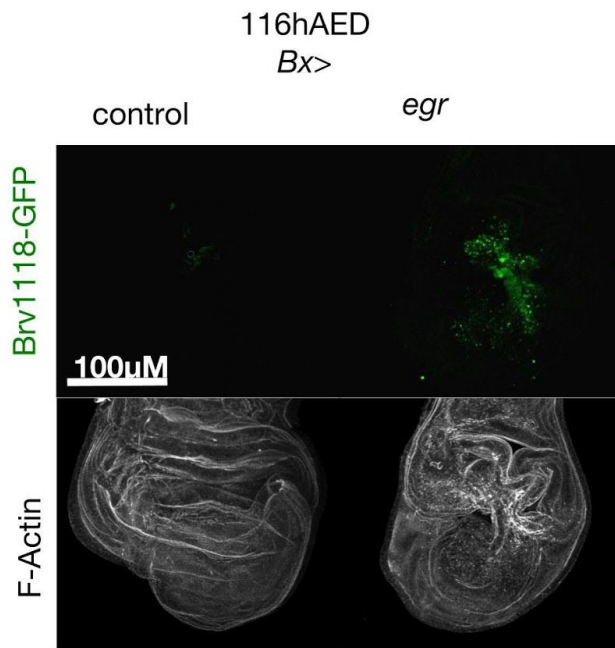


Figure 5. Brv118 transcriptional activity increases in *egr* expressing tissues

Wingless enhancer BRV118-GFP transcriptional activity (green) increases following genetic ablation with UAS/Gal4 *Bx>egr* overexpression in the pouch of the wing disc compared to *Bx>LacZ* controls. The F-actin (gray) shows the shape of the disc, including the pinched tissue caused by *egr* expression. Data from Chapter 2 Figure 2. Scale bar represents 100µM.

Therefore, Wg is necessary for regeneration. In Chapter 2, we observe regenerative activity by measuring fluorescence levels of Brv118-GFP. We find that Brv118 fluorescence levels increase in *egr*-ablated tissue compared to controls (Fig. 3). Thus, in our work, when discussing whether regenerative processes are occurring in our tissues we observe markers for regenerative genes *dilp8* and Wg/BRV118 signaling.

A developmental checkpoint extends larval development and the regenerative period

Wing discs can regenerate while maintaining proper size and allometry following various forms of damage, including X-irradiation damage, physical insult, and genetic ablation^{72,93-97}.

As larvae develop they normally pupate after their wandering L3 stage (relatively from 90-120 hours after egg lay depending on rearing conditions), but after damage, the larval period of development extends and pupariation delays, with the length of delay corresponding to the amount of damage. This delay that gives time for repair is called the regeneration checkpoint delay and also partially pauses the growth of non-injured tissues^{76,97,98}. However, this checkpoint delay is developmentally limited. Imaginal discs can heal if the larvae are injured before the restriction point, or point at which regeneration can no longer heal damaged imaginal discs⁷⁶. For example, larvae injured before the restriction point with ablation or X-irradiation can undergo regenerative checkpoint delay and heal damage to the eye and wing. However, damage after the restriction point prevents this checkpoint delay and in the case of X-irradiated tissues results in a rough eye phenotype and notched wing. The time of the restriction point varies depending on rearing conditions but occurs after larvae begin their wandering phase and slightly before pupariation. (Fig. 6).

Figure 6.

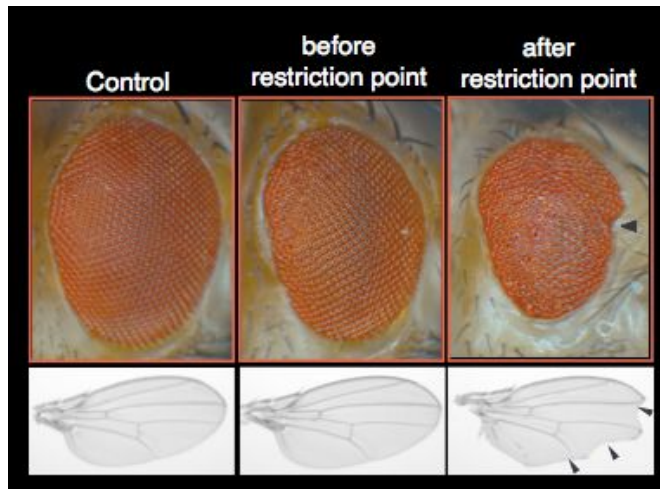


Figure 6. Regeneration is restricted during development

Larvae injured before the restriction point with ablation or X-irradiation are able to heal damage to eye and wing. A rough eye phenotype and notched wing result from damage after the restriction point. (image from Halme et al. 2010).

What signaling pathways are involved in this regenerative process and how does the regeneration checkpoint delay permit growth coordination between damaged and undamaged tissues?

Mechanistically, damaged tissue will secrete signaling peptide Dilp8 to delay pupariation. Dilp8 shares structural features with the insulin/relaxin protein family, and inhibits brain-derived prothoracicotropic hormone (PTTH) expression by binding to Leucine-rich repeat containing G protein-coupled receptor (Lgr3), a relaxin family peptide receptor. Two Lgr3 positive neurons in each brain lobe in the pars intercerebralis of *Drosophila* make physical contact with PTTH neurons, and reducing Lgr3 levels in these neurons via Dilp8 binding disrupts neural circuitry to PTTH^{99,100}. PTTH initiates the normal pulses of steroid hormone 20-hydroxyecdysone from the ring gland, which promotes larval molts and normally halts the period of imaginal disc growth to permit pupariation. If larvae feed on ecdysone they fail to heal X-irradiation damage and die even they are fed before the normal restriction point, indicating that the progression of development prevents normal regenerative checkpoint delay⁷⁶. Thus, Dilp8 checkpoint delay prevents developmental progression. Dilp8 also coordinates growth between regenerating and undamaged tissue by activating nitric oxide synthase in the prothoracic gland, which inhibits ecdysone synthesis and reduces undamaged imaginal disc growth to permit allometric growth of injured tissue compared to undamaged tissues^{97,101}.

In experiments described in this thesis, I use checkpoint delay as a reporter for regenerative activity. Longer checkpoint delay corresponds to higher levels of damage, thus we sought to identify mutations that produce excessive or extended regenerative activity. Dilp8 is one marker we use for regenerative activity (Fig. 1), where we see an increase in Dilp8 in *egr*-ablated tissues.

Apoptosis

As an organism develops, grows, and ages, the balance between the number of cells that proliferate and the number of cells that undergo apoptosis

produces tissue homeostasis. We know that apoptosis is critical during embryogenesis and development to shape tissues and break down unnecessary structures, such as how ecdysone activity increases expression of multiple caspase pathway members, including initiator caspase Dronc, during metamorphosis to break down larval structures¹⁰². Apoptosis also occurs after stress responses, such as when after X-irradiation the p53 pathway upregulates caspase pathway members Reaper, Grim, and Hid to kill off cells that can no longer perform their function^{1,103-106}. In Chapter 2, we discuss the expanded role of apoptosis after the stress of excessive regeneration. Aside from the role of apoptosis in embryogenesis and stress response, we are still discovering new non-apoptotic functions of caspase activation, such as how caspases act to individualize spermatids in *Drosophila*¹⁰⁷.

In *Drosophila*, during these times of embryogenesis and stress response¹, the execution of cell death and degradation of cells depends on caspases, Cysteine-dependent Aspartate directed Proteases. The effector caspase family members that participate in cell death are synthesized as inactive precursors (Drice and DCP-1 in flies) that must have their prodomains proteolytically cleaved by initiator caspase Dronc to form active heterotetramers¹⁰⁸. Ultimately, caspases degrade lamin, inactivate DNA repair proteins, and activate caspase-dependent DNase endonucleases that cleave chromatin, however, caspase activation is tightly regulated.

In addition to the activation of effector caspases by initiator caspases, several regulatory steps prevent caspase activation. In *Drosophila*, apoptosis is tightly regulated by Dark activation of Dronc and regulation of IAP inhibitors by Rpr, Hid, and Grim. First, the initiator caspase Dronc¹⁰⁹ must bind to the *Drosophila* Apaf-1 homolog Dark¹¹⁰ or Tango 7¹¹¹ to form an active protein. Dark is the canonical activator of Dronc in most described cellular contexts, while Tango7 was recently described to act as an activator in the cortex to break down F-actin¹¹¹. Ectopic p35 expression or p49 expression can inhibit caspases by binding to them

in a permanent energetically irreversible manner^{112,113}. Next, caspase activity is limited by Inhibitors of Apoptosis Proteins (IAPs) (in humans XIAP, in flies DIAP1/2, DBruce, and Deterin)^{108,109,114–121}.

Figure 7

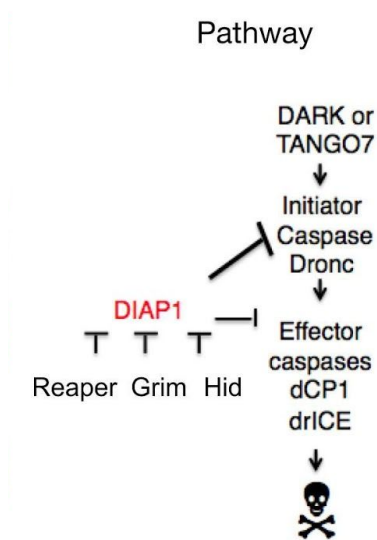


Figure 7. Caspase cell death (apoptosis) pathway. Reaper, Grim, and Hid inhibit Diap1 to promote cell death. Figure by Cristina D’Ancona

IAPs bind to the catalytic site of caspases (BIR domains) and target them for ubiquitination and degradation by acting as an E3 ubiquitin ligase^{108,109,114–121}. In turn, Diap1 is inhibited by Pro-cell death proteins Rpr, Hid, and Grim (in humans Smac/DIABLO, Omi/HtrA2)^{4,108,122–126}. Rpr, Hid, and Grim act most efficiently as a multimeric complex¹²⁷, and all three bind to DIAP1 and induce IAP auto-ubiquitination and degradation to promote programmed cell death³.

The body has many ways to regulate cell death to permit proper homeostasis, prevent cell death in healthy tissue, or to prevent hyperproliferation. Our work focuses on key pro-apoptotic family members and the JNK pathway that increase their expression after ablation or X-irradiation damage. New roles for cell-death genes are described in Chapters 2 and 3, where IAP inhibitor Rpr is

necessary to prevent neoplasia following *egr*-ablation and *rpr*, *grim*, and *hid* overexpression in the wing disc leads to larval growth inhibition.

Cell death in regeneration and cancer

Cell death in regeneration

Cell death and caspase activity are essential for regeneration in many systems. For example, in hydra where fragmented tissue can regenerate to form a new animal, apoptosis is necessary for new basal head formation after the animal is bisected. After the animal is decapitated dying cells are necessary and sufficient to induce Wnt3 secretion. In the hydra Wnt3 itself is necessary for head regeneration, thus apoptosis is necessary and sufficient to induce regenerative activity. Apoptotic cells also promote compensatory proliferation and tissue growth^{2,128}. In response to cell death, surrounding cells undergo compensatory proliferation, or additional proliferation of non-dying cells to compensate for the loss of dead and phagocytized tissue¹²⁹⁻¹³¹. Thus, cell death promotes regenerative activity in hydra by inducing Wnt secretion and promoting compensatory proliferation. Cell death in *Drosophila* also promotes Wnt signaling and compensatory proliferation to increase regenerative activity.

In *Drosophila*, dying cells produce Wnt homologue Wg and Dpp in response to activation of the pathway^{129,132,133}. Wg is required for the proliferative response after ablation with *rpr* or *egr*⁷² and after surgical transection¹³⁴. The *wg* enhancer, regenerative response element/BRV118, is critical for regeneration post *egr*-ablation¹³⁵.

Compensatory proliferation also occurs after damage in *Drosophila*. Initially, compensatory proliferation in *Drosophila* was studied in undead cells (cells that cannot undergo apoptosis) in the wing imaginal disc. In *Drosophila*, one can create cells that are undead or are expressing *p35*, which binds to effector caspases and prevents cell death but does not affect upstream components of the caspase pathway. In this undead cell environment, loss of an allele of *dronc* or *p53*

suppresses compensatory proliferation, indicating cell death pathway member *dronc* and *p53* (which promotes gene expression of IAP inhibitors) are necessary for compensatory proliferation^{104,136}. These studies were done in the wing disc, which proliferates throughout larval development, with the majority of cells remaining undifferentiated until pupal development^{137,138}.

In contrast, cells in the eye disc differentiate during third larval instar. Investigating these differentiating cells posterior to the morphogenetic furrow in the eye shows that compensatory proliferation no longer depends on *Dronc* signaling. Unlike compensatory proliferation in the wing, compensatory proliferation posterior to the morphogenetic furrow requires IAP inhibitor *Hid* expression and effector caspases *DrICE* and *Dcp-1* expression, indicating that different apoptotic factors are necessary for compensatory proliferation in different cell states¹³⁶. Thus, cell death causes compensatory proliferation in both proliferating tissue of the wing imaginal disc and in differentiated tissue of the eye imaginal disc.

Roles of cell death in promoting/preventing cancer

Resisting cell death is considered a hallmark of cancer^{139,140}. Normally, high oncogene activity and/or DNA damage from hyperproliferation or loss of genomic integrity cause cellular stress and apoptosis. However, developing tumors also accumulate mutations in the genes that would normally promote apoptosis (*p53*, *Bcl-2*, *Bcl-XL*, and IAP family members)^{105,141–143}. Loss of apoptotic gene expression alone is insufficient to cause tumor formation, but loss of apoptosis paired with oncogene expression/dysregulation of tumor suppressors causes cancer^{144–148}.

Growth inhibition in *Drosophila*

Chapter 3 focuses on how overexpression of *rpr*, *grim*, or *hid* in the wing disc leads to non-autonomous growth inhibition in whole larval body. We are still determining the mechanism that causes this non-autonomous growth inhibition with these pro-cell death genes expressed in the wing. Here we review how larvae

grow and cease growth during development, and what factors lead to decreased growth that might cause non-autonomous growth inhibition.

As Critical Weight is reached, pulses of Ecdysone end larval growth and push to pupariation

During the larval period, the larvae continuously feed and undergo two molts before reaching critical weight during their third instar. Critical weight is the minimum amount of weight larvae need to reach to have enough energy for pupariation and is determined as the weight needed to pupariate even if the larvae are then starved¹⁴⁹. After critical weight is reached, there is a period called the terminal growth period where the larvae continues to eat and can triple in size. The terminal growth period determines final adult size and is the last point where larvae can gain weight before pupariation^{65,98,149-151}. Coinciding with the attainment of critical weight, pulses of steroid hormone ecdysone are released.

Larval molts and pupariation are determined by pulses of steroid hormone ecdysone, produced by the prothoracic gland. The prothoracic gland (PG) is stimulated to produce ecdysone by the neuropeptide prothoracicotropic hormone (PTTH)^{150,152}. PTTH is produced in by two pairs of lateral neurosecretory cells in the brain that extend axons to the PG^{76,150,153}. Once larvae achieve critical weight, PTTH is released and binds to tyrosine kinase receptor Torso and activates a mitogen-activated protein kinase (MAPK) signaling cascade¹⁵⁴, which increases expression of ecdysone biosynthetic genes.

Ecdysone is secreted into the hemolymph, and is converted to its active form when it reached its target tissues. The P450 monooxygenase Shade acts in periphery tissues such as the epidermis and fat body to convert ecdysone to its active form 20-hydroxyecdysone, which binds the ecdysone nuclear hormone receptor to regulate gene expression¹⁵⁵. There is a small pulse of ecdysone at critical weight, followed by a terminal growth period where the larvae continue to feed before an additional ecdysone peak causes the larvae to stop eating and to wander. Factors that prevent the production of ecdysone can shift critical weight

and thus ultimately give larvae less time for growth. For example, if Torso, Ras, or Raf are overexpressed in the prothoracic gland, animals precociously secrete ecdysone, and pupate early at a small size^{154,156}, leading to non-autonomous growth inhibition.

Disruption of nutrient signaling in the fat body leads to Non-autonomous growth inhibition

The *Bx>rpr* larvae and pupae undergo non-autonomous larval growth inhibition. Unlike cell-autonomous growth inhibition, which affects only the cells/tissues affected directly by manipulation, non-autonomous growth inhibition leads to a reduction in the size of cells or tissues separate from the directly manipulated tissue¹⁵⁷. Non-autonomous growth inhibition is often observed when the larvae are unable to feed or normally process nutrients and grow. The larval fat body, which performs roles comparable to mammalian liver and white adipose tissue, senses nutritional signals and coordinates the growth of imaginal discs and larval tissues¹⁵⁸. Putative amino-acid transporter gene *minidiscs* is required for the fat body to regulate whole-animal growth¹⁵⁹, and without this amino-acid transporter, larvae suffer from imaginal disc growth defects. Also, disruption of fat body cationic amino-acid transporter gene *slimfast(slf)* or TOR activity leads to non-autonomous larval growth inhibition¹⁶⁰. Thus, the fat body regulates the growth of imaginal discs and larval tissue by sensing amino acid levels. The fat body regulates this growth by controlling the release of Dilp2 from the brain. Normally, circulating Dilps, secreted from IPCs in the brain, bind to insulin receptors in target cells to activate PI3K signaling cascades. These cascades inhibit Foxo transcription and promote cell-autonomous growth^{161,162}. When *slif* expression or TOR activity is disrupted in the fat body, an unknown secreted factor from the fat body causes *Drosophila* insulin-like peptide 2 (Dilp2) to accumulate in IPCs in the larval brain^{158,163,164}. Co-Culturing fat bodies from fed larvae, but not from starved larvae, with starved brains is sufficient to cause Dilp2 secretion¹⁶⁴. This result

indicates that the fat body secretes a factor that promotes Dilp2 secretion¹⁶⁴. Thus, the fat body regulates growth in an amino-acid and TOR dependent manner.

Infection in *Drosophila* leads to either inflammatory Toll or Imd pathway cascades involving cellular and humoral defenses. In addition to its previously mentioned role in metabolism, the fat body also synthesizes and secretes antimicrobial peptides into the hemolymph during inflammatory responses¹⁶⁵. Toll pathway activity in the fat body inhibits insulin signaling, which results in decreased triglyceride storage and non-autonomous growth inhibition¹⁶⁶. Thus, it would be ideal to investigate if Toll signaling is increased in the fat body of our *Bx>rpr* expressing larvae in Chapter 3.

Metabolic effects of tumorigenesis

While it is too early to discern whether there really is metabolic disruption with RGH overexpression, in some cases an altered metabolic state is also a hallmark of cancer¹³⁹. First observed in the 1920s by Otto Warburg, cancer cells prefer to use glycolysis even in the abundance of oxygen and upregulate synthesis of glucose transporters¹⁶⁷⁻¹⁷⁰. Tumors also upregulate amino acid and lipid metabolism, increase glutaminolysis, increase mitochondria production, and induce the pentose phosphate pathway as methods to obtain energy and metabolites that promote biosynthesis and continuous proliferation. Disruptions to the normal activity of c-Myc, HIF1alpha, Ras, PI3K, p53, and AMPK permits many of these metabolic changes¹⁷¹.

One outcome of many cancers is wasting or cachexia, which is an involuntary loss of skeletal muscle and adipose tissue that leads to progressive functional impairment¹⁷². In association with reduced treatment response, sixty percent of advanced cancer patients are affected by wasting syndrome, which leads to 20% of cancer-related deaths^{173,174}. Pro-inflammatory cytokines, like TNF alpha and interleukins, are secreted factors implicated with wasting, as are TGF-beta family ligands myostatin and activin, TRAF-6, and IGF-1^{173,175-180}. While the exact mechanisms are unknown, this increase in inflammatory secreted factors

leads to cachexia¹⁷². Figueroa-Clarevega and Bilder (2015) have shown that *Drosophila RasV12/scrib-/-* mutant tumors induce cachexia-like symptoms by secreting ImpL2, which inhibits insulin signaling¹⁸¹. We will begin to explore the possibility of metabolic defects from overexpression of IAP inhibitors *rpr*, *grim*, and *hid* in Chapter 3, but more follow-up experiments will be needed to truly clarify if the growth inhibition phenotype is connected to an altered metabolic pathway.

Summary

The purpose of regeneration is to restore form and function to damaged tissues. Regenerative capacity is variable in nature, and humans have limited regenerative capacity that decreases with age. It is possible that regeneration is limited in nature due to regeneration being energetically costly or because there is a risk of tumorigenesis associated with regenerative activity.

In our research in Chapter 2, we show that the *Drosophila* caspase cell death genes act as a tumor suppressor in cases of prolonged regenerative activity. We also show that prolonged regenerative activity alone can sometimes create overgrowth, which is similar to how cancers can form in cases of chronic illness. When we examine damaged imaginal disc tissues that lack RGH function, we find substantially enhanced levels of regenerative markers Dilp8, Wg, and Wg enhancer regulative regenerative element BRV1118. We then see that inhibiting regeneration in these RGH depleted and damaged discs with a mutant allele of *wg* or a dominant negative allele of JNK partially rescues the overgrowth and delay phenotypes, indicating that this overgrowth is at least partially due to regenerative activity. Overall the research in Chapter 2 supports that cell death prevents neoplasia or neoplasia-like growth in the context of regeneration in *Drosophila*. *Drosophila*, like humans, have limited regenerative capability post development, and undergo wound healing to heal tissues, so it is possible that similar mechanisms occur if IAP inhibitors are disrupted following damage. Hopefully, the insights from our research will be applicable to human regeneration therapy research.

In this introduction, we also reviewed how non-autonomous growth inhibition is caused by alterations of the ecdysone pathway, alterations in TOR or Insulin signaling in the fat body, increase of inflammatory pathway Toll activity in the fat body, or by cachexia-like wasting in *Drosophila*. In Chapter 3, we observe that IAP inhibitor overexpression and ablation in the wing disc also leads to non-autonomous growth inhibition of the larvae and pupa. We observe that this phenotype is likely dependent on apoptotic pathway activity, and the phenotype is partially rescued by Diap1 expression in the wing disc. We found that other damage models, including *egr*-ablation and neoplastic damage, do not recapitulate this growth inhibition phenotype. This growth inhibition is further characterized in Chapter 3.

Chapter 2: Caspase-mediated cell death prevents neoplastic tumor formation in regenerating tissues

Cristina R. D’Ancona¹ and Adrian Halme^{1,2,*}

1. Department of Biology, University of Virginia Charlottesville, VA 22908

2. Department of Cell Biology, University of Virginia School of Medicine
Charlottesville, VA 22908

Abstract

Damage to *Drosophila melanogaster* imaginal discs early in larval development elicits a proportional regenerative response that can repair damaged tissues. Imaginal disc regeneration also produces a systemic response, a developmental checkpoint, which delays pupation and extends the regenerative period of development. We have taken advantage of this delay phenotype associated with imaginal disc regeneration to identify mutants that produce a large regenerative response following damage. Here, we describe an essential regenerative role for the caspase pathway. Mutations that limit caspase activity produce an extension of regeneration checkpoint delay following damage, accompanied by increased expression of regenerative genes *dilp8* and *wingless*. In addition, neoplastic tumors emerge in regenerating tissues that lack IAP-inhibitor function or caspase function. The neoplastic transformation of regenerating tissues that lack apoptotic activity is dependent on JNK-dependent *wingless* transcription. In total, these data support a model in which apoptosis prevents neoplastic transformation of regenerating tissues.

Introduction

There are many features shared between regeneration and tumorigenesis: cell proliferation, cell dedifferentiation, cell migration, and similar inflammatory signals contribute to both regenerative activity and tumor progression^{57,182,183}. However, regeneration and tumor development produce strikingly different outcomes. In regenerating tissues, damaged structures are replaced and functional and differentiated tissues are formed. In contrast, neoplastic tumors fail to differentiate and remain proliferative and dysmorphic. Therefore, it has been unclear whether regeneration and tumor development reflect a shared underlying mechanism, and whether dysregulated regenerative activity contributes to tumor formation. However, one piece of evidence for this connection can be seen in the regeneration of deer antlers. Each spring, male deer regenerate their antlers. However, if male deer are castrated after this regrowth has initiated, the antler regeneration becomes misregulated and produces a dysmorphic overgrowth of the antler tissue. This dysmorphic growth is characterized by histological immaturity and the formation of cystic structures consistent with persistent but poorly regulated regenerative activity⁶².

The fruit fly, *Drosophila melanogaster* has a remarkable capacity to regenerate their imaginal discs—the larval precursors to adult structures. However, this regenerative capacity is limited by development. Imaginal discs can regenerate if damaged early in larval development. Late in larval development, the larvae pass a restriction point (at ~104 hours after egg lay, hAED) where the imaginal discs lose their regenerative capacity.

When damage to imaginal discs at early larval stages produces a regenerative response, there is a corresponding systemic response, activation of a developmental checkpoint, during which larvae will delay their development, postponing pupation and extending the regenerative period⁷⁶. In the experiments described here, we take advantage of this regenerative checkpoint delay to identify

mutations that dysregulate regenerative activity and result in the formation of neoplastic tumors.

We show that loss of pro-apoptotic genes in regenerating tissues produces neoplastic tumors, characterized by loss of apical-basal polarity in the epithelia, and excessive activation of regenerative signaling pathways. These regenerative neoplasias result from excessive JNK activation and activation of the *wg* gene through a regeneration enhancer element. In summary, these results demonstrate that apoptosis acts as a tumor suppressor, preventing tumorigenesis in regenerative tissues.

Results

IAP inhibitors limit regeneration checkpoint activation

To identify genes that limit the size and duration of the regenerative response in tissues we used the developmental checkpoint delay to assess the regenerative activity produced by damage (Fig. 1A and 1B). Regenerative activity in the wing is critically dependent on the transcriptional activation of *wingless* by Jun N-terminal Kinase (JNK)¹³⁵. To demonstrate that checkpoint delay can reflect this transcriptional activity, we sought to determine whether increasing or decreasing transcriptional activation of *wingless* by JNK would produce corresponding increases or decreases in developmental delay. To do this, we expressed the *Drosophila* TNF homolog *eiger* in the wing imaginal disc. *eiger* binds to its receptor Grindelwald to activate JNK phosphorylation to produce a damage response and elicit regeneration. This also causes checkpoint activation and a delay in pupariation (Fig. 1B). Transcriptional activation of *wingless* is increased with its enhancer named *wingless* regeneration regulatory enhancer. The *wingless* regeneration regulatory enhancer is the target of the JNK transcriptional effector AP-1 and is necessary for regeneration following *eiger* ablation damage¹³⁵. If we limit the transcriptional activation of *wingless* in this model by removing one wild type copy of the *wingless* enhancer with the hypomorphic *wg[1]* allele^{135, 208} we

Figure 1.

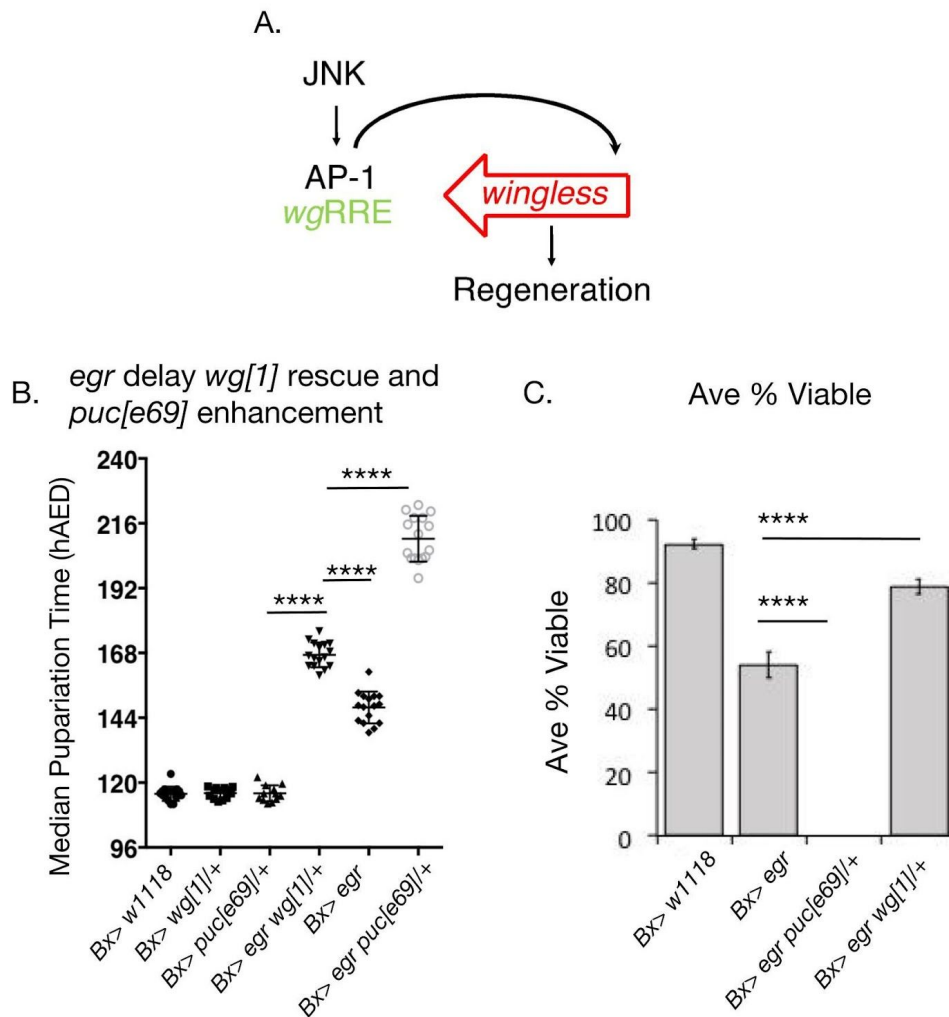


Figure 1. IAP inhibitors limit regeneration checkpoint activation

A.) The pathway models shows that JNK pathway activity causes upregulation of *wingless* regulatory regenerative response element (wgRRE), which is necessary for regeneration. **B.)** JNK pathway upregulation causes an increase in developmental checkpoint delay compared to *Bx> w1118* controls. Further enhancing JNK activity with *puc[1]/+* increases delay, while co expression of *wg[1]/+* inhibits regeneration and delay. (n are Populations of 15-20 individuals: *Bx> w1118* n= 16, *Bx>wg[1]/+* n=12, *Bx> puc[e69]/+* n=12, *Bx> eiger* n=16 populations, *Bx> eiger;wg[1]/+* n=12, *Bx> eiger;puc[e69]* n=16. p values are two-tailed and are all p<0.0001. Significance was calculated with an unpaired Student's t-tests. **C.)** The percent of viable flies that eclose after pupariation is increased with the *wg[1]/+* mutation with *Bx>eiger* co expression compared to *eiger* controls. The percent of viable flies that eclose after pupariation is further diminished with puckerred with *Bx>eiger* co expression compared to *eiger* controls. (populations were of 15-20 larvae *Bx>LacZ* n=8, *Bx>eiger* n=, *Bx>eiger* n=7 *puc[e69]/+* n=7, *Bx eiger;wg[1]/+* n=7) p values are two-tailed and are all p<0.0001. All UAS genes are expressed with Bx Gal4. All significance was calculated with unpaired Student's t-test.

Figure 2.

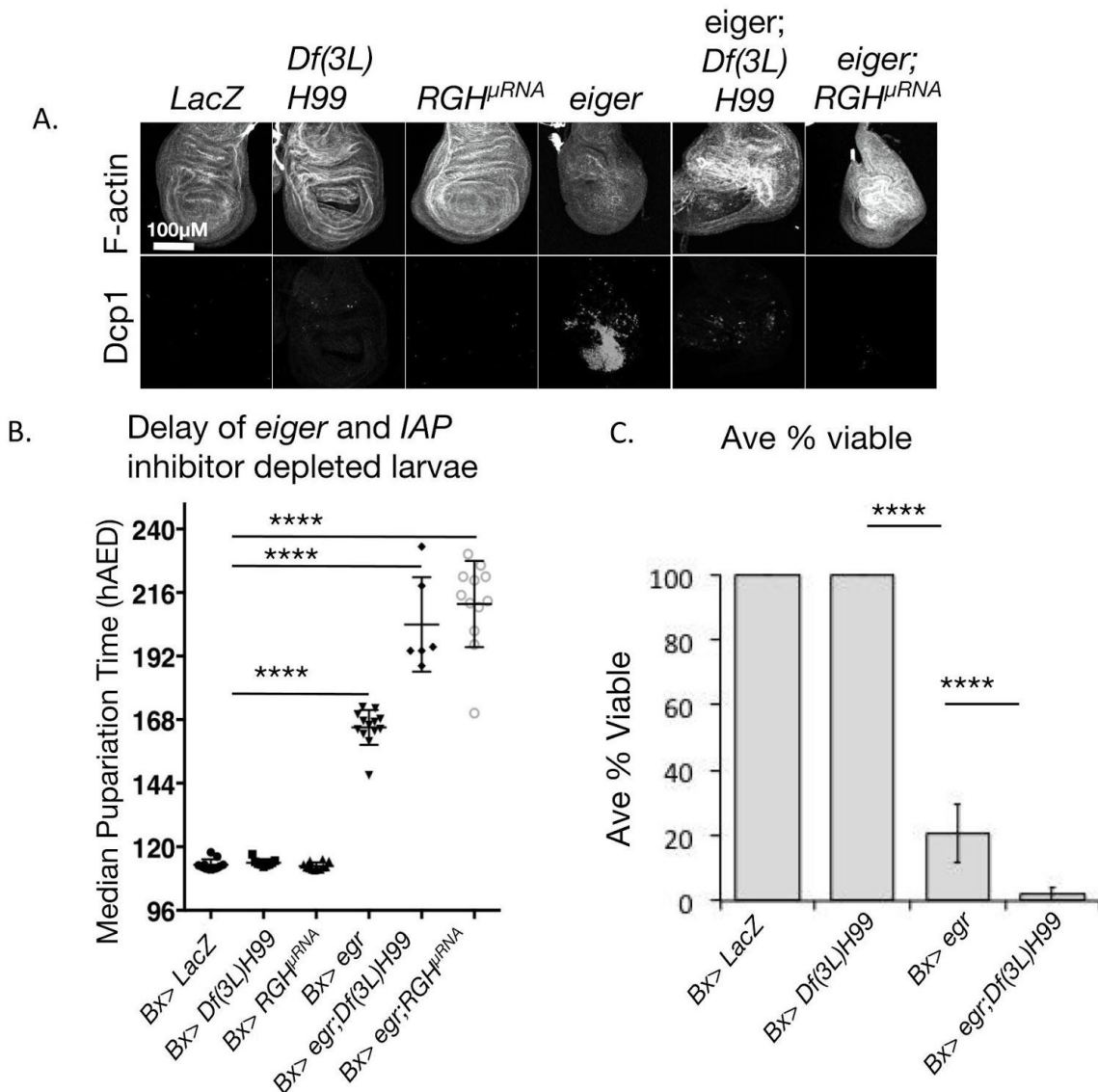


Figure 2. Increased cell death and loss of viability in tissues constitutively expressing *eiger*
A.) *Bx> eiger* and *RGH^{μRNA}* co-expressing discs are no longer express high levels of Dcp1 (shown grayscale, bottom images), but are dysmorphic in shape (visualized with F-actin in grayscale, top images). *Bx>LacZ* controls or *Bx> RGH^{μRNA}* expression alone does not result in dysmorphic shape. Scale bar represents 100μm. Micrograph images represent collapsed stacks of tissue taken at the same fluorescent intensities and edited in ImageJ/Fiji. n=4-5 discs per genotype. **B.)** *eiger* ablated discs that co-express *Df(3L)H99* or *RGH^{μRNA}* delay longer (hours after egg deposition(AED)). (n are populations of 15-20 individuals: *Bx>LacZ* n= 11, *Bx> Df(3L)H99* n=9, *Bx> RGH^{μRNA}* n=12 populations, *Bx> eiger* n=13 populations, *Bx> eiger;Df(3L)H99* n=6, *Bx>eiger;RGHuRNA* n=12) **C.)** The percent of viable flies that eclose after pupariation is further diminished with *RGH* depletion in larvae with the *Df(3L)H99* deficiency compared to *eiger* controls. (populations were of 15-20 larvae *Bx>LacZ* n=11, *Bx>RGHuRNA* n=11, *Bx>eiger* n=8, *Bx eiger;RGHuRNA* n=7) . All UAS genes are expressed with *Bx Gal4*. All significance was calculated with unpaired Student's t-test.

observe a reduction, but now a full rescue, of checkpoint delay (Fig. 1B). In contrast, mutation of the JNK-phosphatase *puckered* with a loss of function allele²⁰⁹ (*puc[e69]*) produces increased JNK activation and a substantial extension of checkpoint delay (Fig. 1B). One caveat is that we do not know if this checkpoint delay is dependent on *wg* expression. However, combined with the data that inhibiting *wg* expression lessens checkpoint delay in *eiger* expression tissues, this data suggests that checkpoint delays reflects JNK-driven *wingless* transcriptional activity during regeneration. When we expressed *eiger* in the wing imaginal disc we observe an increase in pupal lethality compared to controls (Fig 1C). If we limit the transcriptional activation of *wingless* with the *wg[1]* allele we see a rescue of pupal lethality (Fig 1C). In contrast, loss of *puckered* function with the heterozygous *puc[e69]* mutation produces an increase in pupal lethality (Fig 1C). We do not know if this increase in pupal lethality is dependent on JNK activation of *wg*. However, combined with the data that inhibiting *wg* expression lessens pupal lethality in *eiger* expression tissues, suggests that the loss of pupal viability may also reflect JNK-driven *wingless* transcriptional activity during regeneration. Also, the extended regenerative checkpoint delay seen with JNK-driven *wingless* activity is not sufficient to prevent the pupal lethality.

We observe that an extended developmental checkpoint delay is also produced in larvae that carry the heterozygous *Df(3L)H99* deficiency, which removes a portion of Chromosome 3L and deletes genes *rpr*, *hid*, *grim*, and *sickle* (Fig. 2B). We verified that *Df(3L)H99* affected the apoptotic pathway by comparing cleaved caspase activity in *Df(3L)H99* and *eiger* co-expressing discs and discs only expressing *eiger*. We found that depletion of RGH with the *Df(3L)H99* deficiency decreases cleaved caspase activity, indicating less apoptotic pathway activity (Fig. 2A). Larvae with the deficiency do delay their pupariation when there is no damage to imaginal discs (Fig. 2B). However, when regeneration is induced in the wing discs through the targeted expression of *eiger* (*Bx>eiger*) in larvae with the *Df(3L)H99* deficiency there is a much longer checkpoint delay than with larvae with *Bx>eiger*

damage alone (Fig. 2B). The *Df(3L)H99* larvae also have substantially increased pupal lethality following regeneration (Fig. 2C). This increase in pupal lethality indicates that despite the extended regenerative developmental checkpoint delay the damage caused by both targeted *eiger* expression and *RGH* deficiency still coincides with lethality. This loss in pupal viability is also reminiscent of the loss in pupal viability caused by *eiger* expression in larvae with the and pucker[[e69](#)] mutation (Fig. 1C), which led us to believe that there may be additional JNK-driven *wingless* activity occurring in these larvae. Before investigating if there is additional JNK-driven *wingless* activity in these discs, we wanted to test a more direct method of inhibiting *RGH*.

The H99 deficiency removes a copy of the pro-apoptotic genes *rpr*, *grim*, and *hid* (*RGH*) which promote apoptosis by binding Inhibitor of Apoptosis Proteins (IAPs) and targeting them for degradation. Thus, *RGH* is reduced through the entire larvae. To directly test whether these IAP inhibitors are necessary for limiting checkpoint delay and also to determine whether these genes function within the regenerating tissues, we expressed a synthetic microRNA that targets *rpr*, *grim*, and *hid* specifically in the imaginal wing disc using a *Beadex* driver. We verified that the *RGH* microRNA affected the apoptotic pathway by comparing cleaved caspase activity in *RGH* microRNA and *eiger* co-expressing discs and discs only expressing *eiger*. We found that depletion of *RGH* with the *RGH* microRNA decreases cleaved caspase activity, indicating less apoptotic pathway activity (Fig. 2A). We found that co-expression of *eiger* with the *RGH* microRNA in the wing produces significantly more delay to pupariation than *eiger* expression alone (Fig. 2B). While *RGH* microRNA and *eiger* co-expressing larvae do have a higher lethality (data not shown), this lethality is not observed until after mid-way through pupariation, so we can observe these tissues before this point. Once we found this more direct method of inhibiting *RGH* in the imaginal wing disc, we tested if there was an increase in JNK-driven *wingless* activity or regenerative signaling.

Figure 3.

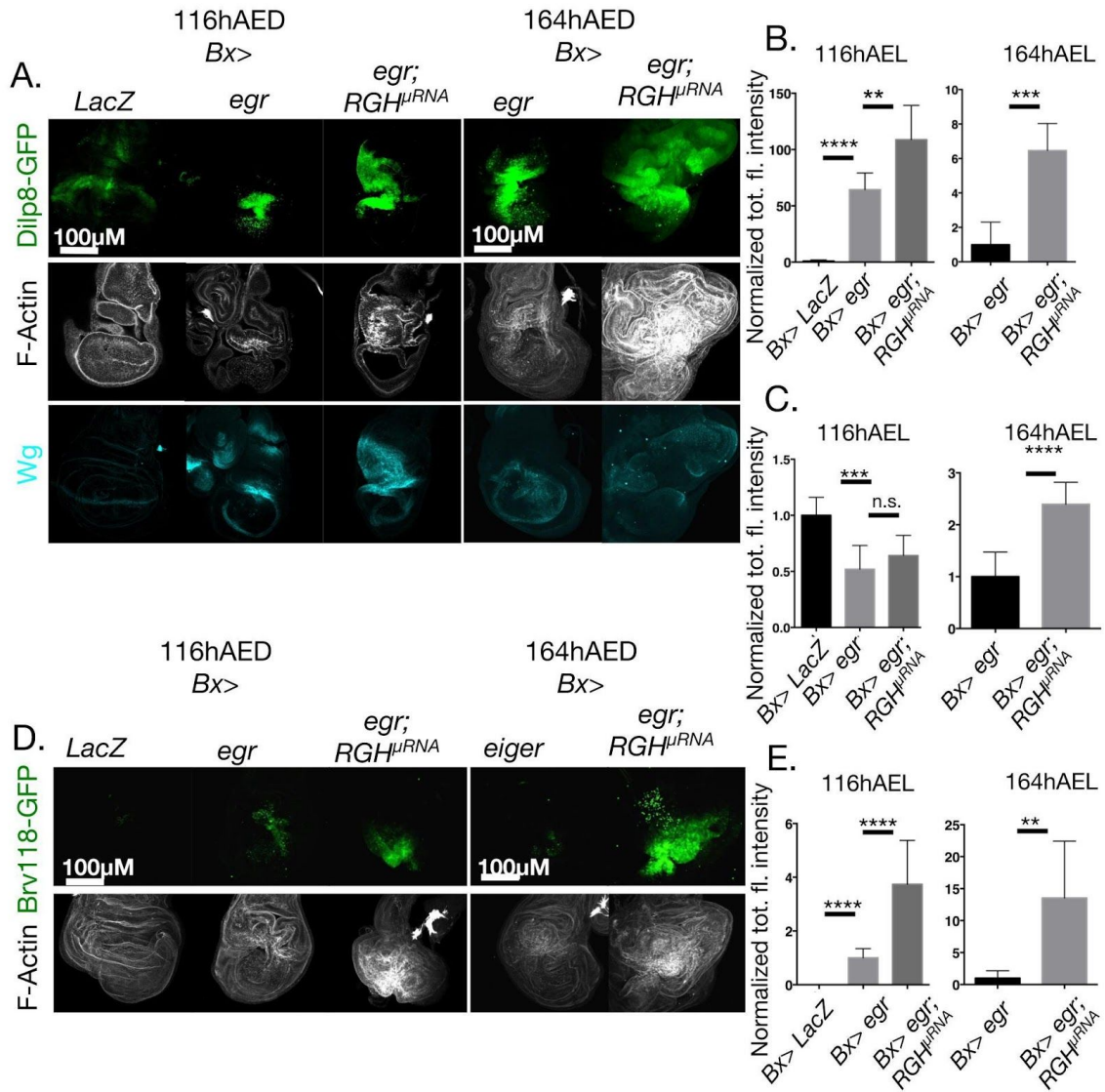
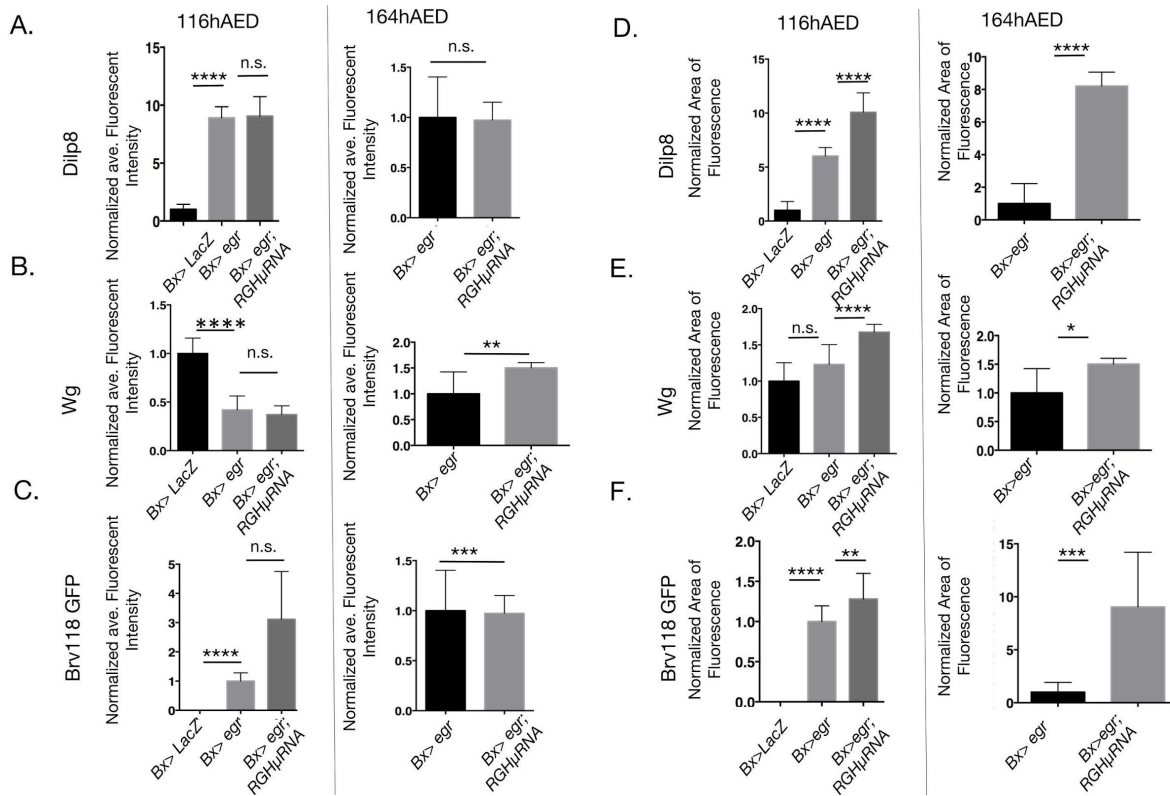


Figure 3. RGH depletion produces excessive regenerative activity

A.) At both 116hAED and 164hAED, *Bx> eiger and RGH^{uRNA}* co-expressing discs have higher levels of Dilp8-GFP expression (green), Wg (cyan) expression, and a distinct increase in intensity of F-Actin (white) compared to *Bx> eiger* discs or *Bx> LacZ* controls. For **A.** and **B.** (116hAED *Bx> LacZ* n= 3, *Bx> eiger* n=12, and *Bx> eiger;RGH^{uRNA}* n=3. At 164hAED *Bx> eiger* n=2 and *Bx> eiger;RGH^{uRNA}* n=12) **B.)** Quantification of total fluorescence, shows that total fluorescent intensity of Dilp8-GFP is higher in *eiger and RGH^{uRNA}* co-expressing discs compared to *eiger* expressing discs or controls at 116hAED and 164hAED. p-values are two tailed. At 116hAED *Bx> LacZ* compared to *Bx> eiger* p< 0.0001 and *Bx> eiger* compared to *Bx> eiger;RGH^{uRNA}* p=0.0022. At 164hAED *Bx> eiger* compared to *Bx> eiger;RGH^{uRNA}* p=0.0008 **C.)** Quantification of total fluorescence, shows that total fluorescent intensity of Wg is higher in *eiger and RGH^{uRNA}* discs compared to *eiger* expressing discs or controls at 164hAED, but not 116hAED. Discs used for quantification are different from ones pictured in **A.** (116hAED *Bx> LacZ* n= 4, *Bx> eiger* n=24, and *Bx> eiger;RGH^{uRNA}* n=9. At 164hAED *Bx> eiger* n=16 and *Bx eiger;RGH^{uRNA}* n=5). p-values are two tailed. At 116hAED *Bx> LacZ* compared to *Bx> eiger* p=0.0002, *Bx> eiger* compared to *Bx> eiger;RGHuRNA* p=n.s. At 164hAED *Bx> eiger* to *Bx> eiger;RGH^{uRNA}* p<0.0001. **D.)** At 116hAED and 164hAED *eiger and RGH^{uRNA}* co-expressing discs have high levels of Brv118-GFP expression (green), Wg (cyan) expression, and a distinct increase in intensity of F-Actin (white) compared to *Bx> eiger* discs or *Bx> LacZ* controls. **E.)** Quantification of total fluorescence, shows that total fluorescent intensity of Brv118-GFP is higher in *eiger and RGH^{uRNA}* discs compared to *Bx> eiger* discs or *Bx> LacZ* controls at 116hAED and 164hAED. (At 116hAED *Bx> LacZ* n= 4, *Bx> eiger* n=20, and *Bx> eiger;RGH^{uRNA}* n=10. At 164hAED *Bx> eiger* n=16 and *Bx eiger;RGH^{uRNA}* n=5). p-values are two tailed. At 116hAED *Bx> egr* compared to *Bx LacZ* p< 0.0001 and *Bx> egr* compared to *Bx> egr;RGH^{uRNA}* p< 0.0001. At 164hAED *Bx> eiger* to *Bx> eiger;RGH^{uRNA}* p=.0010 Total fluorescent intensity was calculated by multiplying average intensity per area of the region of interest by the area of the region of interest. All GFP and Wg micrograph images are collapsed stacks of tissue and all F-actin images are single slices of tissue taken at the same fluorescent intensities and edited in ImageJ/Fiji. Scale bar represents 100µm. All UAS genes are expressed with Bx Gal4. All significance was calculated with unpaired Student's t-test.

Supplemental Figure 1.



Supplemental Figure 1. Normalized Ave. Fluorescent Intensity/ROI of BRV118 GFP and Wg is higher in *eiger* and *RGH^{uRNA}* co-expressing discs. Normalized Area of Fluorescence is higher in *eiger* and *RGH^{uRNA}* co-expressing discs.

A.) Quantification of the average fluorescent intensity per region of interest of Dilp8-GFP expression shows that there is no significant difference in average Dilp8-GFP expression in *eiger* and *RGH^{uRNA}* co-expressing discs compared to *eiger* expressing discs at both 116hAED and 164hAED, although both express more Dilp8-GFP than controls at 116hAED. (116hAED *Bx> LacZ* n= 3, *Bx> eiger* n=12, *Bx> eiger;RGH^{uRNA}* n=3 164hAED *Bx> eiger* n=2, *Bx eiger;RGH^{uRNA}* n=12) p-values are two tailed. At 116hAED *Bx> LacZ* compared to *Bx> eiger* p<0.0001, *Bx> eiger* compared to *Bx eiger;RGH^{uRNA}* p= n.s. At 164hAED *Bx> eiger* to *Bx> eiger;RGH^{uRNA}* p= n.s. **B.)** Quantification of the average fluorescent intensity per region of interest of Wg expression shows that there is no significant difference in average Wg expression in *eiger* and *RGH^{uRNA}* co-expressing discs compared to *eiger* expressing discs at both 116hAED, although there is a significant difference at 164hAED. Additionally, both *Bx> eiger* and *Bx> eiger* and *RGH* microRNA co-expressing discs express less Wg on average than *Bx>LacZ* controls at 116hAED. (116hAED *Bx LacZ* n= 4, *Bx> eiger* n=24, *Bx> eiger;RGH^{uRNA}* n=9 164hAED *Bx> eiger* n=16, *Bx eiger;RGH^{uRNA}* n=5) p-values are two tailed. At 116hAED *Bx> LacZ* compared to *Bx> egr* p<0.0001, *Bx> eiger* compared to *Bx> eiger;RGH^{uRNA}* p= n.s. At 164hAED *Bx> eiger* to *Bx> eiger;RGH^{uRNA}* p= 0.0093. **C.)** Quantification of the average fluorescent intensity per region of interest of Brv118-GFP transcriptional activity shows that there is significantly more average Brv118-GFP activity in *Bx> eiger* and *RGH^{uRNA}* co-expressing discs compared to *Bx> eiger* expressing and control discs at only 164hAED. Additionally, *Bx> eiger* expressing discs, have higher average intensity per area of Brv118-GFP than *Bx> LacZ* controls. (116hAED *Bx> LacZ* n= 4, *Bx> eiger* n=20, *Bx> eiger;RGH^{uRNA}* n=10 164hAED *Bx> eiger* n=16, *Bx> eiger;RGH^{uRNA}* n=5) p-values are two tailed. At 116hAED *Bx> LacZ* compared to *Bx> eiger* p< 0.0001, *Bx> eiger* compared to *Bx> eiger;RGH^{uRNA}* p=0.3534 at 164hAED *Bx eiger* to *Bx> eiger;RGH^{uRNA}* p=.0003. **D-F.)** Quantification of the Region of interest (ROI) area (in this case the pouch of the presumptive wing blade), shows that at 116hAED and 164hAED *Bx> eiger* and *RGH^{uRNA}* co-expressing discs have a larger area of tissue expressing **D.)** Dilp8-GFP, **E.)** Wg, and **F.)** Brv118-GFP compared to *Bx> eiger* expressing discs or *Bx> LacZ* controls. *eiger* expression causes a greater area of Dilp8-GFP and BRV118-GFP expression at 116hAED than *Bx> LacZ* controls. **D.)** At 116hAED *Bx> LacZ* n= 3, *Bx> eiger* n=12, and *Bx> eiger;RGH^{uRNA}* n=3. At 164hAED *Bx> eiger* n=2 and *Bx> egr;RGH^{uRNA}* n=12) **E.)** At 116hAED *Bx> LacZ* n= 4, *Bx> eiger* n=24, and *Bx> eiger;RGH^{uRNA}* n=9. At 164hAED *Bx> eiger* n=16 and *Bx> eiger;RGH^{uRNA}* n=5) p-values are two tailed. All p-values for **D.** are p<0.0001. At 116hAED *Bx> LacZ* compared to *Bx> eiger* p=0.1246 and *Bx> eiger* compared to *Bx eiger;RGH^{uRNA}* p<0.0001. At 164hAED *Bx> eiger* compared to *Bx> egr;RGH^{uRNA}* p=0.0180. **F.)** At 116hAED *Bx> LacZ* n= 4, *Bx> eiger* n=20, and *Bx> eiger;RGH^{uRNA}* n=10. At 164hAED *Bx> eiger* n=16 and *Bx> egr;RGH^{uRNA}* n=5). p-values are two tailed. At 116hAED *Bx> LacZ* compared to *Bx> eiger* p< 0.0001 and *Bx> eiger* compared to *Bx> eiger;RGH^{uRNA}* p=0.0061. At 164hAED *Bx> eiger* compared to *Bx> egr;RGH^{uRNA}* p=.0005. All UAS genes are expressed with *Bx Gal4*. All significance was calculated with unpaired Student's t-test.

RGH depletion produces excessive regenerative signaling in damaged discs

Since blocking cell death leads to an extended developmental checkpoint delay we tested if the longer checkpoint delay reflected increased regenerative signaling in damaged tissues. To test the hypothesis that IAP inhibitor activity not only affects checkpoint delay, but also regenerative signaling, we examined tissues with markers for regenerative genes: *dilp8* and *wingless*. Dilp8 is a signaling peptide released in injured tissues that prevents Ecdysone synthesis⁹⁹. Ecdysone peaks drive larval molts and pupariation, so preventing Ecdysone synthesis permits time for discs to delay and repair injury. To measure Dilp8 we used a fusion protein where *GFP* is inserted into the first intron of *dilp8* and is also transcribed with *dilp8* transcription²¹¹. We found that discs co-expressing *eiger* and *RGH* microRNA in the imaginal wing disc have a higher total fluorescent intensity of Dilp8-GFP than controls in the wing pouch at 116hAED and after delaying for a significant amount of time at 164hAED compared to both control discs and discs only expressing *eiger*, indicating there is more Dilp8 expression (Fig. 3A and 3B). Total fluorescent intensity was calculated by multiplying the average intensity per area of the region of interest by the area of the region of interest (Fig. 3A and 3B).

We also examined the average fluorescent intensity of Dilp8-GFP in these discs to discern if there was more Dilp8 expression. We calculated the average fluorescent intensity of the Dilp8 expressing cells in each disc (averaged over the region of Dilp8 expression). We found that there was no difference in the intensity of Dilp8-GFP between discs co-expressing *eiger* and *RGH* microRNA and discs only expressing *eiger* or controls, indicating that cells are not expressing different amount of Dilp8 (Supplemental Fig. 1A). *eiger* and *RGH* microRNA co-expressing discs have an increased area of Dilp8-GFP expression in the wing pouch at 116hAED and at 164hAED (in larvae that have delayed pupariation) compared to both control discs and discs only expressing *eiger* (Supplemental Fig. 1B). This indicates that the region of Dilp8-GFP expression is larger in discs co-expressing

eiger and RGH microRNA, indicating that a larger number of cells are undergoing regenerative activity.

Another marker for regenerative activity in *Drosophila* is *wg*. By using a Wg antibody, we found that discs co-expressing *eiger* and RGH microRNA in the imaginal wing disc have a higher total fluorescent intensity of Wg than controls in the wing pouch at 116hAED and after delaying for a significant amount of time at 164hAED compared to both control discs and discs only expressing *eiger*, indicating there is more Wg protein (Figure 3A and 3C). We also examined the average fluorescent intensity of Wg in these discs to discern if there was more Wg protein. We calculated the average fluorescent intensity of the Wg expressing cells in each disc (averaged over the region of Wg expression). We found that at 116hAED but not at 164hAED, there was an increase in the intensity of Wg between discs co-expressing *eiger* and RGH microRNA and discs only expressing *eiger* or controls, indicating that cells have higher Wg protein levels (Supplemental Fig. 1A). Discs co-expressing *eiger* and RGH microRNA in the imaginal wing disc do not have an increased area of Wg expression in the wing pouch at 116hAED (Supplemental Fig. 1B) However, discs co-expressing *eiger* and RGH microRNA in the imaginal wing disc have an increased area of Wg expression in the wing pouch after delaying for a significant amount of time at 164hAED (Supplemental Fig. 1B) compared to both control discs and discs only expressing *eiger*. This indicates that the region of Wg expression is larger in discs co-expressing *eiger* and RGH microRNA at 164hAED, and that a larger number of cells are undergoing regenerative activity at this time. Together, these data show an increase in developmental checkpoint delay indicate that there may be higher regenerative activity than expected with *eiger* expression alone.

JNK activates the transcriptional enhancer of *wg* BRV118 (the Wingless Regenerative element) and this enhancer is necessary for proper regeneration following ablation¹³⁵. Thus, we specifically tested if the *wg* regenerative enhancer was upregulated in our *eiger* and RGH microRNA co-expressing wing discs, using a

fluorescent marker for BRV118, BRV118-GFP that measures the enhancer's transcriptional activity. By observing BRV118 fused upstream of a GFP enhancer (BRV118-GFP)¹³⁵, we found that discs co-expressing *eiger* and RGH microRNA in the imaginal wing disc have a higher total fluorescent intensity of BRV118-GFP fluorescence than controls in the wing pouch at 164hAED (but not 116hAED) compared to both control discs and discs only expressing *eiger*, indicating there is more Brv118-GFP enhancer activity (Figure 3D and 3E). We calculated the average fluorescent intensity of the GFP positive tissue in each disc (averaged over the region of *wg* expression). We found that there was an increase in the intensity of GFP between discs co-expressing *eiger* and RGH microRNA and discs only expressing *eiger* or controls, indicating that cells have greater BRV118 enhancer activity (Supplemental Fig. 1A). The BRV118 enhancer is expressed in a larger area in *eiger* and RGH microRNA co-expressing wing discs compared to controls discs or discs only expressing *eiger* at both 116hAED and 164hAED (Supplemental Fig. 1B). This indicates that BRV118 enhancer is active across a larger area, indicating that regenerative activity may be occurring in more cells. Together, these data indicate that there is greater *wg* regenerative activity in discs co-expressing *eiger* and RGH microRNA.

IAP inhibitors prevent neoplasia in regenerating tissues

When examining the regenerating tissues, we observe that expressing RGH microRNA alone does not cause a morphological tissue phenotype, however co-expression with *eiger* causes a dysmorphic disc (Fig. 2A and 3A). In normal tissues, the imaginal wing disc pouch is organized as a single sheet of pseudostratified epithelia. *eiger* expression results in a pinched pouch with a bolus of dead cells underneath. In discs co-expressing *eiger* and RGH microRNA we observe that folded epithelia in the pouch reminiscent of hyperplasia. To better observe the epithelia we stained the wing imaginal discs with Phalloidin which visualizes filamentous actin (F-actin). High F-Actin localization is associated with neoplastic tumors in *Drosophila*^{184,185}. Thus, we stained our tissues to visualize the

epithelia and to determine if F-actin levels were increased. We observe a dysmorphic overgrown shape, with an increase in F-actin in the cluster of disorganized cells in the center of the wing imaginal disc pouch in 116hAED and 164hAED tissues (Fig. 4) (high F-actin marked with red arrows). The cluster of disorganized cells is surrounded by hyperplastic-like folds of tissue that do not have the same striking increase in F-actin. The increase in F-actin indicated that there could be neoplasia. We observed the cross sections of epithelia to better characterize its structure. The locations of the cross sections are marked on the Z-slices with red lines (Fig. 4). In epithelial cross sections we observe a loss of epithelial monolayer and a central clusters of cells in the pouch (Fig. 3).

The loss of epithelial monolayer is a characteristic of neoplasia in *Drosophila*. To further investigate if the phenotype resembled neoplasia, we characterized if apicobasal polarity was disrupted. Neoplastic tissue in *Drosophila* lack normal apicobasal polarity, thus loss of apicobasal polarity markers such as apical marker (aPKC) is associated with neoplasia¹⁸⁶. By examining cross sections of imaginal wing disc epithelia we found that aPKC localization is decreased in areas with high cortical F-actin (Fig. 4, Loss of aPKC marked with cyan arrows). In *eiger* expressing discs, we see that the area where tissue pinches together to regenerate after the ablation loses aPKC localization at 116hAED. At 164hAED, when larvae with *eiger* ablated discs are about to pupariate we no longer observe this loss of aPKC. This indicates that the loss of aPKC in *eiger* ablated discs may be at the site of regenerating tissue. In wing imaginal discs co-expressing *eiger* and RGH microRNA we see loss of aPKC at sites where cells are piled in multi-layered clusters and contain high levels of F-actin at both 116hAED and 164hAED (Fig. 4). Larvae with *eiger* and RGH microRNA co-expressing discs are still undergoing regenerative checkpoint delay at 164 hAED as they pupariate closer to 188hAED, and thus these tissues may still be regenerating. Further images (Supplemental Fig. 2) show the *eiger* and RGH microRNA co-expressing discs. Together the characterization of *eiger* expressing and *eiger* and RGH microRNA co-expressing

Figure 4.

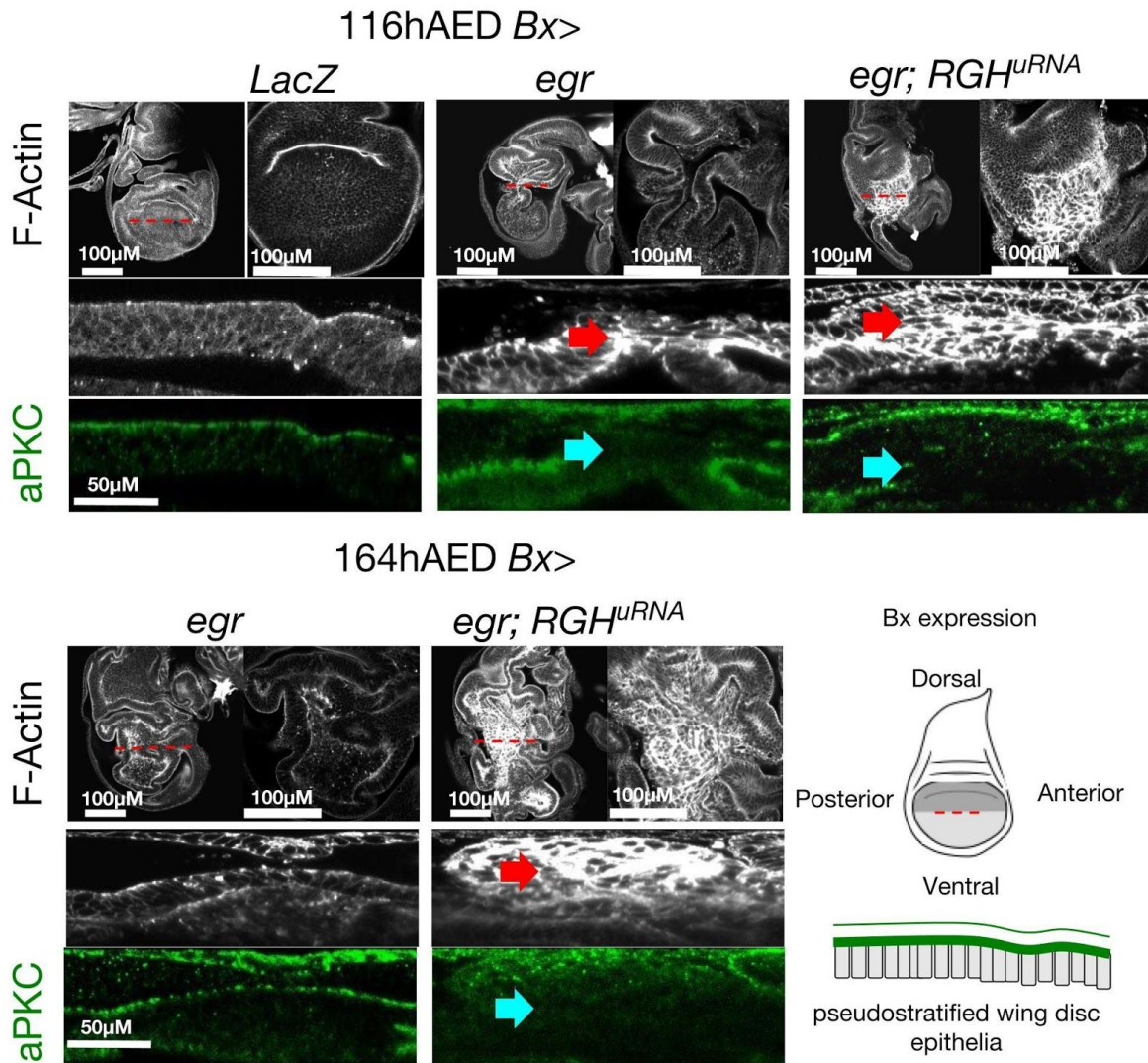
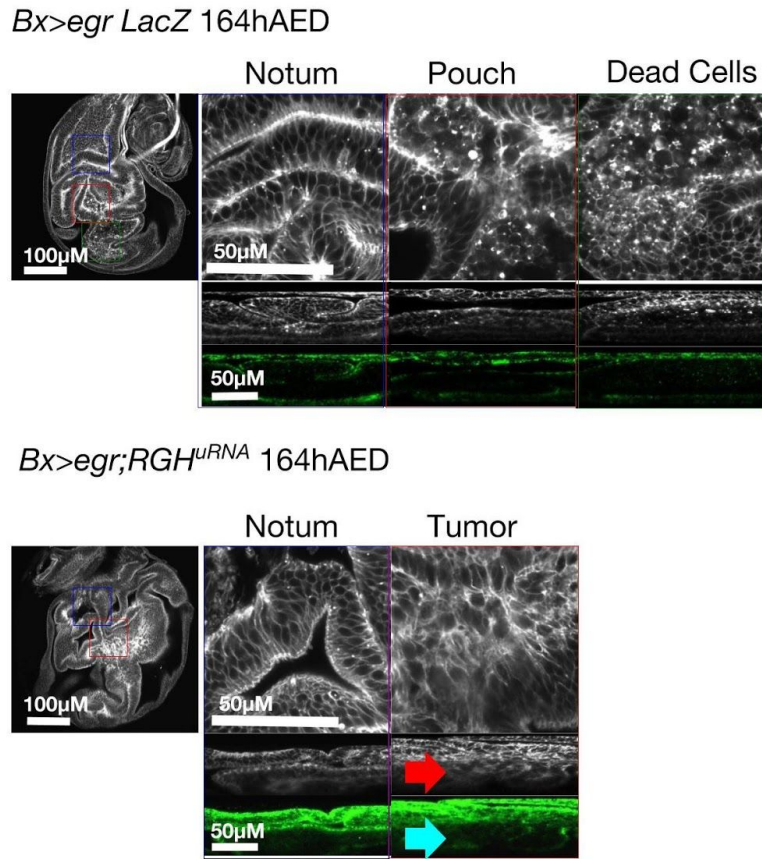


Figure 4. IAP inhibitors prevent neoplasia in eiger ablated regenerating tissues

Z-plane images and zoomed Z-plane images show the F-actin (white) is disorganized indicating neoplasia in the presumptive wing blade. Scale bar represents 100µm in Z-plane images. The orthogonal view shows the neoplastic areas with F-actin (white) and the aPKC stain (green). *Bx> eiger;RGH^{uRNA}* discs have mislocalization and partial reduction of aPKC (green, marked with cyan arrows) in areas of high F-Actin (white, marked with red arrows) at both 116hAED and 164hAED compared to *Bx> LacZ* controls and *Bx> eiger* discs. Scale bar represents 50µm in orthogonal images. aPKC is also mislocalized in the dead cells of *Bx>eiger* discs, but there is no neoplasia. The cartoon shows the area where *Bx* expresses and where we make our orthogonal slice. The cartoon orthogonal slice shows typical aPKC pattern in a control, where aPKC is apically localized in the pseudostratified epithelia. At 116hAED *Bx> LacZ* n= 7, *Bx> eiger* n=9, and *Bx> eiger;RGH^{uRNA}* n=12. At 164hAED high quality images: *Bx> eiger* n=2 and *Bx> eiger;RGH^{uRNA}* n=2). Micrograph images are shown as individual slices of tissue and taken at the same fluorescent intensities and edited in ImageJ/Fiji. All UAS genes are expressed with Bx Gal4.

Supplemental Figure 2.



Supplemental Figure 2. The pouch of *eiger* and *eiger* RGH discs is abnormal

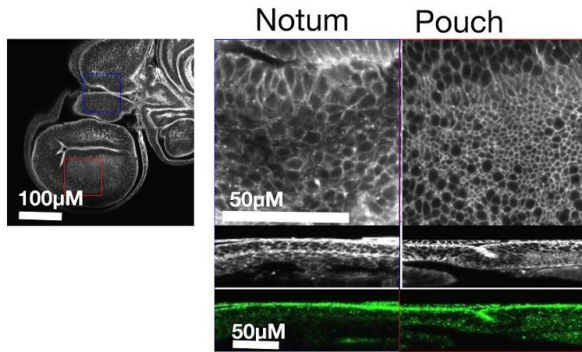
Z-plane images and zoomed Z-plane images show the F-actin (white) is disorganized indicating neoplasia in the presumptive wing blade. Scale bar represents 100µm in Z-plane images and 50µm in the zoomed in Z-plane images. Additional orthogonal slices show that *Bx> eiger;RGH^{uRNA}* disc tissues have an increase in cortical F-actin activity (white) (marked with red arrow) which is indicative of neoplasia, and these tissues have mislocalization and partial reduction of aPKC (marked with a cyan arrow). Tissues were dissected at 116 or 164 hAED. At 164hAED *Bx> eiger* n=2 and *Bx> eiger;RGH^{uRNA}* n=3). Micrograph images are shown as individual slices of tissue and taken at the same fluorescent intensities and edited in ImageJ/Fiji. All UAS genes are expressed with Bx Gal4.

discs indicated that regenerating areas of tissue had high F-actin localization and a decrease in aPKC localization. We also observed that the *eiger* and RGH microRNA co-expressing discs have a loss of epithelial monolayer, with a mass of cells in the center of the imaginal wing disc pouch. Together these characterizations indicate that the pouch region of *eiger* and RGH microRNA discs are most likely neoplastic.

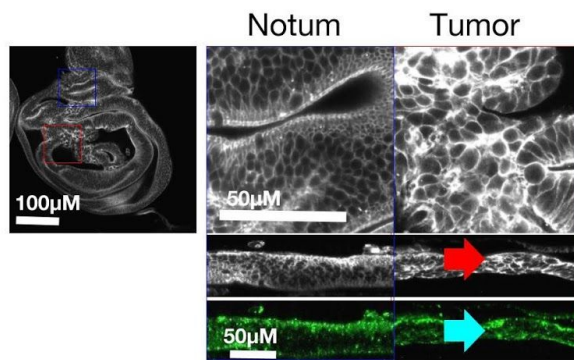
Next, we wanted to test whether the neoplastic phenotype is dependent on the persistent expression of *eiger*. To see if brief-temporally limited damage causes neoplasia in discs expressing RGH microRNA, we irradiated Bx>RGH microRNA expressing larvae and control larvae at 56hAED with 2500 Rads of X-irradiation. In the pouch area of the wing disc where RGH is depleted, we see small areas of epithelia disorganization, high cortical F-actin, and an increase in the area of *wingless* expression (Fig. 5A). These small neoplastic areas indicate that neoplasia is possible in an RGH depleted background with other damage models aside from *eiger* ablation. The number and size of the neoplasia varies from disc to disc, with neoplastic areas defined as areas with an increase in F-actin, a larger area of Wg expression, and tissue disorganization. The neoplastic areas are more common in the pouch of tissues than the notum (Fig. 5B), indicating the neoplasias are forming specifically in the area of RGH depletion. On average, each RGH depleted disc has two tumors that cause an increase in the expression area of *wingless* (Fig. 5B, significance calculated with Student's t-test). Additional images characterizing the neoplastic tissue by comparing neoplastic to non-neoplastic regions are shown in Supplemental Figure 3.

Supplemental Figure 3.

Bx> LacZ 140hAED
(Irradiated with 2.5k R at 56hAED)



Bx> RGH^{uRNA} 140hAED
(Irradiated with 2.5k R at 56hAED)



Supplemental Figure 3. The pouch of X-irradiated RGH discs is abnormal, unlike control X-irradiated discs Z-plane images and zoomed Z-plane images show the F-actin (white) is disorganized indicating neoplasia in the presumptive wing blade. Scale bar represents 100µm in Z-plane images and 50µm in the zoomed in Z-plane images. Additional orthogonal slices show that *Bx> RGH^{uRNA}* disc tissues have an increase in cortical F-actin activity (white) (marked with red arrow) which is indicative of neoplasia, and these tissues have mislocalization and partial reduction of aPKC (marked with a cyan arrow). Tissues were dissected at 116 or 164 hAED. At 140hAED *Bx> eiger* n=2 and *Bx> egr;RGH^{uRNA}* n=2). Micrograph images are shown as individual slices of tissue and taken at the same fluorescent intensities and edited in ImageJ/Fiji. All UAS genes are expressed with Bx Gal4.

JNK activity is necessary and sufficient for neoplasia in RGH depleted background

We observed an increase in *wg* transcriptional activity in *eiger* and RGH microRNA co-expressing discs. Regenerative *wg* transcriptional activity is dependent on JNK activity¹³⁵, but it is unknown if the neoplastic phenotype is dependent on JNK pathway activity. AP-1 is a heterodimer of the JNK's phosphorylation target cJun and the protein cFos. Ap-1 acts as a transcription factor. Ap-1 transcriptional activity can be observed with fluorescence of a transcriptional GFP reporter. Ap-1 binding sites were inserted upstream of a GFP-promoter, so GFP is activated with Ap-1 transcriptional activity²¹⁰. We found that expression of *eiger* increases AP-1 GFP transcriptional activity and the Normalized Total Fluorescence of Ap-1 GFP and that co-expression of *eiger* and RGH microRNA increases the Normalized Total Fluorescence of Ap-1 GFP further compared to *LacZ* expression (Fig. 6A and 6B). We also find that there is a larger area of AP-1 GFP transcriptional activity (Supplemental. Fig. 4). This increase in AP-1 GFP area indicates that there are more cells expressing AP-1 in these tissues. We also note that there is a higher average Fluorescent Intensity/Area of AP-1 GFP in the wing pouch, indicating that there is more AP-1 transcriptional activity in these tissues (Supplemental. Fig. 4). Thus, to specifically test if the JNK activity is sufficient to produce the neoplastic phenotype in *eiger* and RGH microRNA co-expressing tissue, we also expressed an active allele of the JNK kinase hemipterous (carries the amino acid replacements S346D, T350D and S352D)⁸⁵ with RGH microRNA in the wing disc. In this experiment, we see an increase in F-actin in a neoplastic center of cells in the wing pouch and an increase in wingless signaling similar to *eiger* and RGH microRNA co-expression in the wing disc (Fig. 6C). We also see that an increase in folded hyperplastic-like tissue surrounding the neoplastic cells, although this hyperplastic-like tissue is even more noticeable with activated

Figure 6.

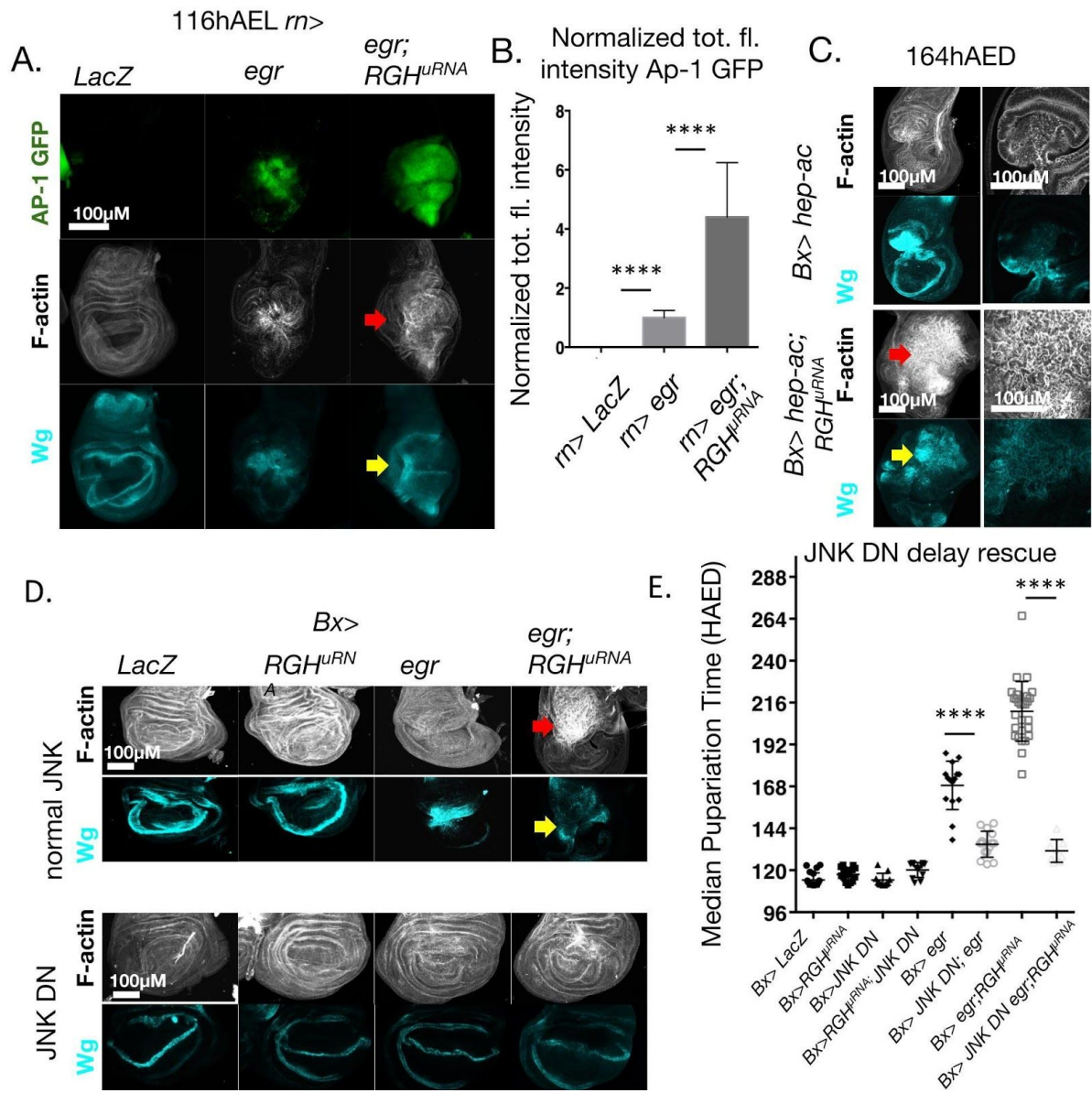
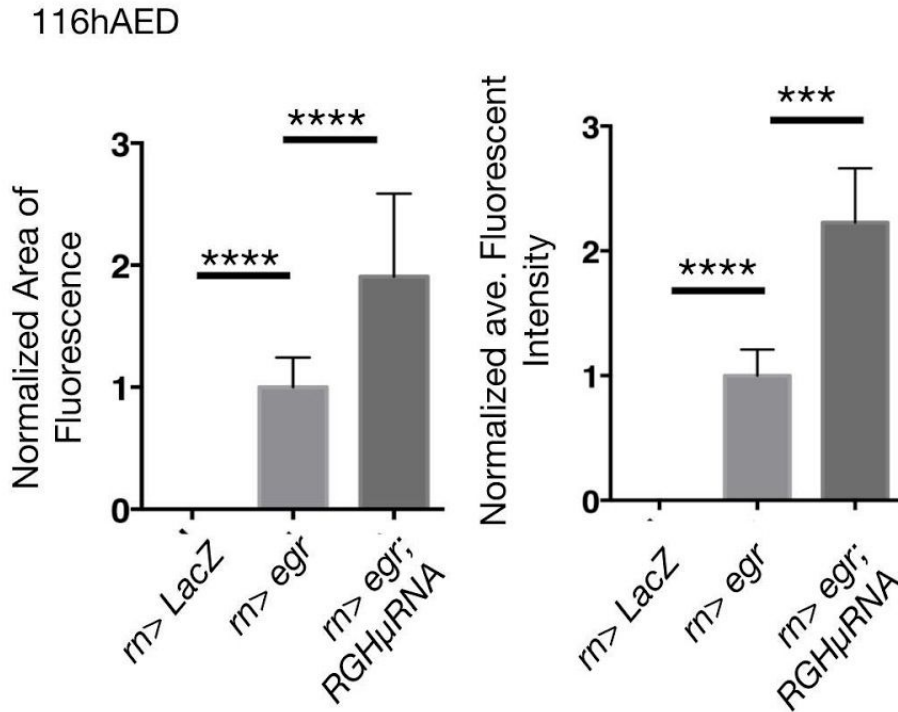


Figure 6. JNK activity is necessary and sufficient for neoplasia in RGH depleted background

A.) AP-1 GFP fluorescence (green) is increased with *Bx> eiger* expression compared to *Bx> LacZ* control discs at 164hAED in the wing imaginal disc. AP-1 GFP fluorescence is further increased in *eiger* and *RGH^{uRNA}* tissue at 164hAED. High F-actin (white) and dysmorphic neoplastic regions are marked with red arrows and increased Wg area is marked with yellow arrows. (For 116hAED *rn> LacZ* n= 10, *rn> eiger* n=10, *rn> eiger;RGH^{uRNA}* n=11). **B.)** The normalized total fluorescent intensity of AP-1 GFP transcriptional activity is larger in *eiger;RGH^{uRNA}* tissue at 164hAED than in tissue expressing *eiger*. (same n as **A.**) p values are two-tailed. All p values are p<0.0001 **C.)** Activated *hemipterous (hep-ac)* and *RGH^{uRNA}* co-expression is sufficient to cause neoplasia (164hAED). Z-plane images and zoomed Z-plane images show the F-actin (white) is disorganized indicating neoplasia in the presumptive wing blade and that Wg (cyan) area is increased. High F-actin and neoplasia are marked with red arrows and excessive Wg activity is marked with yellow arrows. (*Bx> hep-ac* n=3, *Bx>hep-ac;RGH^{uRNA}* n= 3. The experiment was repeated with an additional 5 discs of each genotype imaged.) **D.)** Inhibition of JNK activity with JNK dominant negative (DN) prevents neoplastic phenotype in *Bx> eiger* and *RGH^{uRNA}* co-expressing tissue and *Bx> eiger* tissues. Control and *RGH^{uRNA}* discs are unaffected by JNK DN. F-actin (white) shows tissue shape and Wg (cyan) shows regenerative activity. High F-actin and neoplasia are marked with red arrows and Excessive wg activity is marked with yellow arrows. (*Bx> LacZ* n= 3, *Bx> JNK DN* n=3, *Bx> RGH^{uRNA}* n=3, *Bx JNK DN;RGH^{uRNA}* n=3, *Bx>eiger* n=5, *Bx> JNK DN;eiger* n=5, *Bx> eiger;RGH^{uRNA}* n=5, and *Bx> JNK DN eiger;RGH^{uRNA}* n=3) **E.)** JNK DN expression rescues developmental checkpoint delay in *eiger* ablated RGH depleted tissues. p values are two tailed. For all p values p<0.0001. (n=populations are 10-20 individuals. *Bx> LacZ* n= 20, *Bx> JNK DN* n=15, *Bx> RGHuRNA* n=11, *Bx JNK DN;RGHuRNA* n=12, *Bx> eiger* n=15, *Bx> JNK DN;eiger* n=15, *Bx> eiger;RGHu* n=28, *Bx> JNK DN;eiger;RGHuRNA* n=8) All micrograph images are shown as individual slices (actin high magnification) and collapsed stacks (actin, wg, and AP-1 GFP) and taken at the same fluorescent intensities and edited in ImageJ/Fiji. All significance was calculated with an unpaired Student's t-test. Micrograph images are shown as collapsed stacks of tissue for and taken at the same fluorescent intensities and edited in ImageJ/Fiji. All UAS genes are expressed with Bx Gal4, except for in panels **A.** and **B.** where rn Gal4 was used. All Scale bars represents 100µm.

Supplemental Figure 5.



Supplemental Figure 4. *eiger* and *RGH* microRNA co-expressing discs have greater area of AP-1 GFP activity and a higher average AP-1 GFP activity The Area of the Region of Interest (ROI) in *Bx> eiger* and *RGH* microRNA co-expressing discs is higher than in *Bx> eiger* expressing discs or *Bx> LacZ* control discs at 164hAED. Additionally, the average intensity per area of region of interest of AP-1 GFP expression is higher in *eiger* and *RGH* microRNA co-expressing discs than in *eiger* expressing discs or control discs at 164hAED. (At 116hAED *m> LacZ* n= 10, *m> eiger* n=10, and *m> eiger;RGH^{uRNA}* n=11). p values are two-tailed. For area of AP-1 GFP all p values are p< 0.0001. For the average fluorescent intensity *m>LacZ* to *m> eiger* p<0.0001, *m> eiger* to *m>egr RGHuRNA* p<0.0008. All UAS genes are expressed with *m Gal4*. All significance was calculated with an unpaired Student's t-test.

hemipterous expression (Fig. 6C). Perhaps, because *hemipterous* is more downstream of *eiger* and directly phosphorylates JNK, the neoplastic phenotype and surrounding hyperplastic-like phenotype are enhanced. Thus, JNK pathway activity is sufficient to produce neoplasia if RGH are depleted. Next, we tested if JNK pathway activity is necessary for the neoplastic phenotype and *eiger* ablation. We used a JNK dominant negative allele to remove JNK activity in wing discs expressing *eiger* alone and found that the discs no longer appeared ablated or have upregulated *wg*, indicating that the *eiger* ablation and subsequent regeneration is dependent on JNK activity (Fig. 6D). We also see that the JNK dominant negative allele (T181A nonactivatable mutant)⁸⁵ prevent neoplasia and *wg* activity in wing discs co-expressing *eiger* and RGH microRNA (Fig. 6D). Since there is no ablation damage, this indicates that the neoplasia phenotype is dependent on the *eiger* ablation damage caused through JNK signaling. Thus, JNK activity is necessary for the ablation damage that causes neoplasia in the RGH depleted tissue. We also observed that without ablation damage there was not regenerative checkpoint delay (Fig. 6E). Thus, JNK activity is necessary for the ablation damage that causes neoplasia in the RGH depleted tissue.

Regeneration through Wingless is necessary for the neoplastic phenotype.

While the neoplasia caused by RGH depletion is dependent on ablation caused by the *eiger*/JNK pathway activity, we needed to test if the neoplasia is also dependent on the subsequent regenerative activity. Earlier, we observed an increase in the activity of the *wg* regenerative element BRV118 in *eiger* and RGH microRNA co-expressing neoplastic wing discs, indicating an increase in JNK-driven *wingless* activity. We also observe that these *eiger* and RGH microRNA co-expressing tissues have an increase in regenerative checkpoint delay, indicating that there is high regenerative activity in these tissues. To test whether regeneration is necessary for the neoplasia phenotype we tested whether depletion of Wg using a *wingless*

Figure 7.

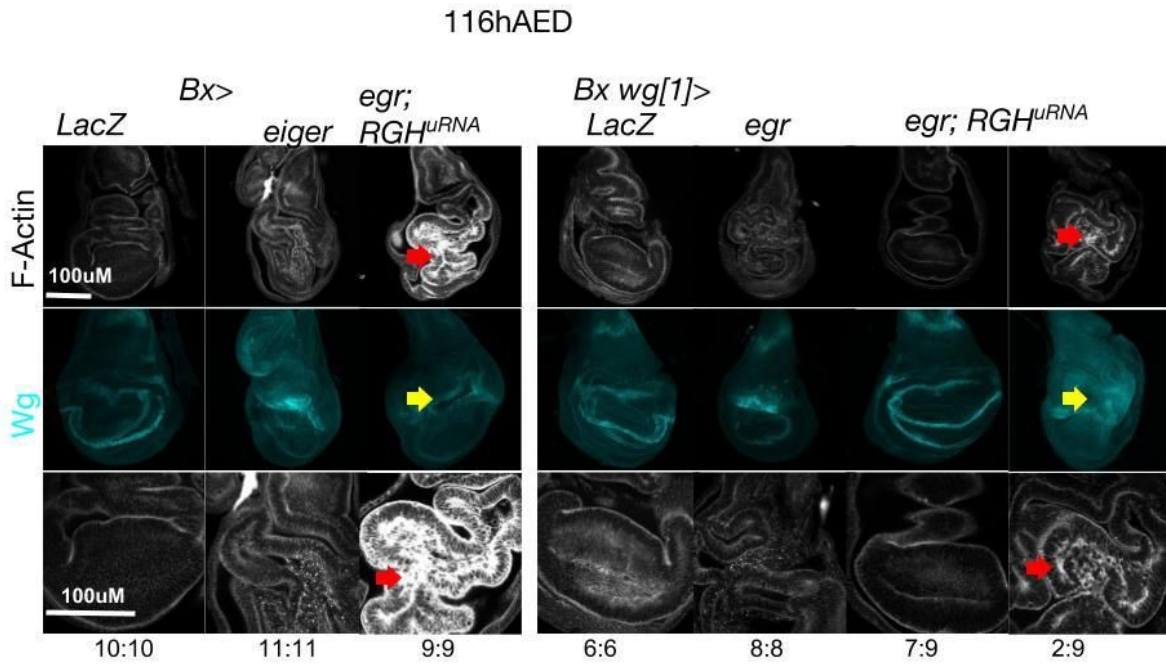


Figure 7. Regeneration through Wingless is necessary for the neoplastic phenotype.

A.) Z-plane images and zoomed Z-plane images show the F-actin (white) and Wg (cyan). *Bx> wg[1]/+* mutation co-expression leads to a dominant rescue of the neoplastic F-actin (white) phenotype (marked with red arrows) and increase in the are of Wg expression (marked with yellow arrows) in *Bx> wg[1]/+ eiger* and *RGH* microRNA co-expressing discs in 7:9 discs. In the remaining 2 discs, the tissue is still dysmorphic, but there is a decrease in F-actin(white) activity compared to *Bx> eiger* and *RGH* microRNA co-expressing discs. *Bx> LacZ* n=10, *Bx> eiger* n=11, *Bx> eiger;RGH^{uRNA}* n=9, *Bx> wg[1]/+;LacZ* n=6,, *Bx> wg[1]/+;eiger* n=8, *Bx> eiger wg[1] eiger;RGH^{uRNA}* n=9). Micrograph images are shown as individual slices (actin) and collapsed stacks (wg) and taken at the same fluorescent intensities and edited in ImageJ/Fiji. All UAS genes are expressed with Bx Gal4. All Scale bars represents 100μm.

mutant *wg[1]*, which removes the *wg* enhancer BRV118, prevents the neoplasia (marked with red arrows) in *eiger*-ablated RGH microRNA co-expressing wing discs (Fig. 6A). We found that the *wg[1]* mutation does not prevent ablation when co-expressed with *eiger* at 116hAED (Fig. 7A). However, the *wg[1]* mutation prevents the neoplasia characterized by high F-actin, epithelial disorganization, and an increase of *wg* activity (increase in *wg* activity marked with yellow arrows) in a majority (7:9) *eiger* and RGH depleted tissues at 116hAED (Fig. 7A). In the remaining dysmorphic tissues there was a decrease in F-actin stain. This result indicates that *wg* regenerative element BRV118 activity is likely necessary for the neoplastic phenotype observed with *eiger* and RGH microRNA co-expression.

Inhibition of IAP inhibitors via other caspase pathway members produces neoplasia

To determine if any individual IAP inhibitor is necessary to prevent neoplasia in regenerating tissues, we inhibited each IAP inhibitor individually in an *eiger* damage background using microRNA. We found that co-expression of *eiger* with *rpr* microRNA, but not *hid* or *grim* microRNA, lead to a neoplastic phenotype similar to one seen with RGH depletion and *eiger* co-expression with high F-actin (marked with red arrows), loss of an epithelial monolayer, high *wg* activity (marked with yellow arrows), and loss of aPKC (marked with cyan arrows) (Fig. 8). The result indicates that Rpr is the IAP inhibitor necessary for the neoplastic phenotype, but that other IAP inhibitors may play a role in the phenotype. It also remains to be seen if other RNAi lines or methods of depleting *hid* or *grim* could produce a similar neoplastic phenotype. Discs co-expressing *eiger* and *rpr* microRNA do not have aPKC signaling in the cells that are clustered in the neoplasia (marked with a cyan arrow), indicating that those cells have lost apicobasal polarity. Finally, in *eiger* and *rpr* microRNA co-expressing discs there is increase in the area of *wg* signaling (marked with a yellow arrow), indicating an increase in regenerative activity

compared to *eiger* expressing wing discs. Together, these results suggest that Rpr expression is responsible for preventing neoplasia.

Figure 8.

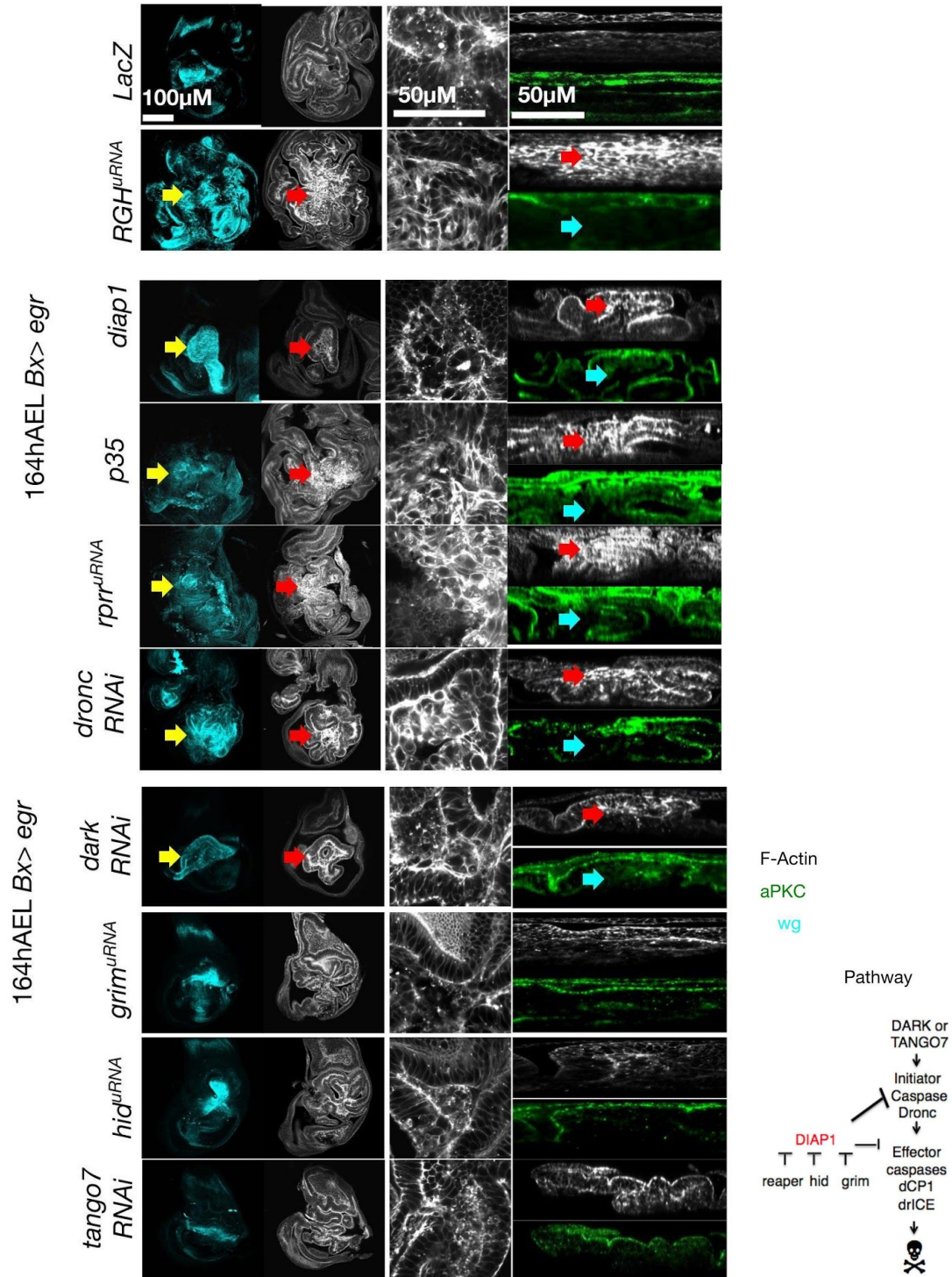


Figure 8. Inhibition of IAP inhibitors via other caspase pathway members produces neoplasia.

Z-plane images and zoomed Z-plane images show if F-actin (white) is disorganized (indicating neoplasia) in the presumptive wing blade. Scale bar represents 100µm in Z-plane images and 50µm in the zoomed in Z-plane images. Additional orthogonal slices show if tissues have an increase in cortical F-actin activity (white) (marked with red arrow) which is indicative of neoplasia, and if these tissues have mislocalization and partial reduction of aPKC (marked with a cyan arrow). In the orthogonal slices scale bar represents 50µm. Depletion of *rpr* with *Bx> eiger* expression leads to a similar neoplastic phenotype with high F-actin(white) (red arrows), loss of aPKC (cyan arrows), and high *wg* activity (yellow arrows) indicating the *rpr* depletion and *eiger* co-expression is sufficient to cause neoplasia (164hAED). Overexpression of p35, DIAP1, or Dronc RNAi leads to a similar neoplastic phenotype in *Bx> eiger* expressing tissue. Expression of *tango7* RNAi in *Bx> eiger* expressing tissue does not lead to neoplasia. Pathway model shows the cell death pathway. (*Bx> eiger* n= 3, *Bx> eiger;RGH^{uRNA}* n=3, *Bx> eiger;diap1* n= 5, *Bx> eiger;p35* n=5, *Bx> eiger;reaper^{uRNA}* n=5, *Bx> eiger;dronc RNAi* n= 5, *Bx> eiger;dark RNAi* n=5, *Bx> eiger;hid^{uRNA}* n=3, *Bx> eiger;grim^{uRNA}* n=3, and *Bx> eiger;tango7 RNAi* n=5) Micrograph images are shown as individual slices (actin and aPKC) and collapsed stacks (Wg) and taken at the same fluorescent intensities and edited in ImageJ/Fiji. All UAS genes are expressed with Bx Gal4.

We then tested if depletion of other pro-cell death caspase members also leads to the neoplastic phenotype with after *eiger* expression. First, we expressed *eiger* and depleted caspase expression by either depleting initiator caspase Dronc with RNAi, by expressing Diap1 which targets caspases for degradation, or by expressing p35 which binds to effector caspases. We found that blocking initiator or effector caspases led to a neoplastic phenotype (marked with red arrows) characterized by a dysmorphic wing disc with a neoplastic cluster of disorganized cells, increase in *wg* activity (yellow arrows), and loss of aPKC (cyan arrows) (Fig. 8). These cells have high F-actin and a loss of aPKC signaling. These caspase-depleted tissues also had an increase in Wg signaling. Together, this data suggests that *eiger* expression and depletion of initiator or effector caspases is sufficient to cause a neoplastic phenotype and that apoptosis prevents neoplasia after *eiger* damage. We also tested if brief, temporally-limited damage would cause neoplasia in caspase depleted discs. Expression of p35, which blocks effector caspases, led to neoplastic areas (marked with red arrows) forming and an upregulation of *wg* (marked with yellow arrows) (Fig. 5A). Thus, we irradiated tissues overexpressing p35 at 60hAED with 2500 Rads of X-irradiation and observed that the neoplastic phenotype occurs at 140hAED (Fig. 5). These irradiated tissues where effector caspases were depleted had an average of two neoplastic clusters in the pouch of their imaginal wing disc. Thus, initiator and effector caspases prevent neoplasia in *eiger* ablated or X-irradiated wing discs.

The initiator caspase Dronc is activated by adaptors Dark or Tango7 depending on cellular context. While depletion of initiator caspase activity in an *eiger* expressing tissue causes neoplasia, we decided to test if depletion of these adaptors would do the same. Dark is the canonical activator of Dronc in most described cellular contexts, while Tango7 was recently described to act as an activator in the context of the cortex to break down F-actin¹¹¹. However, expression

of Tango7 RNAi in an *eiger-ablation* background does not lead to an obvious neoplasia phenotype, indicating that the increase of Tango7 expression that leads to an increase in cortical F-actin is not the cause of neoplasia in these discs (Fig. 8). The caveat to this experiment is that the Tango7 RNAi may not effectively prevent Tango7 expression. Dark RNAi overexpression, however, leads to a neoplasia phenotype, characterized by neoplastic regions of clumping cells that do not form a monolayer, lose aPKC signaling and have high F-actin. These Dark depleted tissues also have an increase in the area of *wg* expression indicating regenerative activity. These results indicate that the caspase activity that prevents the neoplastic phenotype in *eiger* expressing tissues likely relies on Dark activating Dronc.

Discussion

To identify genes that limit the size and duration of the regenerative response in tissues we measured the developmental checkpoint delay to assess the regenerative activity produced by damage. We found that *eiger* ablation causes damage that promotes a developmental checkpoint delay. Previous studies indicate that regenerative activity in the wing is critically dependent on the transcriptional activation of *wingless* by Jun N-terminal Kinase (JNK)¹³⁵. If we limit the transcriptional activation of *wingless* in this model we observe a reduction in checkpoint delay. In contrast, mutation of the JNK-phosphatase *puckered* (*puc[e69]*) produces a substantial extension of checkpoint delay. Therefore, checkpoint delays reflect JNK-driven *wingless* transcriptional activity during regeneration and supports a pathway where upregulation of JNK activity after tissue damage causes *wg* dependent regenerative activity.

We then searched for other genes that alter developmental checkpoint delay. We found that depletion of IAP inhibitors *rpr*, *grim*, and *hid* in *eiger* expressing tissues produces a substantial extension of checkpoint delay. We found that *eiger* and RGH microRNA co-expression leads to an increased area of tissue that expresses Dilp8, which promotes regenerative developmental checkpoint delay. We

then found that the area of *wg* enhancer Brv118 activity is increased in *eiger* and RGH microRNA co-expressing tissues. We found that there was an increase in the average fluorescent intensity of Wg expression or Brv118-GFP activity, indicating increased Wg expression or Brv118 activity in these discs co-expressing *eiger* and RGH microRNA. As the *wg* Brv118 enhancer region is necessary for regeneration, this indicates an increase in regenerative activity in these discs, supporting a model where *eiger* ablation increases regenerative activity.

We next observed the phenotype of imaginal wing discs co-expressing *eiger* and RGH microRNA. We observed that these discs produce regions of tissue in the wing pouch that lose epithelial structure, lose aPKC signaling, and express high levels of cortical F-actin. All these phenotypes are consistent with neoplasia^{185,186}. We found that temporally-limited X-irradiation damage also caused this neoplastic phenotype in RGH depleted tissues, indicating that more temporal damage also can cause neoplasia if there is no apoptotic activity. We did not test if the X-irradiation induced neoplasia in RGH depleted discs was due to JNK activity. We also tested if depletion of other caspase pathway members was sufficient to cause neoplasia following damage. We found that inhibition of initiator caspase or effector caspase activity with Dronc RNAi, Dark RNAi, expression of Diap1, or expression of p35 was sufficient to recapitulate the neoplastic phenotype. We also found that depletion of IAP inhibitor Rpr alone was sufficient to induce neoplasia in *eiger* expressing tissues, but that Hid or Grim depletion with microRNA was not sufficient to induce neoplasia in *eiger* expressing tissues. Thus, without caspase activity after *eiger* or X-irradiation damage neoplasia can result.

We observed an increase in *wg* transcriptional activity in *eiger* and RGH microRNA co-expressing discs. Regenerative *wg* transcriptional activity is dependent on JNK activity¹³⁵, but it was unknown if the neoplastic phenotype is dependent on JNK pathway activity. We found that JNK pathway activity with an activated allele of *hemipterous* in RGH depleted tissues was sufficient to cause a neoplastic phenotype, indicating that the JNK activity is involved in the neoplasia.

We also found that inhibiting JNK prevents *eiger* ablation. Without JNK-dependent *eiger* ablation there is no neoplastic phenotype in RGH depleted tissues or regenerative checkpoint delay. Thus, JNK activity is necessary for the ablation damage that causes neoplasia in the RGH depleted tissue.

Whereas we observed an increase in regenerative activity and regenerative checkpoint delay, we also tested if *wg* enhancer Brv118 was necessary for the neoplastic phenotype. We found that regenerative element BRV1118 activity is likely necessary for the neoplastic phenotype observed with *eiger* and RGH microRNA co-expression.

Together, these data help us form our model (Fig. 9). Our data supports a model in which after damage from *eiger* ablation, JNK signaling promotes *wg* enhancer BRV118 activity. The ablation and delay are dependent on not just *eiger* but also JNK activity. Previous work has shown that transcriptional activation of wingless by JNK is necessary for regenerative activity¹³⁵. We have found that a decrease in caspase pathway activity in this damaged and regenerating tissue leads to neoplasia and that *wg* activity is necessary for this neoplastic phenotype. We hypothesize that excessive JNK/*wg* regeneration, if not properly regulated, can cause neoplasia. We do not directly show how caspase activity limits regenerative activity. We theorize that Rpr, initiator caspase Dronc, Dark, and effector caspases prevent excessive regeneration by killing cells that express high levels of JNK signaling (Fig. 8B) or killing neoplastic cells (Fig. 8A). We also do not show that *eiger*/JNK activity directly increases *rpr* expression or caspase pathway activity in this model, although JNK activity is known to increase transcription of *rpr* and *hid* to cause cell death in the eye disc⁸⁶. We also suspect that neoplastic cell activity further increases *JNK* expression, as the JNK pathway is activated as a stress response⁸³. Cell death after JNK response to *eiger* ablation damage or X-irradiation prevents neoplasia.

Figure 9.

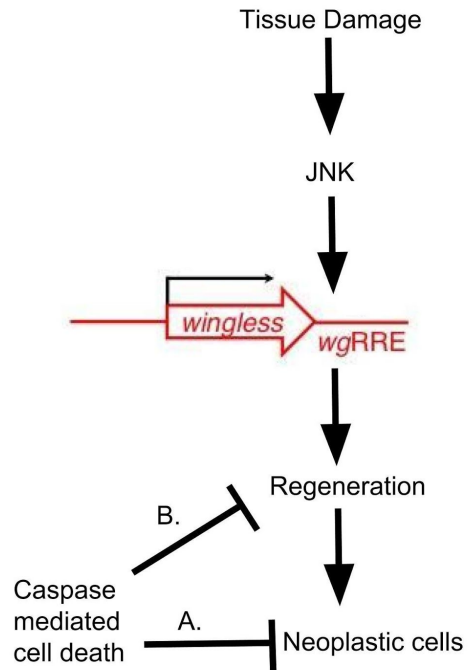


Figure 9. Model: Cell death prevents neoplasia caused by JNK and Wg regenerative activity. Following injury, JNK activity increases Wg transcription via the wgRRE and permits regenerative activity. With high levels of damage and JNK signaling, apoptotic gene transcription increases, leading to an increase in death. This increase in cell death prevents neoplasia caused by excessive regeneration either by causing the death of neoplastic cells (A.) or by limiting regeneration by killing cells expressing high levels of JNK (B.)

This work shows a role for apoptotic pathway genes to act as tumor suppressors after *eiger* or X-irradiation damage in *Drosophila* initiates regenerative activity. Resistance to apoptosis is a hallmark of cancer^{139,140}. The loss of apoptotic gene expression alone is insufficient to cause tumor formation but the loss of programmed cell death paired with oncogene expression/dysregulation of tumor suppressors causes cancer¹⁴⁴⁻¹⁴⁸. Here, we would argue that regeneration has tumorigenic potential and that this tumorigenic potential of regeneration is limited by the activity of IAP inhibitors.

Activating regeneration in non-regenerating tissue has been a focus of research in regenerative medicine^{44,45,187,188}. However, it is unclear whether tissues that have lost the ability to regenerate will retain the ability to effectively limit regenerative therapies. Understanding the pathways that limit regenerative activity may help to develop safer regenerative therapies going forward.

Materials and Methods

Stocks- Sp/CyO; UAS-eiger(III) / (TM6C) and UAS Rpr(III) was provided by Ishwar Hariharan⁷². RGH^{miRNA}, Rpr^{miRNA}, Hid^{miRNA}, and Grim^{miRNA} were provided by Sarah Siegrist^{189,190}. All other stocks were obtained from the Bloomington *Drosophila* Stock Center or the Vienna *Drosophila* RNAi Center. Identifying stock numbers are referenced in the Supplementary text.

***Drosophila* Culture and media.** Unless otherwise stated, larvae were reared at 25°C in a 12-hour light cycle on standard cornmeal-yeast media in vials (Archon Scientific B101) or from melted and poured cornmeal-yeast media (Archon Scientific B110 - 500 cc) supplemented with live baker's yeast. Larvae were developmentally synchronized by collection after a 4-hour egg-laying period on grape agar plate. Larvae were transferred to vials or plates containing standard cornmeal-yeast media 24 hours after egg lay (AED) at first instar and placed in an incubator at 25°C in a 12-hour light cycle. Larvae were collected at 116hAED as wandering third instars.

X-irradiation damage Irradiation was performed as previously described (Halme, Cheng, and Hariharan 2010), with staged larvae on media plates being floated up with a drop of DI water to be exposed to X-irradiation at 80hAED. Larvae were exposed to 0, 1, 1.5, 2, 2.5, 3, or 4K Rads using the Hewlett-Packard, Model: 48305N operating at 130kV and at 3.0mA. Larvae were then raised at 25°C in a 12-hour light/dark cycle.

Measurement of delay to pupariation

Time to Pupariation, the time at which half the population had pupated was measured by recording the number of newly pupariated individuals at 12-hour intervals. Graphs, Student t-tests, and Anovas were done using Prism Software.

Wing Disc fixation

Larval fat body tissue was dissected at 116 HAED (wandering third instars) or at later stages (140 HAED and 164hAED) as noted in Phosphate Buffered Saline (PBS), fixed in 4% paraformaldehyde in PBS before being fixed in 4% paraformaldehyde for twenty minutes. Tissues were then washed in PBS three times for ten minutes each, and permeabilized in 0.3% Triton X-100 (PBST) twice for ten minutes each. Tissues were washed in 10% Goat Serum (Block) for 30 minutes before being placed in Primary antibody for 4 hours at RT. Tissues were washed in PBST twice for 10 minutes, washed in Block for 30 minutes before being placed in Secondary antibody for 4 hours at RT. Tissues were washed in PBS twice for ten minutes and mounted in 80% glycerol. Images were taken on confocal Zeiss LSM 710 or on Olympus Fluoview

Immunohistochemistry

Primary antibodies used included:

Rabbit anti-cleaved caspase-3 (Asp175) **1:100**, Cell Signaling Technology, MA.

Rabbit anti-aPKC ζ C-20:sc216) **1:1000**, Santa Cruz Biotechnology, INC.

Mouse anti-wg (4D4-S) **1:100**, Developmental Studies Hybridoma Bank.

Rhodamine-conjugated Phalloidin (R415) 1:100 Life Technologies Corporation.

Secondary Antibodies: Alexaflour 406, 488, and 633 **1:1000**, Invitrogen

Quantifications and Statistical Analysis

Graphs and Unpaired (two-tailed) T-tests were created using GraphPad Prism Version 6.0f Software. Data is normally distributed.

Chapter 3: Imaginal disc expression of *Drosophila* pro-apoptotic genes reaper, hid, and grim produce non-autonomous larval growth inhibition

Abstract

Apoptosis can eliminate abnormal or dying cells, which can be replaced through the proliferation of adjacent healthy cells maintaining tissue homeostasis. However, apoptotic pathways may play additional roles during development. The experiments in this chapter explore the role of pro-apoptotic proteins Reaper (Rpr), Grim, and Head involution defective (Hid) in regulating larval growth during development.

In response to localized imaginal disc damage, *Drosophila* larvae can delay developmental progression and slow growth to coordinate the regeneration of damaged tissues with the development and growth of undamaged tissues. Previously, the Halme lab and others have demonstrated that targeted expression of the Tumor Necrosis Factor (TNF) homologue *eiger* in the wing imaginal discs produces localized apoptosis and tissue damage and limits the growth of undamaged imaginal discs⁸⁵. However, larval growth is not affected by *eiger*-induced damage in the wing, whereas expressing pro-apoptotic genes *rpr*, *grim*, and *hid* in wing imaginal discs strongly restricts larval growth. Consequently, *eiger rpr*, *grim*, and *hid* expression but not apoptosis uniquely causes growth inhibition. Rpr, along with Grim, and Hid promote apoptosis by directly binding and degrading Inhibitor of Apoptosis proteins (IAPs). Overexpression of *Drosophila* IAP1 partially rescues *rpr*-induced growth inhibition in the wing, indicating IAP inhibition plays a role in promoting the growth inhibition. Other types of imaginal disc damage do not recapitulate the larval growth inhibition seen with expression of Reaper,

Grim, or Hid. Though the mechanism of this non-autonomous growth inhibition is presently unknown, this research indicates that IAP inhibitors *reaper*, *grim*, and *hid* play a novel role in regulating systemic growth, which can be the focus of future studies.

Introduction:

Ecdysone pulses transition the larvae from their growth period to pupariation

During the larval period, the larvae grow in mass 200-fold¹⁹¹. Larvae feed and molt twice until reaching critical weight during their third instar, which initiates a cascade of hormones that eventually lead to the cessation of feeding and larval growth so the larvae can pupariate^{65,98,149–151}. Pulses of ecdysone from the prothoracic gland determine the timing of larval molts and pupariation. Ecdysone synthesis is triggered by Prothoracicotrophic hormone (PTTH), which activates a mitogen-activated protein kinase (MAPK) signaling cascade in the prothoracic gland¹⁵⁴, that increases expression of ecdysone biosynthetic genes. The ecdysone pulses that end the larval growth period can be delayed by damage. Damaged tissue secretes signaling peptide Dilp8, which inhibits PTTH expression by binding to Lgr3 receptors to disrupt neural circuitry to PTTH^{99,100}. Damage and Dilp8 secretion prevent the pulses of 20-hydroxyecdysone by inhibiting PTTH and ultimately prevent the end of larval growth and pupariation.

Growth is coordinated during larval development

While the larvae are feeding, the larval fat body senses nutritional signals and coordinates the growth of imaginal discs and larval tissues. Disruption of fat body specific TOR signaling/cationic amino-acid transporter gene *slimfast* leads to non-autonomous larval growth inhibition¹⁶⁰ and prevents *Drosophila* insulin-like peptide 2 (DILP2) secretion into the hemolymph (causing it to accumulate in IPCs)^{158,163,164,192}. Circulating Dilps bind to insulin receptors in target cells to activate PI3K-responsive signaling cascades that inhibit FOXO transcription and promote

cell-autonomous growth. Thus, a lack of Dilp signaling limits growth^{161,162}. Infection in *Drosophila* leads to inflammatory Toll pathway cascades. This Toll pathway activity in the fat body inhibits Insulin signaling and thus results in decreased triglyceride storage and non-autonomous growth inhibition.

Can cell death affect growth?

However, very little is known about the effect that cell-death genes could either affect one of the aforementioned pathways or if cell death could independently alter adult body size. In *Drosophila*, programmed cell death occurs when initiator caspase Dronc cleave and activate effector caspases DrICE and Dcp-1, which proceed to proteolytically process cellular substrates to degrade the cytoskeleton, release signals that attract phagocytes, and activate nucleases that digest genomic DNA^{108,109,114,115}. In flies, cell death is regulated mainly by Diap1, an E3 ubiquitin ligase that binds and targets caspases for degradation^{116,121}. Pro-cell-death proteins Rpr, Grim, and Hid bind to and inhibit Diap1^{4,122-126}, induce IAP auto-ubiquitination and degradation to promote programmed cell death.

Programmed cell death can cause compensatory proliferation through Dronc, Hid, DrICE, or Dcp-1^{104,129,136}. However, compensatory proliferation is a local effect and does not affect whole larva or adult body size¹⁴³. In the following results, we investigate how overexpression of IAP inhibitors in the developing wing imaginal disc produces non-autonomous larval growth inhibition.

Results

reaper expression in the wing imaginal disc causes larval growth inhibition

Previous research in our lab showed that ablation with *eiger* (*egr*) in the wing disc slows the growth of non-injured imaginal discs⁹⁷. This systemic response to damage and regeneration could give damaged tissues time to repair and coordinate their growth with undamaged imaginal tissue⁹⁷. We originally hypothesized that another ablation model, *reaper* (*rpr*) expression⁷², would cause similar systemic growth inhibition in other imaginal discs. This turned out to be correct. However, we

also observed that constitutive expression of *rpr* in the wing imaginal disc using the Beadex-Gal4 expression pattern produced non-autonomous growth inhibition of the whole larvae (Fig. 1A). Our hypothesis was that this larval growth inhibition was not due to this specific expression pattern of Beadex (Bx), but is instead due to *rpr* expression in the wing pouch. Bx expresses in the entire wing pouch (though is more concentrated dorsally), but may also be expressed non-specifically in other tissues. Thus, to avoid a non-specific Gal4 expression from Bx, and to demonstrate that wing expression of reaper can produce a systemic regulation of larval growth, we expressed *rpr* with other Gal4 drivers that are expressed in the wing disc: Apterous-Gal4 (Ap), which is expressed in the dorsal wing pouch and notum, and Nubbin-Gal4 (*nub*) and Rotund-Gal4 (*rn*), which are both expressed throughout the wing pouch. Constitutively overexpressing pro-apoptotic gene *rpr* in the wing disc in the expression pattern of Bx, Ap, *nub*, or *rn* produces a significant decrease in larval growth (Fig. 1A). The degree of reduction is not uniform and bi-modal indicating that the phenotype has variable expressivity and that the data is non-parametric. Thus, significance was tested with the Kruskal-Wallis test. However, on average *rpr* expressing larvae are smaller than controls (Fig. 1B). While, we did not test this, it is possible that the phenotype may be stronger in some larvae due to sex difference, as female larvae and flies are larger than males¹⁹³. Alternatively there may be variability in levels of UAS expression of *rpr*. Next, we looked into effects of other ablation models to see if non-autonomous growth inhibition occurs.

Constitutive expression of TNF alpha homolog *eiger* (*egr*) is another method that is used to ablate the wing disc⁷². Thus, we tested if larval area was affected by *eiger* overexpression (Fig. 1A and Fig. 5A), but found that, unlike with *rpr* overexpression, there was no difference between Bx>*egr* and control larval size (normalized area in micrometers squared). This is consistent with previous work in our lab by Jacob Jaszczak (2015), which also shows that damage caused by *egr* overexpression does not cause a decrease in larval size⁹⁷.

Figure 1.

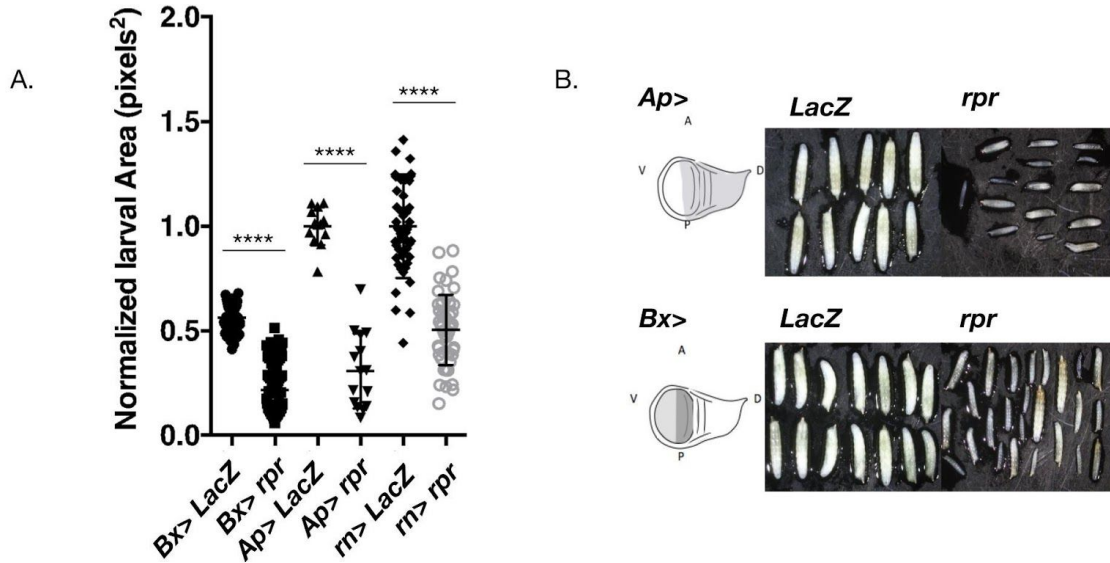


Figure 1 Beadex, Apterous, or Nubbin promoter driven reaper expression causes larval growth inhibition A.) Constitutive expression of *rpr* with Gal4 drivers Bx, Ap, Nub, or RN leads to non-autonomous growth inhibition (area pixels squared) at 116hAED. Eggs were collected during a 4-hour staging period. Ap and Bx data collected at 116hAED separately from Nub and Rn which were collected at 80hAED. 53 *Bx> UAS LacZ III* larvae, 82 *Bx> UAS rpr III* larvae, 13 *Ap> UAS LacZ III* larvae, 15 *AP> UAS rpr III* larvae, 46 *m> UAS LacZ III* larvae, 52 *Rn> UAS rpr III* larvae, 51 *Nub> UAS LacZ III* larvae, 48 *Nub> UAS rpr III* larvae. p values are two-tailed. All p values are $p < 0.0001$. **B.)** The reduction in larval size is not uniform **C.)** Previous work has shown that while overexpression of *eiger* can affect the area of other imaginal discs (the eye disc) total larval area (mm^2) is not affected (eye 10 *Bx> UAS GFP* and 9 *Bx> UAS egr III*: larval area 21 *Bx> UAS GFP* and 19 *Bx> UAS egr III*). Significance calculated with Kruskal-Wallis nonparametric test.

Thus, *rpr*-ablation, and not *egr*-ablation, in the wing disc causes non-autonomous growth inhibition. However, as we still do not know what period of development is sensitive to $Bx > rpr$ expression, we decided to constrain *rpr* expression to specific periods of development to better understand when $Bx > rpr$ can produce growth inhibition.

Reaper expression in the wing imaginal discs produces larval growth inhibition

In the previous experiment, we saw that constitutive expression of *rpr* leads to non-autonomous growth inhibition, but to see what period of larval development is critical for this growth inhibition we tested whether larval growth is still inhibited when *rpr* is only expressed in the wing imaginal disc during the last larval instar. We limited UAS *rpr* expression using the temperature-sensitive Gal80^{ts} allele. With Gal80 control, we can repress UAS-driven *rpr* expression at low temperatures (18°C) while promoting UAS-driven *rpr* expression at high temperatures (29°C) (Fig. 2A).

To determine whether the non-autonomous growth inhibition caused by *rpr* expression is dependent on *rpr* expression early in the embryo, larval stage, or only the late larval stage after the second to third instar transition, we divided $Bx > rpr$ expressing larvae into three groups. With the first group, we tested if expression of *rpr* in the wing disc at the embryonic stage alone could lead to non-autonomous growth inhibition compared to controls reared at the same temperature. While we do not know if *rpr* expresses at the embryonic stage, this experiment is designed to test if possible *rpr* expression at this time would cause growth inhibition. We repressed *rpr* in the first group by shifting larvae to 18°C at 24 hours (at the end of embryogenesis) after egg laying (Fig. 2A). We found that there was no growth inhibition in either *rpr* expressing larvae as compared to similarly treated controls that did not express *rpr*, indicating that growth inhibition is not dependent on embryonic expression of *rpr* (Fig. 2B) (Significance calculated with Kruskal-Wallis nonparametric test).

Figure 2.

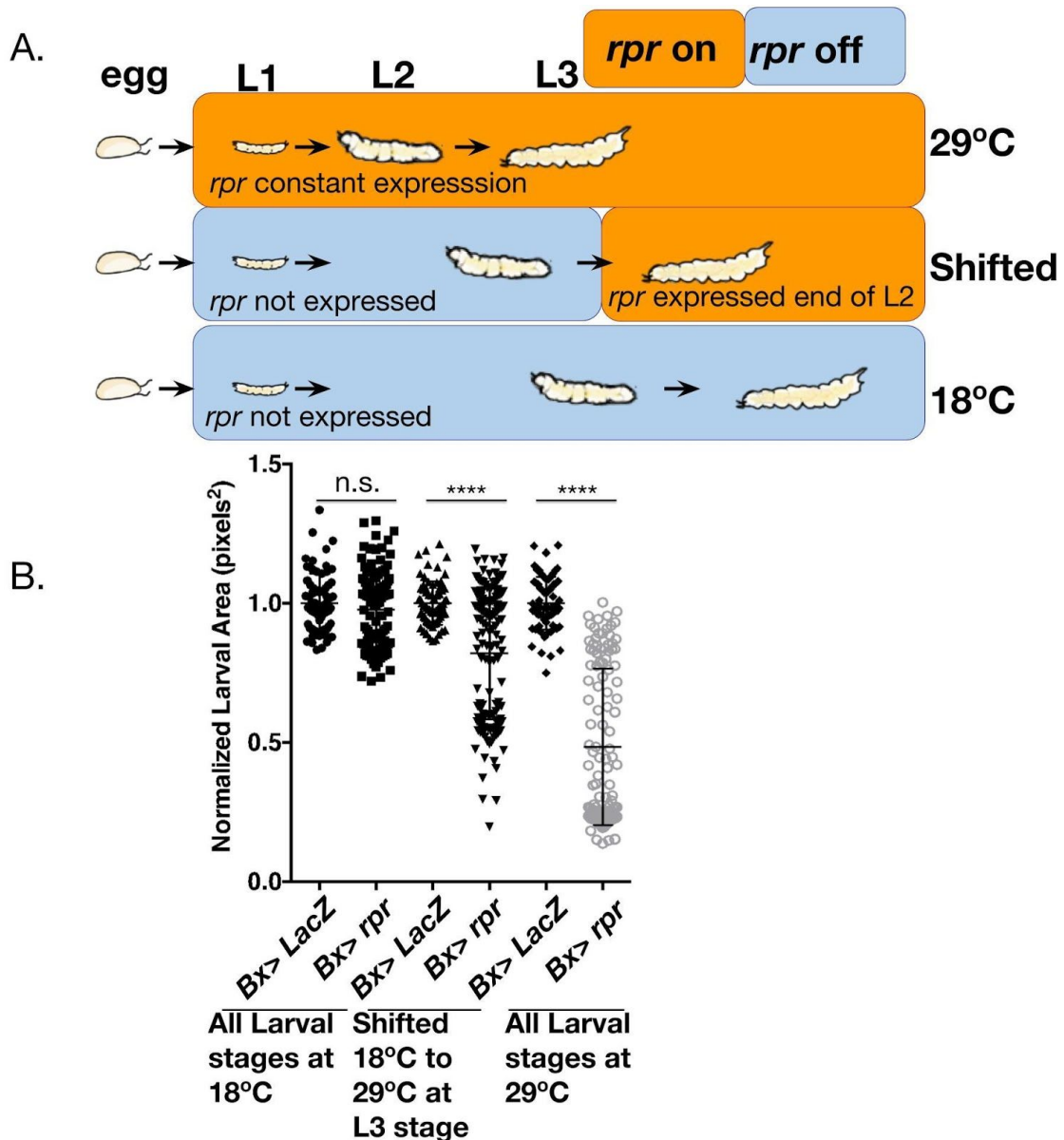


Figure 2. Temporally-limited reaper expression is sufficient to limit larval growth.

A) Populations of larvae shifted to turn on UAS reaper expression at both 24hAED (72 *Bx> UAS LacZ III* and 143 *Bx> UAS rpr III* larvae collected at wandering L3 stage) and late L2 (73 *Bx> UAS LacZ III* and 120 *Bx> UAS rpr III* collected at wandering L3 stage) show a significant decrease in larval size (pixels squared) compared to control larvae. The Gal80 TS construct prevents UAS reaper expression and any difference in larval size when larvae are kept at 18°C (68 *Bx> UAS LacZ III* and 111 *Bx> UAS rpr III* collected at wandering L3 stage). **B)** Cartoon of scheme showing the temperature shift. At lower temperatures, larvae develop more slowly, so the L2-L3 transition at 18°C is closer to 72 hAED than 56 hAED. p values are two-tailed. All significant p values are $p < 0.0001$. Significance calculated with Kruskal-Wallis nonparametric test. All UAS genes are expressed with Bx Gal4.

With the second group, we tested if the expression of *rpr* from the first larval instar onward was sufficient to cause non-autonomous growth inhibition. We shifted newly hatched larvae from 18°C to 29°C at 24hAED to inactivate Gal80 and permit Gal4-driven expression of *rpr* in the wing (Fig. 2A). Therefore, developing animals did not express *rpr* at embryonic stages. These larvae showed non-autonomous larval growth inhibition (normalized pixels squared) compared to controls reared at the same temperatures (Fig. 2A) (Significance calculated with Kruskal-Wallis nonparametric test). Again, the degree of growth reduction is not entirely uniform, indicating that the phenotype has variable expressivity, but on average *rpr* expressing larvae are smaller. Therefore, expressing *rpr* in the wing discs at some point from the first instar onward leads to a uniform phenotype, where all larvae undergo growth inhibition.

Third, we tested whether limiting *rpr* expression in the wing disc to the final larval instar is sufficient to cause growth inhibition. This experiment was designed to show if *rpr* expression at or after the L2-L3 transition no longer affects growth either because *rpr* expression must occur over a larger period of time to have an effect or because after the L2-L3 transition whatever mechanism *rpr*-ablation uses to cause growth inhibition is no longer at play. We shifted larvae from 18°C to 29°C at the L2-L3 transition (72h AED at 18°C) (Fig. 2A) (As the Data is bimodal, significance calculated with Kruskal-Wallis nonparametric test). A subset of the *rpr*-expressing larvae undergo non-autonomous larval growth inhibition (normalized pixels squared) compared to controls reared at the same temperatures (Fig. 2A). These smaller larvae have mouth hook morphology that indicates they are at the third larval instar, indicating they are not delaying their molts. This shows that *rpr* expression is partially sufficient to cause non-autonomous growth inhibition when expressed in the wing disc at this time, but that the phenotype is no longer penetrant. This result indicates that earlier expression of *rpr* or a longer expression of *rpr* in the wing disc is necessary for a penetrant phenotype. Overall, these results

show that *rpr* expression in the imaginal wing disc is capable of causing growth inhibition

Figure 3.

A.

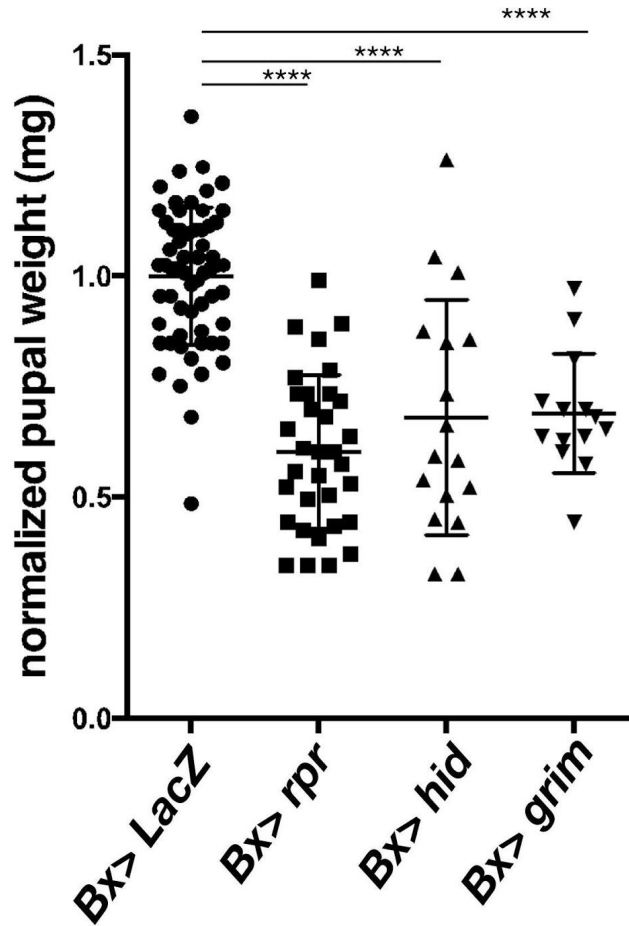


Figure 3. RGH expression in imaginal wing discs produces a decrease in pupal weight

Normalized pupal weight (mg) of *rpr*, *grim*, or *hid* overexpressing larvae show a significant reduction in weight compared to control (*LacZ*). (177 *Bx> UAS LacZ* pupae, 106 *Bx>UAS rpr III* larvae, 99 *Bx> UAS hid III* larvae, and 90 *Bx> UAS grim* larvae were collected over several weeks of staging). *p* values are two-tailed. *Bx> LacZ* compared to *Bx> rpr* $p < 0.0001$, *Bx> LacZ* compared to *Bx> hid* $p = 0.0002$, and *Bx> LacZ* compared to *Bx> grim* $p < 0.0001$. Significance calculated with Kruskal-Wallis nonparametric test. All *UAS* genes are expressed with *Bx Gal4*.

throughout larval development. We asked if other IAP inhibitors besides *rpr* would cause non-autonomous growth inhibition if expressed in the larval wing disc.

Expression of other IAP inhibitors *hid* or *grim* in the wing imaginal disc produces similar larval growth inhibition

Another method to assess larval growth is to examine pupal weight, which reflects the weight achieved at the end of larval growth. We tested if other IAP inhibitors Grim and Hid, which often work cooperatively with Rpr to inhibit Diap1, would cause a similar phenotype to *rpr* overexpression. This tests whether the phenotype is *rpr* specific and whether it is likely caused by IAP inhibition. We found that Beadex-driven *rpr*, *grim*, and *hid* expression all produce a significant reduction in pupal weight compared to *LacZ* expressing controls (Fig. 3) (Significance calculated with Kruskal-Wallis nonparametric test). The degree of growth reduction is not entirely uniform, indicating that the phenotype has variable expressivity, but on average RGH expressing pupa weigh less. This result indicated that the mechanism that permits *rpr* to inhibit larval growth may be through IAP inhibition. Next, we wondered if the effect of larval growth inhibition was reflected in the pupal phase because larvae were not delaying.

***Bx>rpr* expression in imaginal wing discs produces checkpoint delay, with the smallest larvae delaying longest**

We observed *Bx>rpr* expressing larvae and compared them to control larvae to see if they failed to delay, but, as seen in Fig. 1B, there is some variation in the amount of growth inhibition seen in larvae. We wondered if there was a correlation between the variable larval sizes and delay. At 116hAED (before pupariation), larvae overexpressing *rpr* were separated into three size categories: small, smaller, and smallest (measured by areas pixels squared). Larvae were separated qualitatively by observation under a dissecting microscope and photographed live while crawling across the microscope stage, with their area measured (Fig. 4A). Larvae

were then transferred to vials in groups of approximately 20 animals each, separated by size

Figure 4.

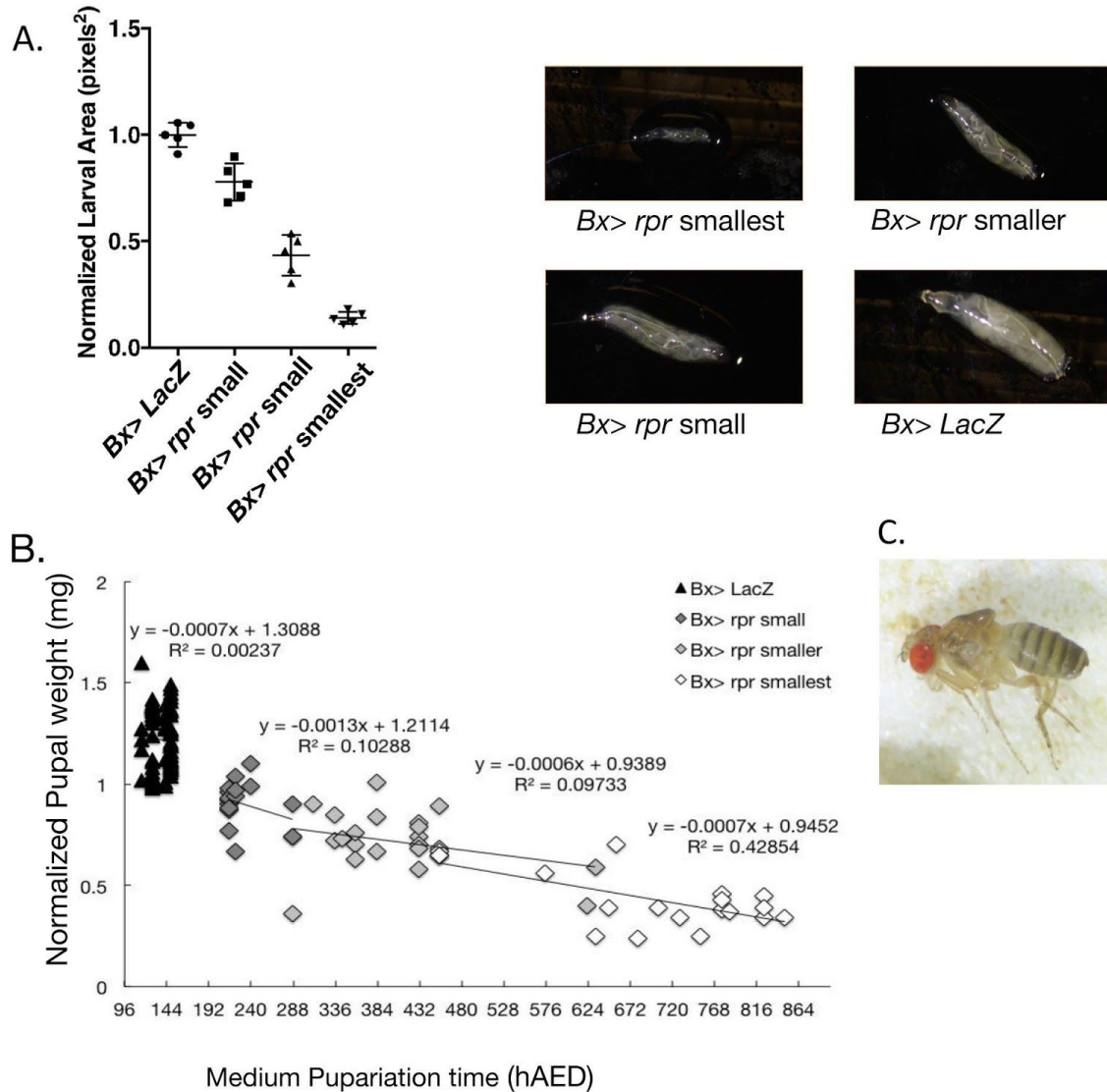


Figure 4. Reaper expression in imaginal wing discs produces checkpoint delay, with the smallest larvae delaying longest.

A) *Bx> GFP PH* larvae expressing *LacZ* or *rpr* were separated by size, with pixel area measured at 116hAED and photographed (5 *Bx> GFP PH UAS LacZ III* larvae, 5 *Bx> GFP PH UAS rpr III* larvae in all three size categories). **B.)** By following three size categories of *rpr* expressing larvae, small, smaller, and smallest, we see that the smallest larvae delay longest to pupariation and become pupae that weigh the least. *rpr* expressing larvae are significantly smaller than controls and delay longer. There is a negative correlation between pupal weight and delay with all size categories,

indicating that longer delay does not lead to higher pupal weight (73 *Bx> GFP PH UAS LacZ III* pupae, 17 *Bx> GFP PH UAS rpr III* small, 22 *Bx> GFP PH UAS rpr III* smaller, 20 *Bx> GFP PH UAS rpr III* smallest). **C.**) Once eclosed, the wing ablation phenotype is apparent. All UAS genes are expressed with *Bx Gal4*.

category. The larvae then developed to pupation, with their pupation timing and pupal weight recorded. We observed delay that was significantly longer than control larvae for all three size categories of *Bx>rpr* expressing larvae (Fig. 4B), and that the smallest larva tracked became the lowest weight pupae, despite having the longest larval period (Fig. 4A and B). There is a negative correlation between pupal weight and delay, indicating that longer delay does not lead to higher pupal weight (Fig. 4B.) Thus, the reason for the low pupal weight is not due to lack of delay during ablation damage.

Although pupae were smaller, viable adults eclosed from all pupae in all three-size categories (Fig. 4C). One interesting note is that all eclosed adults are female, indicating that males die at some point in development. As expected, all eclosed *Bx>rpr* flies have ablated wings but are otherwise superficially normal on the outside demonstrating that the *rpr* ablation is specific to the wing disc and that the *rpr* overexpression is indeed causing ablation in our model.

There is a fundamental difference in the amount of delay that *egr*-ablated larvae and *rpr*-ablated larvae undergo. Our lab observes that *egr*-ablation usually causes about forty additional hours of delay, which is much less than the additional five hundred hours (on average) seen in some larvae (Chapter 2 Fig. 1B). In the *egr*-ablation model, all delay is dependent on Dilp8 signaling⁹⁷, while delay caused by *rpr* ablation is only partially dependent on Dilp8 signaling¹⁰⁰. We noted that *egr* ablation damage does not cause larval growth inhibition (Fig. 6A). Similarly pupal weight is not decreased in *Bx>egr* expressing pupa (Fig. 6B) compared to control pupa (Significance calculated with Kruskal-Wallis test). Also, delay with overexpression of Dilp8 also does not decrease larval area (Fig. 6C) or pupal weight (mg) (Fig. 6D), and instead larval area and pupal weight are higher (Significance calculated with Kruskal-Wallis test). This result indicates that the mechanism that

causes the delay in *Bx>rpr* overexpressing pupa is not only Dilp8 delay and suggests that there is some other source of delay in *Bx>rpr* larvae such as delay to

Figure 5.

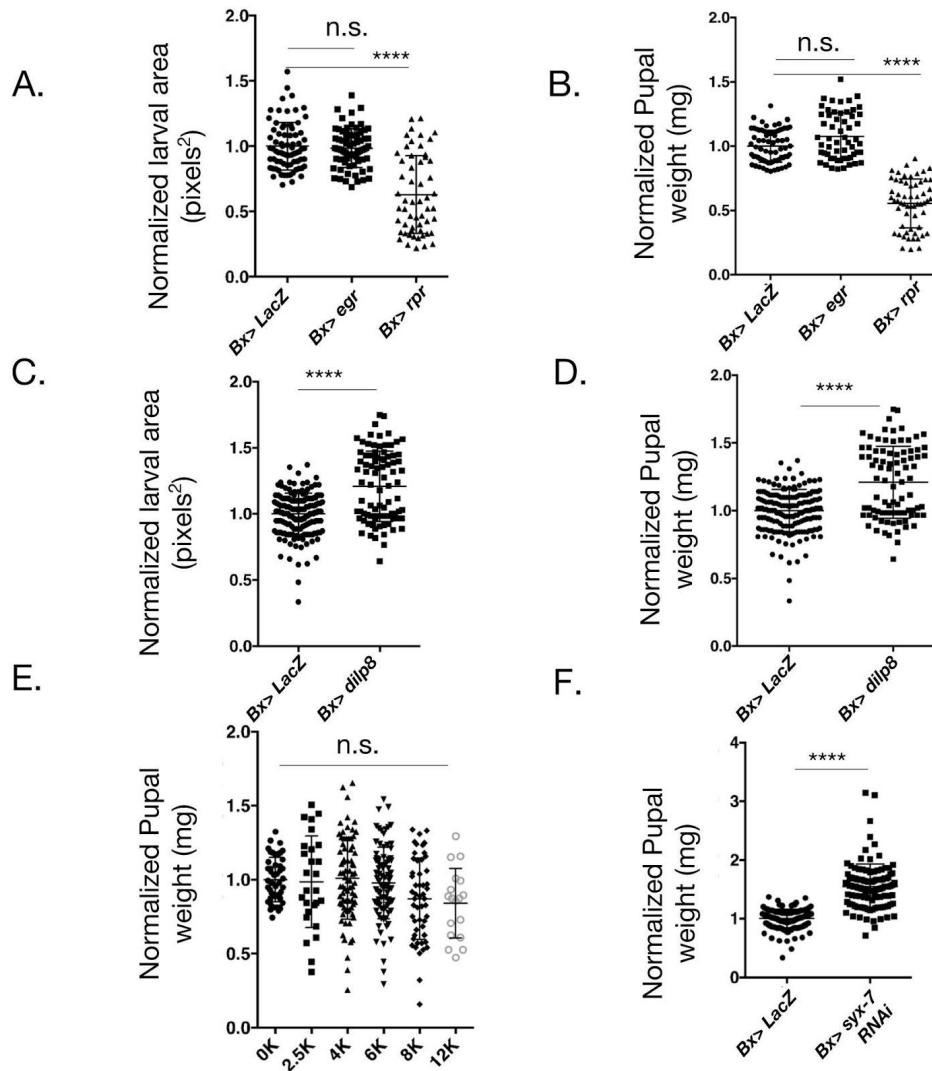


Figure 5. Other methods of causing injury or delay do not recapitulate the growth inhibition phenotype. Constitutive eiger ablation damage does not reduce the area of larvae (pixels squared) (76 *Bx> UAS LacZ III* larvae, 71 *Bx> UAS egr III* larvae, 56 *Bx> UAS rpr III* larvae measured at 80hAED) **A.** or reduce pupal weight (mg) **B.** Overexpression of *dilp8*, which causes delay, did not lead to a decrease in larval size (pixels squared) (36 *Bx> UAS LacZ III* larvae and 76 *Bx> UAS dilp8* larvae collected at 116hAED over a two-day period.) **C.** or a decrease in pupal weight (mg) if anything larvae and pupa were significantly larger than controls after delay (177 *Bx> UAS LacZ III* pupae and 88 *Bx> UAS dilp8* pupae collected over a several week staging series) **D.** Damage by X-irradiation at 2.5, 4, or 6k, 8K, or 12K Rads did not decrease pupal weight (mg) although there is larger variability on pupal weight (w1118 larvae were irradiated at 80hAED (47 0K controls, 27 2.5K irradiated pupae, 76 4K irradiated pupae, 90 6K irradiated pupae, 52 6K irradiated pupae, 19 12K

irradiated pupae were collected over a 2-day staging series) **E.**) Neoplastic damage by overexpression of *Syx-7 RNAi* did not decrease pupal weight (mg), and instead, lead to a significant increase in pupal weight (177 *Bx*> *UAS LacZ III* pupae and 113 *Bx*> *Syx-7 RNAi* pupae collected over a several week staging series). p values are two-tailed. All significant p values are $p < 0.0001$ Significance calculated with Kruskal-Wallis nonparametric test in A-C. Significance calculated with student t-test in F. All UAS genes are expressed with *Bx Gal4*.

critical weight. Next, we test if other damage models also produce this non-autonomous growth inhibition.

Other methods of producing delay do not produce a significant decrease in pupal weight

Other mechanisms that activate the regeneration checkpoint and induce developmental delay include X-irradiation damage in imaginal discs and neoplastic transformation of imaginal tissues. X-irradiation can be used to damage entire *Drosophila* larvae including the mitotically dividing discs⁷⁴⁻⁷⁶. X-irradiation also causes double-stranded breaks in DNA to cause p53-dependent upregulation of IAP inhibitors and subsequent apoptosis of diploid cells in imaginal discs⁷⁷. As with temperature dependent *Gal4/UAS* driven *rpr* ablation, X-irradiation damage creates temporally-limited damage. Critically, we were testing if damage to the entire system leads to growth inhibition. We found that X-irradiation from 2.5-12K Rads at 80hAED does not produce a statistically significant decrease in pupal weight (mg) (Significance calculated with Student t-test). Interestingly, some pupae are smaller than controls, indicating that some larvae undergo growth inhibition (Fig. 5E). One caveat with these results and the following results which use pupal weight as a readout of larval growth inhibition is that any damage method that produces delay gives larvae additional time to feed. This additional feeding time can offset any non-autonomous larval growth inhibition. Thus, just because there no observable difference in pupal weight does not mean larvae did not have a slight reduction in growth.

In Chapter 2, I demonstrated that neoplasia leads to a decrease in pupal viability. Thus, to see if damage caused by tumorigenic effects that leads to pupal death caused growth inhibition we damaged larvae with overexpression of

syntaxin-7 RNAi in the imaginal wing disc. This neoplastic tumor damage model¹⁸⁵ does not lead to a decrease in pupal weight and instead leads to a surprisingly significant increase in pupal weight (Fig. 5F) (Significance calculated with Student t-test). Therefore, it is not likely that the damage caused by *rpr* ablation is causing growth inhibition through neoplasia. Although, it is important to note that there are many other misregulated genes that cause neoplasia in *Drosophila*, and it is possible that misregulation of a different neoplastic gene in the wing disc may cause growth inhibition.

Overall, X-irradiation, which causes cell death in imaginal wing discs via p54, also causes growth inhibition in a subset of pupa. Expression of other IAP inhibitors *hid* and *grim* also causes pupal growth inhibition. Thus, we investigated if growth inhibition caused by RGH in the wing disc could be due to IAP inhibition as opposed to a separate unknown pathway of these IAP inhibitors.

Diap1 repression in the wing disc contributes to the larva growth suppression

IAP inhibitors such as Rpr bind to *Drosophila* Inhibitor of Apoptosis 1 (Diap1) to target it for ubiquitination and degradation. Diap1 normally binds to caspases and targets them for degradation, thus IAP inhibitors promote caspases to initiate the apoptotic cascade. To determine whether the growth inhibition we observed was dependent on the interaction between Rpr and Diap1, we co-expressed *diap1* and *rpr*. We use two UAS *rpr* insertions, one on Chromosome II and one on Chromosome III, in case either construct differentially expresses *rpr*. We observed that *diap1* expression alone leads to an increase of larval size (Significance calculated with Kruskal-Wallis nonparametric test). As, *diap1* expression alone causes an increase in larval size, it is difficult to determine if the *rpr* and *diap1* co-expressing larvae are larger than *rpr* expressing larvae due to *diap1* expression alone, or Diap1 and Rpr protein interactions (Fig. 6) (Significance calculated with Kruskal-Wallis nonparametric test). *diap1* co-expression with *rpr* may partially rescue the growth inhibition produced by expression of *rpr* in the imaginal wing disc with *rpr* constructs either on Chromosome II and III. Diap1 inhibition may play a role

in limiting *Bx>rpr* growth inhibition, but *Diap1* expression may simply increase larval size. Currently, this result does not clarify if the non-autonomous growth inhibition is due to caspase pathway activity or an unknown pathway caused by IAP inhibition.

Thus, we have seen that IAP inhibition causes non-autonomous growth inhibition in the imaginal wing disc during larval development, and that despite extensive delay, pupa also weigh less than control individuals. As pupa weigh less, it is possible that *Bx>rpr* larvae delay pupariation because they delay obtaining critical weight due to lack of nutrients or an altered metabolism.

Metabolic observations indicate there may be an altered metabolism

One factor that alters metabolism is lack of nutrition. *Bx>rpr* pupae with reduced weight (mg) are comparable to pupa with reduced weight after starvation (Fig. 7A) (Significance calculated with Kruskal-Wallis nonparametric test). Thus, we decided to investigate whether *Bx>rpr* larvae were feeding properly, in case larvae are starving due to a feeding defect. By dyeing the larval food blue with standard food coloring, we could visualize their gut, and see that it contained dye (Fig. 7B). We also observe the larvae burrowing through blue dyed 1% agar when placed in it, indicating normal feeding behavior (Fig. 7C). A look at the larval fat body does show a smaller, less opaque fat body, but the fat body is proportional to the smaller larvae (Fig. 7D). Together, these results show that gross feeding behavior is normal. To test if local *rpr* expression causes a decrease in insulin receptor activity in the fat body we measured insulin receptor/phosphoinositide 3-kinase (Inr/PI3K) activity via a pleckstrin-homology domain-linked GFP protein (GFP-PH) in the fat bodies of larvae with either no damage or targeted wing damage induced by *rpr* or *egr* expression (Fig. 7E). The pleckstrin homology domain of cytohesin/GRP1 binds specifically to phosphatidylinositol-3, 4, 5- P_3 (PIP₃), a product of PI3-kinase activity, and is thus recruited to the plasma membranes of cells with increased insulin receptor activation²⁰⁴. PI3K activity is high when there are available dietary proteins

and low in starvation conditions. Insulin signaling in the trophocytes of the fat body serves as a nutrient sensing system that maintains energy homeostasis¹⁵⁸.

Figure 6.

A.

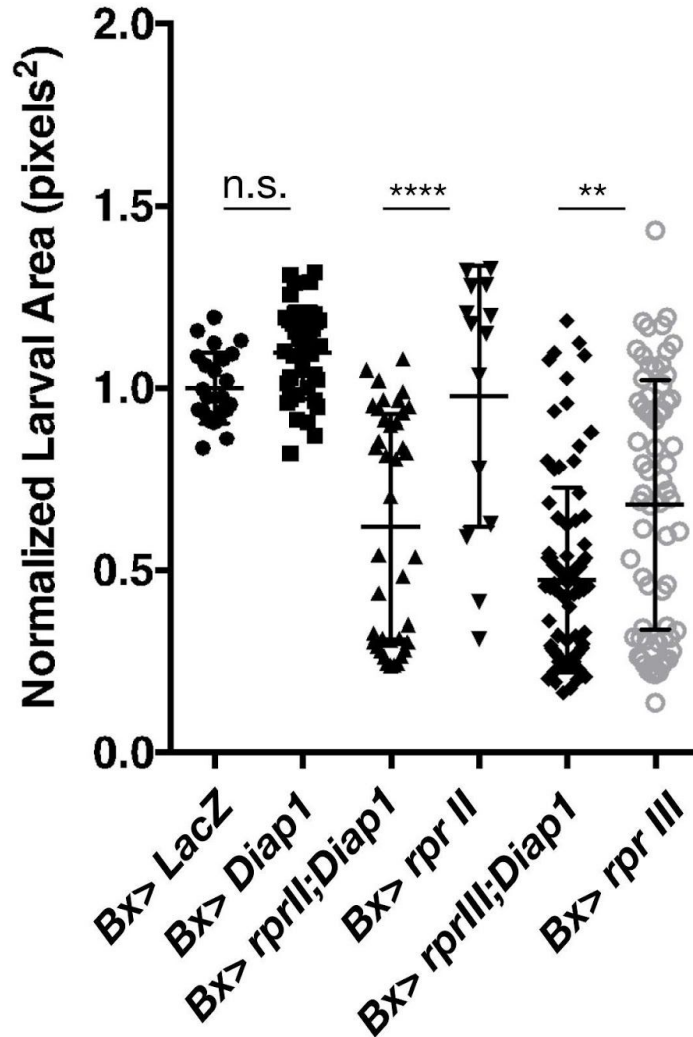


Figure 6. Diap1 inhibitor co-expression partially rescues larval size. Compared to reaper expression alone, co-expression of *diap1* with *rpr* on II or III partially rescues the larval growth inhibition (pixels squared). Data Collected at 116hAED from two separate experiments and pooled (24 *Bx> UAS LacZ III* controls, 38 *Bx> UAS diap1*, 40 *Bx> UAS rpr II*, 14 *Bx> UAS rpr II; UAS diap1*, 88 *Bx> UAS rpr III*, 68 *Bx> UAA rpr III; UAS diap1*). p values are two-tailed. *Bx> rpr II;Diap1* to *Bx> rpr II* $p < 0.0001$ and *Bx> rpr III;Diap1* to *Bx> rpr III* $p = 0.00029$. Significance calculated with Kruskal-Wallis nonparametric test. All UAS genes are expressed with Bx Gal4.

Figure 7.

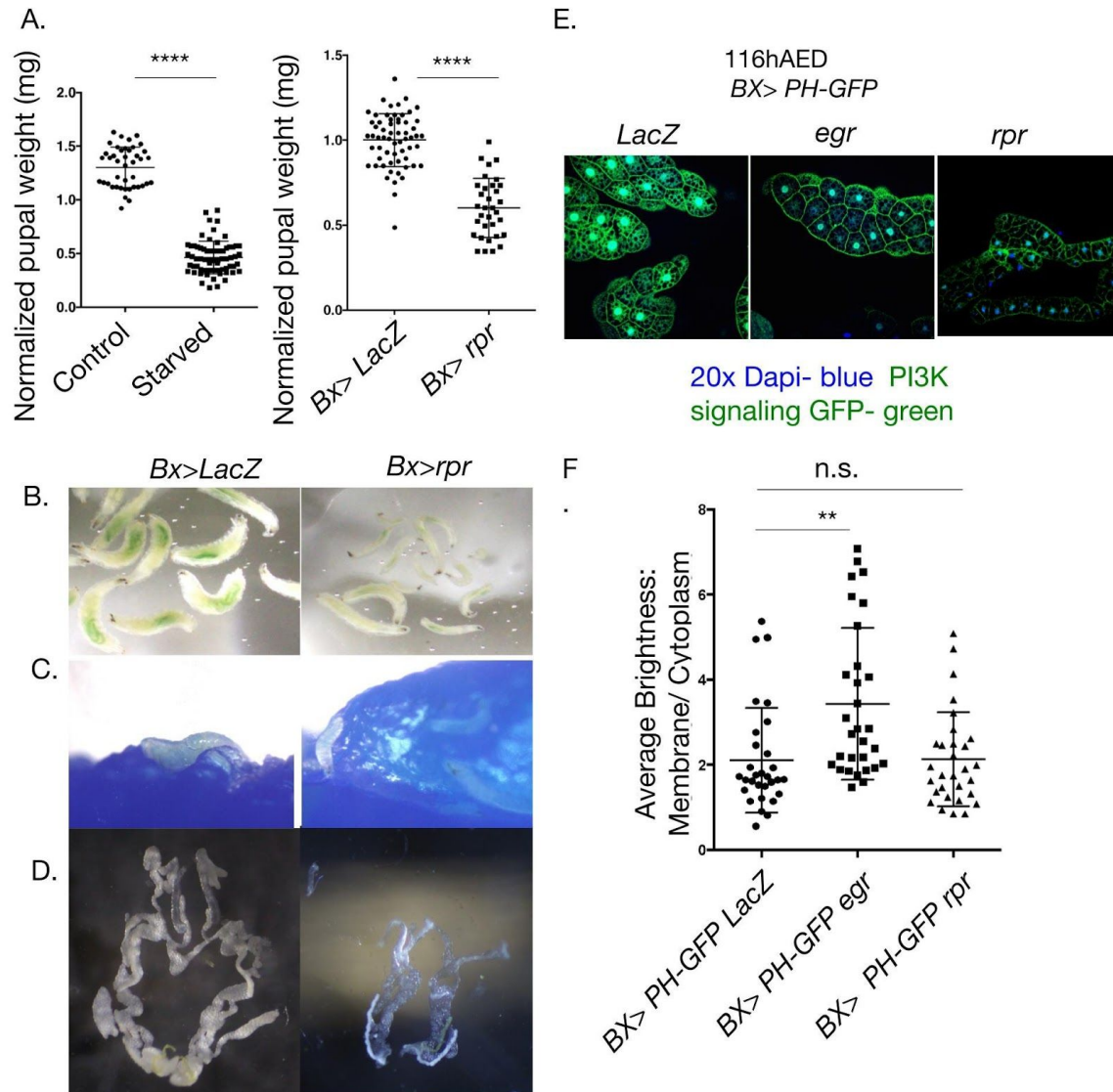


Figure 7. Metabolic observations indicate there may be an altered metabolism

A.) The low weight of Bx> *rpr* pupa (mg) is reminiscent of starved pupa, which also have decreased weight (mg) (89 Bx>LacZ non-starved and 68 Bx> LacZ starved) (177 Bx> UAS LacZ III larvae and 106 Bx> UAS *rpr* III pupae also shown in Figure 3. p values are two-tailed. p values in **A.)** are both p < 0.0001 **B.)** dye in guts of Bx>*rpr* larvae indicate food is being consumed. **C.)** Larvae exhibit normal tunneling behavior. **D.)** Their fat bodies (the energy storage tissue) are proportionally smaller compared to controls. **E.)** Overall, there is less PI3K signaling in these smaller *rpr* ablated tissues (6 Bx> PH-GFP UAS LacZ III fat body images, 11 Bx> PH-GFP UAS *egr* III fat body images, and 8 Bx>PH-GFP UAS *rpr* III fat body images collected over 3 days) **F.)** The ratio of PI3K in the membrane to the cytoplasm in *rpr*-ablated tissues are similar to control tissue, but significantly different than the ratio in the fat bodies of larvae with *egr*-ablated wing discs (30 cells analyzed for Bx> PH-GFP UAS LacZ III, Bx> PH-GFP UAS *egr* III, and Bx> PH-GFP UAS *rpr* III). p values are two-tailed. Bx> ph-GFP LacZ compared to Bx> ph-GFP *rpr* is 0.80155, Bx> ph-GFP LacZ compared to Bx> ph-GFP *egr* is 0.00022, and Bx> ph-GFP *rpr* compared to Bx> ph-GFP *egr* is 0.00098 (not on image). Significance calculated with Kruskal-Wallis nonparametric test. All UAS genes are expressed with Bx Gal4.

Thus, we can use the GFP-PH reporter to compare insulin signaling in the fat bodies of *Bx>rpr* larvae compared to that of controls. Phosphatidylinositol-3, 4, 5-P₃ (PIP₃) is a product of PI3-kinase activity, and is thus recruited to the plasma membranes of cells with increased insulin receptor activation. We found that *Bx>rpr* fat body trophocytes are substantially smaller than *LacZ* or *eiger* controls, but they have similar ratios of GFP-PH localization in the membrane to cytoplasm compared to controls. Interestingly, *Bx>rpr* larva fat bodies and the control fat bodies have a significantly lower ratio of PI3 kinase in the membrane to the cytoplasm compared to *Bx>egr* larval fat bodies (Fig. 7F), perhaps indicating that there is excessive insulin signaling in *Bx>egr* larvae.

Together, these initial observations indicate that if there is a nutrient deficiency caused by the systemic response to *rpr*-induced damage it may not be detectable by observing PI3 kinase activity ratios in the membrane and cytoplasm of the fat body.

Discussion and Future Directions

Apoptosis appears to have a role in larval growth regulation. We observe that IAP inhibitor overexpression and ablation in the wing disc leads to non-autonomous growth inhibition of the larvae and pupa, that is unique from *egr*-ablation, suggesting a novel role for the apoptosis pathway members Rpr, Grim, and Hid. We observe that IAP inhibition plays a role in this non-autonomous growth phenotype. Finally, the decrease in pupal weight, which reflects larval growth, is similar to pupae that were starved as larvae, indicating that larvae have altered critical weight and may have an altered metabolism that causes the non-autonomous growth inhibition.

Characterization of the growth inhibition phenotype

First, we observe that *rpr* expression in the wing disc using a variety of expression patterns leads to non-autonomous larval growth inhibition. We could follow-up this result and see if *rpr* expressed in other non-wing disc tissues, such as the eye imaginal disc or the fat body, also lead to non-autonomous growth inhibition. This experiment would help narrow down if the overall mechanism that causes growth inhibition is specific to the wing disc, imaginal tissues, or any larval tissue. To further characterize the non-autonomous growth inhibition, we used Gal80 temperature sensitive control of the Gal4/UAS system to express *rpr* only when larvae were at high temperatures. We found that the non-autonomous larval growth inhibition is not dependent on *rpr* expression in the presumptive wing disc at embryonic stages, and is instead dependent on expression sometime from the first instar stage onward. We also found that limiting *rpr* expression to after the second to third instar transition, caused a subpopulation of *Bx>rpr* larvae to no longer have non-autonomous growth inhibition. This result could be because there is a cutoff where *rpr* expression no longer causes larval growth inhibition or because the *rpr* expression needs to occur for a longer period of time for it to cause non-autonomous growth inhibition. One way to differentiate between these two possibilities is to see if restricting *rpr* expression to an even shorter window that encompasses only L1 or only L2 leads to a penetrant growth inhibition or non-penetrant growth inhibition. If the non-autonomous growth inhibition is no longer penetrant when *rpr* is expressed for one of these smaller windows of time, the result indicates that the duration of *rpr* expression is critical for the growth inhibition. If the phenotype is still penetrant, the result indicates that the specific larval stage that *rpr* is expressed at is what causes the non-autonomous growth inhibition. Another follow-up experiment would be to test if the population of larvae that do not undergo non-autonomous growth inhibition reach critical weight. To test this we could starve both populations of larvae and see if both groups or only the population that does not undergo growth inhibition is able to pupate at 116hAED

and then eclose. If only the population that does not undergo non-autonomous growth inhibition pupariates and ecloses it indicates that the smaller larvae delay reaching critical weight.

Finally, we see that the larval growth inhibition is not recovered by pupariation, with *Bx>rpr* expressing pupa showing reduced weight compared to control pupa. This indicates that at some point larvae are obtaining critical weight, but that afterwards, they do not have a long terminal growth period to promote additional growth.

IAP inhibition has a role in the non-autonomous growth inhibition phenotype

We also find that this growth inhibition phenotype is partially rescued by Diap1 expression in the wing disc, indicating that IAP inhibition has a role in the non-autonomous growth inhibition. Although a partial rescue normally would indicate that there may be an alternate mechanism by which RGH are causing growth inhibition, it is also likely that expression of *diap1* may not produce the same amount of Diap1 protein as *rpr* expression produces Rpr protein. Thus, unless we measure protein levels, we do not know if Diap1 could fully rescue the phenotype if there was enough Diap1 protein. We could consider using a Western blot to measure both Diap1 protein levels and Rpr protein levels and see if they are even or not. Next, to clarify if Diap1 activity is necessary for the phenotype we could inhibit Diap1 expression with RNAi. We could also try to co-express p35 with *rpr*, as p35 also inhibits the caspase pathway by binding to effector caspases. If p35 co-expression rescues the *Bx>rpr* non-autonomous growth inhibition phenotype or delay, it would further indicate that the phenotype is dependent on effector caspase activity.

To show that this phenotype is due to IAP inhibition we observe that expression of other IAP inhibitors, *grim* and *hid* also leads to a pupal growth inhibition phenotype. This could be further cemented if overexpression of other pro cell death pathway members such as initiator caspase Dronc in the wing disc leads to a similar growth inhibition phenotype. Another follow up experiment would be to

see if inhibition of one IAP inhibitor paired with overexpression of *rpr* would partially rescue the phenotype. Rpr, Grim, and Hid can act more efficiently in a complex together¹²⁷, so it would be interesting to test if that was true in our model.

We also find that X-irradiation damage, which causes cell death in diploid cells of imaginal wing disc tissue, has a non-significant subset of pupa undergo growth inhibition. Thus, it is possible that temporally-limited X-irradiation systemic damage that causes cell death can cause growth inhibition to some larvae. Not all larvae undergo growth inhibition following X-irradiation, and one explanation for this is that our phenotype depends specifically on *rpr* expression in the wing disc or on high levels of damage to imaginal discs. Because X-irradiation damage is random, larvae that fail to exhibit growth inhibition may not receive enough damage to their wing disc to see non-autonomous growth inhibition. Another experiment to follow-up experiment would be to express *rpr* in tissues besides the wing disc, such as other imaginal discs, and see if the growth inhibition caused by IAP expression is specific to the wing disc. We could also see if other damage models that cause cell death, such as heat-shock, also cause growth inhibition in larvae. Finally, neoplastic damage caused by overexpression of *syntaxin-7* RNAi did not cause non-autonomous growth inhibition but we may wish to test if other tumor models cause non-autonomous growth inhibition in the wing disc. Overall, damage methods that increase *rpr/hid/grim* expression cause at least some amount of non-autonomous growth inhibition and this phenotype can be partially rescued by inhibiting apoptosis with *Diap1* expression. However, these results do not clarify if the phenotype is due to caspase activity or only IAP inhibition.

The difference between the *rpr*-ablation and *egr*-ablation phenotype indicate that non-autonomous growth inhibition may be due to altered metabolism

Expression of another ablation causing gene *egr* does not cause growth inhibition, which first suggests that the growth inhibition is not due to an off-target ablation effect as *eiger* ablation would likely also kill off-target tissue, but secondly indicates that there is something fundamentally different about *rpr* ablation

compared to *egr* ablation. Although *rpr* and *egr* expression both cause cell death, it is possible that *rpr* expression more directly or efficiently promotes caspase-mediated cell death or that *rpr* activates another pathway that causes growth inhibition.

Another difference observed between the two ablation models is that while *egr*-ablated larvae do delay their pupariation by approximately forty more hours than control larvae (seen in Chapter 2.), *rpr*-ablated larvae delay can delay an additional one-hundred sixty to seven-hundred sixty hours. Initial observations show all observed *Bx>rpr* pupa eclosed to adults, whereas many *egr* expressing pupa die, indicating the *Bx>rpr* expression still permits survival. These *rpr*-ablated pupae eclose into females with ablated wings, but no males have ever been observed. As the Beadex-Gal4 driver is on the X chromosome, the effect could be due to dosage compensation, a process which balances the transcription of genes on the single X chromosome that males have to be equivalent to transcription from both X chromosome copies in females (Lucchesi and Kuroda 2015). Perhaps as a side effect of this dosage compensation *rpr* expression is causing lethality in males, since males will express genes at greater levels to make up for having one less chromosomal copy of the gene. First, we could test if *Bx>GFP* causes more *GFP* expression in males than females. Alternatively, we could test if expressing *rpr* using genes with wing expression drivers on an autosome, such as the Rotund-Gal4 driver which would not be under the effect of dosage compensation, permits males to eclose at the same rate as females. If this were the case, it would help confirm that the lack of male animals with the Bx-Gal4 driver is due to dosage compensation with *Bx>rpr* expression.

Altogether, this fundamental difference in delay can be explained by the fact that *egr*-ablation delay is fully dependent on Dilp8 checkpoint delay⁹⁷, while *rpr*-ablation delay is only partially dependent on Dilp8 checkpoint delay¹⁰⁰. Dilp8 delay is not known to cause growth inhibition, and our results confirm that there is not non-autonomous growth inhibition due to *dilp8* expression in larvae or pupa.

Thus, other mechanisms that cause delay to pupariation, such as delay to reach critical weight due to an altered metabolism, may be occurring.

An altered metabolism could be caused by a variety of factors, including decreased intake of food, decreased ability to process food, improper TOR or insulin/Dilp2 signaling from the fat body or brain, a Toll-mediated immune response in the fat body, or energy wasting due to a disorder like cachexia. Preliminary experiments show that *Bx>rpr* are feeding (due to the presence of dyed food in their gut and burrowing behavior). Careful examination of the mouth hooks of larvae should be done, to see if there are any gross deformities that would slow food intake. The rate at which the *Bx>rpr* larvae feed should be compared to control larvae, perhaps by giving larvae an equal amount of food and seeing how long it takes larvae to process the food. We also tested if *Bx>rpr* expression causes a decrease in dietary proteins in larvae by seeing if there was a decrease in membrane to cytoplasm ratio PI3K activity in the *Bx>rpr* fat bodies compared to *Bx>egr* or control larvae. We found that *Bx>egr* fat bodies had a higher ratio of PI3K activity in the membrane compared to cytoplasm, but that there was no difference between *Bx>rpr* and controls. If there were a difference in insulin signaling in the larval fat body other experiments that more directly measure insulin would have to be done. We could, for example, measure if Dilp2 is being sequestered in IPCs in *Bx>rpr* larvae compares to controls. We could also see if TOR or *slimfast* signaling is decreased in the fat body of *Bx>rpr* larvae using an antibody stain, or see if co-expression of *slimfast*/TOR in the fat body rescues the non-autonomous growth inhibition in *Bx>rpr* expressing larvae.

To test other models that alter metabolism, we could test if there is increased Toll signaling in *Bx>rpr* larvae by using a fluorescent marker that shows the activity of a Toll pathway member, such as Drosomycin-GFP, to see if Toll pathway activity is increased in *Bx>rpr* larvae. Another syndrome that causes growth inhibition is cachexia. *Drosophila* Ras mutant tumors interrupt insulin signaling by increasing expression of ImpL2/IGFBP to induce cachexia like wasting (Figueroa-Clarevega

and Bilder 2015). Inhibition of ImpL2 with RNAi prevents this energy wasting phenotype. It would be worth co-expressing ImpL2 RNAi with *Bx>rpr* overexpressing larvae to see if the non-autonomous growth inhibition phenotype could be rescued.

We anticipate that further research will help discern whether there are alterations of TOR, Dilp insulin signaling, or Toll signaling in fat bodies or brain tissue of *Bx>rpr* larvae. We will also investigate if inhibition of ImpL2 or other wasting genes may rescue the non-autonomous growth inhibition phenotype. If the growth inhibition and delay are related to an altered metabolism, then perhaps then the purpose of *rpr*, *hid*, or *grim* non-autonomous growth inhibition would ultimately be to allocate amino acid and lipids to repair following high levels of damage, to promote survival.

In conclusion, we observe a novel role for pro-apoptotic IAP inhibitors in the larval wing disc, where their overexpression causes growth inhibition. Although this phenotype seems to be dependent on caspase pathway activity, the exact mechanism behind this non-autonomous growth inhibition is unclear. Follow-up experiments can help determine whether factors that are known to alter metabolism such as nutrient deficiency or inflammation/Toll signaling will clarify the biological purpose of this growth inhibition.

Methods

Stocks- UAS-Reaper on III and UAS-Eiger were provided by Ishwar Hariharan⁷². UAS-Avl RNAai (Syx-7) was provided by David Bilder¹⁹⁵. PH-Gal4 was provided by Michelle Bland. UAS-Dilp8 construct from Pierre Leopold. UAS hid III was provided by Matthew Pahl of Sarah Siegrist's laboratory. UAS-GFP was provided by Yassi Hafezi of the Hariharan Laboratory. All other stocks listed are from Bloomington or Vienna.

***Drosophila* Culture and media.** Unless otherwise stated larvae were reared at 25°C in a 12-hour light cycle on standard cornmeal-yeast media in vials (Archon Scientific B101) or from melted and poured cornmeal-yeast media (Archon Scientific B110 - 500 cc) supplemented with live baker's yeast. Larvae were developmentally synchronized by collection after a 4-hour egg-laying period on grape agar plate. Larvae were transferred to vials or plates containing standard cornmeal-yeast media 24 hours after egg lay (AED) at first instar and placed in an incubator at 25°C in a 12-hour light cycle. Larvae were collected at 116hAED as wandering third instars. For temperature sensitive Gal80 UAS experiments, larvae were transferred at 24hAED as newly hatched first instars from grape plates to media and place at 18°C in an incubator or at 29°C respectively. Larvae that were shifted from 18°C to 29°C were shifted at 72hAED at the L2-L3 transition.

Food Dye Food vials were re-melted, and one drop of McCormick blue food coloring was evenly mixed into the standard cornmeal-yeast media. Animals were transferred into this food at 24hAED and observed at 116hAED. For clear blue food, 1% Agar was made, with one drop of McCormick blue food coloring mixed in. 72 hAED larvae were transferred temporarily into the food and photographed a few hours after transfer. For photography the Olympus DP21 microscope digital camera was used.

X-irradiation damage Irradiation was performed as previously described (Halme, Cheng, and Hariharan 2010), with staged larvae on media plates being floated up with a drop of DI water to be exposed to X-irradiation at 80hAED. Larvae were exposed to 0, 2.5, 3, or 4K Rads using the Hewlett-Packard, Model: 48305N operating at 130kV and at 3.0mA. Larvae were then again reared at 25°C in a 12-hour light cycle.

Measurement of delay to pupariation

Time to Pupariation, the time at which half the population had pupated was measured by recording the number of newly pupariated individuals at 12-hour intervals. Graphs and Kruskal- Wallis nonparametric test were done using Prism Software.

Fat Body dissections Larval fat body tissue was dissected at 116 HAED (wandering third instars) in Phosphate Buffered Saline (PBS), fixed in 4% paraformaldehyde in PBS before being washed in PBS. Tissues were then permeabilized in 0.3% Triton X-100 for twenty minutes. Tissues were stained with DAPI at 1:10,000 for 5 minutes, and then washed in PBS, and mounted in 80% glycerol. Images were taken on confocal Zeiss LSM 710.

Larval Area Quantification

Larvae were collected at 80hAED or 116 hours after egg lay into Eppendorf tubes filled with DI water. Larvae were poached at 80°C for 5 minutes before being dried on a Kimwipe and transferred to the microscope stage for photography on an Olympus DP21 microscope digital camera. Larval area was measured using ImageJ/Fiji. Area was measured by photographing larvae apically or laterally and then decreasing threshold in the image until only the larva was highlighted. The ImageJ/Fiji area measurement tool was then used to measure total pixel area.

Pupal Weight Pupae were frozen overnight, washed with a paintbrush, and dried before weighing on a Radwag Scale, Model: AS 60/220.R2

Chapter 4: Discussion

Summary

The experiments in this dissertation explore the role of the apoptotic pathway and IAP inhibitors Reaper, Grim, and Hid (RGH) in both regeneration and larval growth. Inhibitors of Apoptosis Proteins (IAPs) bind to the catalytic site of executioner caspases and use their RING domain to act as an E3 ubiquitination ligase to degrade themselves and bound caspases. RGH proteins bind to IAPs and induce IAP auto-ubiquitination and degradation to promote programmed cell death³. Apoptosis promotes localized cell death and promotes growth through compensatory proliferation, however apoptosis also has more nuanced roles. Through the use of immunohistochemistry, observation of developmental checkpoint delay, and careful characterization of larval, pupal, and wing phenotype, we see that apoptotic genes act as tumor suppressors during regeneration and that IAP inhibitor overexpression in the wing imaginal disc limits larval growth. In this research, there are still a number of unanswered questions that I will discuss below.

In Chapter 2, I demonstrated that depletion of apoptotic genes in the imaginal wing disc leads to an increase in developmental checkpoint delay, loss of viability, and overgrowth resembling neoplasia. This neoplastic overgrowth is characterized by high cortical F-actin in cells, loss of aPKC apical polarization and disorganization of epithelia compared to damaged discs that do not lose apoptotic capability. We know depletion of IAP inhibitor Reaper or depletion of caspases with Dronc RNAi, p35 expression, Diap1 overexpression, or loss of Dronc adaptor Dark in *egr*-ablated tissue also leads to a neoplastic phenotype. This result leads to our first lingering question: In regenerating wing disc tissue, how do caspase pathway members limit regenerative activity to prevent neoplasia (4.1)? In this research, we also focus solely on neoplasia formation after RGH depletion in the wing disc. Thus, we also discuss: Is the role of caspase pathway members to limit regenerative

activity specific to the imaginal wing disc (4.2)?

When we examine damaged imaginal disc tissues that lack RGH function, we find substantially enhanced expression of Dilp8, high transcriptional activity generated by the *wingless* regeneration enhancer BRV118, and higher levels of Wingless protein expression. All these signaling events are consistent with increased regenerative activity in these tissues^{72,99}. We observe that *egr*-ablated tissues with depleted RGH have higher levels of AP-1 activity, measured by measuring fluorescence of a transcriptional GFP reporter, than *egr*-ablated or control tissues. AP-1 is a transcription factor that is the homo- or hetero-dimer of cJun and cFos, which are phosphorylated and activated by the JNK pathway. Thus, an increase in AP-1 transcriptional activity suggests an increase in JNK pathway activity. Limiting JNK pathway activity using a JNK DN allele in *egr*-ablated RGH depleted tissue prevents the neoplastic phenotype. Also, co-expression of JNK pathway member hemipterous in RGH-depleted tissue also leads to the same neoplastic phenotype, indicating that JNK pathway activity is necessary for the ablation and sufficient for the neoplastic phenotype. We then see that inhibiting regeneration in these RGH-depleted and damaged discs with a mutant allele of *wg* rescues the overgrowth and delay phenotypes, indicating that this overgrowth is due to regenerative activity. However, these regenerative pathways are large, and it is possible other downstream members have a role in the observed phenotype. Thus, we discuss: What other members of pro-regenerative JNK or Wg pathway may be involved with the phenotype? (4.3)?

These results support a model that RGH-mediated cell death prevents neoplastic growth in regenerating tissues. Following injury, low levels of JNK activity increase *wg* expression through the enhancer BRV1118 and promote regenerative activity. With high levels of damage and JNK signaling, RGH activity is increased^{186,196,197}. This increase in cell death prevents neoplasia caused by excessive regeneration. In the case of X-irradiation, cell death genes expression is increased by p53 dependent JNK signaling, so it possible that caspase activity is

necessary to prevent neoplasia caused by high levels of JNK signaling following X-irradiation¹⁹⁸. Together, these data show that apoptosis has the capacity to act as a tumor suppressor with JNK pathway or X-irradiation damage. We also observe that JNK signaling and *wg* regenerative activity are necessary for the neoplastic phenotype, indicating that regenerative activity from JNK/*wg* signaling can cause neoplasia if misregulated. This suggests that IAP inhibitors limit regenerative activity to prevent tumorigenesis. This leads us to the question: What are the selective disadvantages of regeneration (4.4)?

In Chapter 3, we describe experiments demonstrating that IAP inhibitor overexpression in larval stages leads to non-autonomous growth inhibition in the larvae. Previously, the Halme lab has demonstrated that targeted expression of the Tumor Necrosis Factor (TNF) homolog *eiger* in the wing imaginal discs produces localized apoptosis and tissue damage, and systemically limits the growth of undamaged imaginal discs, but not the whole larvae⁹⁷. However, another ablation model, *rpr*-driven ablation in the imaginal wing disc⁷² does cause non-autonomous growth inhibition. The IAP inhibitors Rpr, Grim, and Hid promote apoptosis by directly binding and inhibiting the activity of *Drosophila* Inhibitor of Apoptosis 1 (Diap1). Co-expression of *Diap1* partially rescues *rpr* induced growth inhibition in the wing, indicating that Diap 1 inhibition plays a role in limiting *Bx>rpr* growth inhibition. IAP inhibitors expression in the wing imaginal discs also produces pupal growth inhibition. This pupal growth inhibition is only partially recapitulated with X-irradiation damage and is not recapitulated with *syntaxin-7* RNAi knockdown. Together these data indicate the non-autonomous growth inhibition is likely due to IAP inhibitor activity and inhibition of DIAP1.

However, we do not understand the mechanism behind the growth inhibition. The non-autonomous growth inhibition produces a starvation-like phenotype. Therefore, one hypothesis is that *Bx>rpr* expression disrupts metabolism, and that this alteration of metabolism is the mechanism that causes non-autonomous growth inhibition. There could be a disruption of feeding behavior or a disruption of

normal signaling from the larval fat body and brain. Our paper started to investigate if feeding behavior or nutrient signaling was altered in our larvae by looking into larvae burrowing, food intake in the gut, and insulin signaling in the larval fat body, but additional experiments must be completed to discern if metabolism is altered in larvae with *rpr*-ablated wing discs. Thus, we discuss: How does expression of IAP inhibitors in the wing disc produce non-autonomous larval growth inhibition (4.5)?

Another difference is that unlike *egr*-ablation, which often causes a decrease in viability, initial observations indicate that all *rpr*-ablated pupae eclose to adults. While the adults have not been characterized in terms of the length of their lifespan or their fecundity, they survive. Unlike damage caused by *egr*-ablation, *rpr*-ablation causes longer delays to pupariation, and perhaps this longer delay promotes more repair of damaged tissue that permits higher survival. If the hypothesis that RGH ablation alters metabolism to cause growth inhibition is true, it may indicate that RGH ablation may be altering metabolism to promote survival after damage. Thus, to explore if *rpr*-ablation alters metabolism to permit repair and survival, we discuss: Is the RGH growth inhibition critical for survival (4.6)?

In Chapters 2 and 3 we show that manipulating IAP expression in the *Drosophila* wing disc leads to neoplasia following damage and that causing ablation with *rpr*, *grim*, or *hid* leads to non-autonomous larval growth inhibition. Are these findings applicable to other systems besides *Drosophila* (4.8)? Together, the results in this thesis demonstrate a broader role for IAP inhibitors during regeneration of injured tissues which we discuss in our conclusion.

4.1 In regenerating wing disc tissue how do Reaper and other caspase pathway members Dark and Dronc limit regenerative activity to prevent neoplasia?

Cell-death pathways respond to oncogenic signaling and cellular stresses to eliminate damaged or abnormal cells and prevent tumorigenesis. In our model, perhaps the simplest explanation for why Rpr and pro-caspase activity prevent neoplasia is that they eliminate abnormal cells or cells that do not contribute to

restoring proper form and function or begin to emit oncogenic signals.

Perhaps this process involves cell clearance following apoptosis and compensatory proliferation. It could be possible that without proper apoptotic regulation, there are also errors in compensatory proliferation and that normal healthy cells would no longer be able to compete with unhealthy cells that should die (undead cells) or are oncogenic. Accompanying apoptosis, surrounding cells undergo compensatory proliferation, or additional proliferation of non-dying cells to compensate for loss of dead and phagocytized tissue¹²⁹⁻¹³¹. In *Drosophila*, studies of undead p35 overexpressing cells showed that pro-apoptotic protein Dronc coordinates mediating apoptosis and compensatory proliferation and that loss of an allele of *dronc* suppresses compensatory proliferation^{104,136}. In another example of compensatory proliferation in *Drosophila*, apoptosis caused by *hid*, *drice* and *dcp-1* expression in cells posterior to the morphogenetic furrow in the eye and is required for compensatory proliferation¹³⁶.

Apoptosis is also necessary for normal regenerative activity. For example, in hydra cell death and the resulting cell clearance is necessary for head regeneration². Caspases are also necessary for tail regeneration in *Xenopus*¹⁹⁹. To further test these theories in *Drosophila*, we could observe if in clonal model tissue we could have a portion of cells expressing normal Rpr levels while others have depleted Rpr signaling. By irradiating these tissues, we could observe cell clearance with and without RGH.

4.2 Is the role of caspase pathway members to limit regenerative activity wing disc specific?

In our model, depletion of IAP inhibitor Rpr or inhibition of caspase activity leads to neoplasia with excessive JNK pathway signaling in the wing disc. This neoplasia, despite being in a tissue that is not needed for survival leads to death in the pupal stage. To determine if depletion of caspase family genes combined with excessive JNK signaling leads to neoplasia in other tissues we could try depleting

caspase family genes in other imaginal disc tissues such as the eye or leg disc, or even in other expression patterns in the eye disc. Different spatial limitations of caspase family member gene depletion and damage from *egr*-ablation or X-irradiation damage may lead to a stronger or weaker phenotype, which would help us understand if there are any parts of imaginal discs more or less susceptible to tumor formation. This experiment would help narrow down if the overall mechanism that causes growth inhibition is specific to the wing disc, imaginal tissues, or any larval tissue. Other neoplastic tumor suppressing genes cause neoplastic overgrowth in multiple imaginal disc tissues¹⁸⁵, and showing that caspase-family gene depletion and high JNK activity is also capable of causing neoplasia in other tissue types would help expand our model and show that there is a higher probability for apoptosis to act as a tumor suppressor in a variety of systems. Further experiments in other imaginal discs and non-imaginal tissue will elucidate whether this is an imaginary disc tissue specific effect or can occur in other larval tissue.

4.3 What other members of pro-regenerative JNK or Wg pathway may be involved with the phenotype?

To better understand the mechanism that causes neoplasia in *Rpr* depleted tissues, we could investigate what other JNK or Wg pathway members contribute to the phenotype. Recent work by Pinal et al. (2018) show that temporal JNK pathway activity with sixteen-hour pulses of JNK activator p53 or *hemipterous* in the wing disc in a cell-death-deficient background also leads to overgrowth²⁰⁵. Additionally, JNK activity increases *rpr* and *hid* expression^{85, 86}, and we see AP-1 transcriptional activity (using an AP-1 GFP marker) increases when RGH is depleted in regenerating *eiger* damaged tissue. We could repeat this experiment and see if AP-1 activity is increased following X-irradiation. However, to test if AP-1 is necessary for the neoplastic phenotype we could inhibit AP-1 with siRNA in RGH depleted tissues following X-irradiation or *eiger* damage and see if neoplasia still

occurs. This experiment would show that the downstream factor that causes neoplasia in regenerating RGH depleted tissue is AP-1, as opposed to other factors upregulated by JNK, such as Foxo.

We also observe that our phenotype is dependent on *wg* transcriptional activation. In *Drosophila*, during compensatory proliferation, JNK signaling increases caspase pathway activity and WNT/Dpp^{132,133,200}. *wg* is required for regeneration after ablation with *rpr*⁷², after surgical transection¹³⁴, or after irradiation¹³⁵. Specifically, the *wg* regeneration enhancer element BRV118 is necessary for transcriptional activation of *wg* in regenerating tissues. *wg* then promotes growth and proliferation through the expression of *myc*⁷². *myc* misregulation is oncogenic and causes hyperplasia²⁰¹. Although it would not explain our neoplastic phenotype, it may explain the hyperplastic region surrounding the neoplasia that we observed but did not carefully characterize. A follow-up experiment where we inhibit Myc signaling in this IAP depleted damage model could provide insight on whether the surrounding hyperplastic phenotype is produced through *myc* activity.

4.4 What are the selective disadvantages of regeneration?

In Chapter 2, we show that excessive regenerative activity through JNK pathway activity (marked by increased or high Dipl8 delay and *wg*/Brv118 fluorescence) can lead to tumorigenesis if apoptosis is inhibited. Normal regenerated activity does not lead to tumorigenesis and, in fact, may protect against it. For example, regenerating dorsal newt limbs do not form tumors when carcinogenic agents are applied^{53,54}.

Altogether, we see many similarities between wound healing and the tumor environment including an increase in fibrin matrix and collagen, inflammatory cells, and genes such as *SDF1* that are activated during wound healing and to promote tumor growth. We also observe that wounded sites are more at risk of tumorigenesis than non-wounded sites after infection with tumorigenesis Rous Sarcoma virus⁶⁰ and that in cases of chronic injury neoplasias have a risk of

forming. We observe that longer-lived organisms may have developed more tumor suppressors to prevent cancer risk and that hormonal misregulation leads to overgrowth during deer antler regeneration. Altogether, this data indicates that regeneration may be limited because there is at least an associated risk between regenerative activity and tumorigenesis.

Altogether, this shows there is some risk associated with regenerative activity or the inflammation caused by extensive regenerative activity that can lead to neoplasia if oncogenes or tumor suppressors are misregulated. Our research shows an additional risk of tumorigenesis following X-irradiation or *egr*-ablation damage if tumor suppressor activity of the apoptotic pathway is inhibited.

4.5 How does expression of IAP inhibitors in the wing disc produce non-autonomous larval growth inhibition?

In Chapter 3, *rpr*-ablation damage in the wing disc during the larval growth period causes non-autonomous growth inhibition. Although we found that this growth inhibition is partially rescued by Diap1 inhibition, indicating that the inhibition of caspase activity may play a role in limiting *Bx>rpr* growth inhibition, we do not know how cell-death could signal to other tissues that regulate growth in *Drosophila*.

It might be useful to contrast the global growth phenotype in *Rpr* (which produces cell death) with *eiger* (which also produces IAP dependent cell death). What hypotheses could one advance that might explain this and how could one test them? This seems important to address.

Growth depends on nutrient levels, which when high cause the brain to secrete *Drosophila* insulin like peptides (Dilps), which bind to insulin receptors in target cells to activate PI3K signaling cascades that inhibit *foxo* transcription and promote cell-autonomous growth^{161,162}. During times of starvation or decreased nutrient availability, the transcription of *dilp3/5* is suppressed, while the transcription of *dilp2* remains the same. Instead, secretion of Dilp2 is suppressed, and it accumulates in IPCs of the brain, indicating that there serotonergic neuronal

input controls Dilp2 secretion^{163,192,202}. Culturing fat bodies from fed larvae, but not from starved larvae, with starved brains is sufficient to stimulate the brain to secrete Dilp2, indicating that the fat body secretes a factor that promotes Dilp2 release from IPCs in the brain¹⁶⁴. To test if the wing disc is affecting metabolism in other organ tissues we could test if Dilp2 is accumulating in the IPCs of larvae with *rpr*-ablated wing discs and if co-culturing *rpr*-expressing wing discs with brains and fat bodies from a control animal would lead to increased Dilp2 accumulation in these brains or altered TOR/*slimfast* expression in the fat body, similar to what occurs with starvation. This experiment would show that through some signaling or factor in the damaged wing imaginal disc tissue is capable of affecting growth signaling in other tissues. The injured wing disc could be secreting factors that affect other tissues or could be removing normally secreted signaling molecules (such as Dilps) that permit normal growth. We could examine hemolymph in *Bx>rpr* larvae, and see if it contains a normal level of Dilps to start characterizing if the phenotype is due to a decrease in signaling molecules or an unknown secreted factor.

We could also test if this IAP inhibitor ablation also causes non-autonomous growth inhibition if *rpr*, *grim*, or *hid* is expressed in other imaginal discs and if signals from these tissues could similarly affect growth signaling in the fat body or brain. This experiment would help narrow down if the overall mechanism that causes growth inhibition is specific to the wing disc, imaginal tissues, or any larval tissue. Different imaginal discs will also have different ablation patterns and may affect a larger or smaller amount of tissue than RGH expression in the wing disc, so expressing RGH genes in these discs could show if these different ablation patterns or if a larger ablation or smaller ablation pattern causes more or less non-autonomous growth inhibition.

4.6 Is the RGH growth-inhibition critical for survival?

rpr-ablated tissues may be limiting growth through several possible mechanisms: limiting the ability to absorb nutrients, suppressing activation of the

TOR pathway in the fat body, reducing systemic Insulin signaling, or by activating Toll signaling in the fat body. Could RGH non-autonomous growth inhibition promote survival following stress? Cell death occurs after a stress response such as heat shock, X-irradiation, hypoxia, or cutting or bruising. After cell-death occurs, the resulting wound repair of the injured imaginal discs may require energy that would otherwise go to increasing the size of the larvae. *rpr*-ablation damage may affect energy allocation, so that energy does not go to lipid storage in the trophocytes of the fat body, but instead goes to regeneration following injury.

It is also interesting to think that expression of IAP inhibitors in an organ such as the wing, which is nonessential for survival to adulthood, could lead to a systemic growth inhibition that is reflected in a low pupal weight. To see if there are any negative repercussions of this growth inhibition we could test if adult flies whose wing discs were ablated suffer any loss of fecundity.

4.7 Are these findings applicable to other systems?

The work in Chapter 2 may be a model for human disease. In humans, apoptotic machinery is also compromised during tumorigenesis to the point where resisting cell death is considered a hallmark of cancer^{139,140}. Apoptosis and the genes involved are conserved from flies to humans. In mammals (Bcl-2, Bcl-XL, and IAP family members), defects in apoptosis reduce the body's ability to eliminate unhealthy tissue¹⁴¹. Loss of apoptosis paired with oncogene expression or dysregulation of tumor suppressors causes cancer¹⁴⁴⁻¹⁴⁸. In our model, excessive JNK pathway activity during regeneration is tumorigenic, and it is possible that this is the case in other systems.

The purpose of regeneration is to restore form and function to damaged tissues, and humans have limited regenerative capacity. In the search to develop regenerative therapy for patients who have suffered limb or digit loss or suffer from other severe injuries, it is vital to increase our knowledge of what is necessary for normal regenerative repair. Many groups are currently interested in activating regeneration in non-regenerating tissue^{44,45,187,188}. Reactivating proliferative potential

in humans has enormous potential, but if a regenerative pathway is artificially induced in tissues that have lost the ability to regenerate, then how can we ensure the tissue is capable of regulating the regenerative process? By studying cell death and other methods that regulate regeneration we can make sure these regulators are present when developing safe regenerative therapies.

The work in Chapter 3 is less complete but speaks to either a new function of IAP inhibitors to cause non-apoptotic growth inhibition, or a possible novel non-apoptotic role of IAP inhibitors death genes *rpr*, *grim*, and *hid*. IAP inhibitor expression in the wing disc limits systemic growth. Growth involves using the energy from amino acids and fats consumed by the larvae to increase the size of imaginal discs. This is from the same pool of energy the system uses to repair after regeneration. The energetic cost of regeneration is observed in other systems, where when an organism re-grows an appendage the cost can be up to half of the organisms' total energy (measured in lipids and joules per milligram of the dry weight of lizards)²⁰³. The energetic costly process of regeneration can also affect an organism's fecundity. Regeneration causes a decrease in fecundity in several regenerative species⁴⁷⁻⁵¹ either by lowering the times an organism mates or preventing an organism from mating for a while. Perhaps due to the energetic and reproductive cost of regeneration after damage *Drosophila* need to find methods to carefully balance growth and repair of damaged tissue during development.

Conclusions- the expanded role of apoptosis and IAP inhibitors

The ability of different phyla to regenerate tissue after injury varies substantially. As development progresses, most animals lose the capacity to regenerate tissue either by limiting the proliferation potential of progenitor cells and/or by repression of developmental genes. The remaining ability to regenerate or heal wounds, therefore, needs to be tightly regulated by tumor suppressors. In researching the potential to regenerate tissues we need to understand what regulates regeneration.

Here, I show how apoptosis functions to suppress tumorigenic effects of regeneration caused by JNK activity following *egr*-ablation or X-irradiation damage. Resisting apoptosis is considered a hallmark of cancer, as normally oncogene signaling and DNA damage from hyperproliferation cause cellular stress and cell death^{139,140}. It is also known that inactivating mutations in DNA damage sensor p53 lead to tumor resistance to apoptosis^{105,142,143}. In our model, regeneration itself has the potential to be tumorigenic and cell death prevents this process as a response to this stress.

This model shows an additional apoptotic role for caspase pathway genes to prevent neoplasia post-regeneration, and expands our understanding of the potential risks of regeneration in *Drosophila*. Considering how many tumor models rely on the inhibition of cell death pathways, I believe that this work is applicable to other systems.

Next, we show that ablation caused by *rpr*, *grim*, or *hid* expression causes non-autonomous growth inhibition in the larvae and long delays to pupariation. IAP inhibitor Hid has been described to alter growth by causing compensatory proliferation, the additional proliferation of adjacent, viable cells to compensate for the loss of tissue after cell death¹³⁶. However, compensatory proliferation is a local effect, does not affect whole larva or adult body size, and if anything promotes growth instead of inhibiting it (Grasso et al. 2012). Thus, the result of IAP inhibitors *rpr*, *grim*, and *hid* causing non-autonomous growth inhibition is a novel finding.

Currently, we know that RGH ablation causes growth inhibition and that DIAP-1 inhibition plays a role in this phenotype. We currently do not know if the mechanism that causes the growth inhibition is through activation of caspases or a novel non-apoptotic pathway mechanism. More work must be done to understand the mechanism by which RGH expression limits growth and if the mechanism is related to decreasing nutrient availability and delaying critical weight obtainment. As mentioned, these larvae appear similar to larvae that are starved, and this resemblance may indicate that these larvae have altered metabolism. Although

more research needs to be done, this may indicate a model where RGH function to limit growth following damage, to promote energy to be allocated to wound repair. Considering the conservation of the cell death pathway it is possible that this model of growth inhibition would be applicable to other systems.

Together, this data shows that caspase pathway members have additional apoptotic roles in preventing neoplasia in *Drosophila* and a novel role in potentially regulating larval growth and repair following damage. Apoptosis in *Drosophila* occurs in development as in response to genotoxic stress and tissue damage. Understanding how caspase pathway members respond after damage to prevent excessive regenerative activity that causes neoplasia or to limit growth to possibly permit energetic resources go to healing gives us a deeper understanding of the wound healing process.

Citations

1. Martín, F. a & Morata, G. Compartments and the control of growth in the *Drosophila* wing imaginal disc. *Dev. Cambridge Engl.* **133**, 4421–6 (2006).
2. Bergmann, A. & Steller, H. Apoptosis, stem cells, and tissue regeneration. *Sci. Signal.* **3**, re8 (2010).
3. Bader, M. & Steller, H. Regulation of cell death by the ubiquitin-proteasome system. *Curr. Opin. Cell Biol.* **21**, 878–84 (2009).
4. Goyal, L., McCall, K., Agapite, J., Hartwig, E. & Steller, H. Induction of apoptosis by *Drosophila* reaper, hid and grim through inhibition of IAP function. *EMBO J.* **19**, 589–97 (2000).
5. Oviedo, N. J. & Beane, W. S. Regeneration: The origin of cancer or a possible cure? *Semin. Cell Dev. Biol.* **20**, 557–64 (2009).
6. Morgan, T. H. *Regeneration*. New York, *The Macmillan Company; London, Macmillan & Co., ltd.* (1901). doi:10.19030/iber.v8i1.3094
7. Reddien, P. W. & Alvarado, A. S. Fundamentals of planarian Regeneration. *Annu. Rev. Cell Dev. Biol.* **20**, 725–57 (2004).
8. Agata, K., Tanaka, T., Kobayashi, C., Kato, K. & Saitoh, Y. Intercalary regeneration in planarians. *Dev. Dyn.* **226**, 308–16 (2003).
9. Agata, K., Saito, Y. & Nakajima, E. Unifying principles of regeneration I: Epimorphosis versus morphallaxis. *Dev. Growth Differ.* **49**, 73–8 (2007).
10. Bosch, T. C. G. Why polyps regenerate and we don't: Towards a cellular and molecular framework for *Hydra* regeneration. *Dev. Biol.* **303**, 421–33 (2007).
11. Chan, R. J. & Yoder, M. C. The multiple facets of hematopoietic stem cells. *Curr Neurovasc Res* **1**, 197–206 (2004).
12. Bonner-Weir, S. *et al.* β -cell growth and regeneration: Replication is only part of the story. *Diabetes* **59**, 2340–8 (2010).
13. Oates, P. S. & West, A. R. Heme in intestinal epithelial cell turnover, differentiation, detoxification, inflammation, carcinogenesis, absorption and motility. *World J.*

- Gastroenterol.* **12**, 4281–95 (2006).
14. Lee, L., Lau, P. & Chan, C. A simple and efficient treatment for fingertip injuries. *J. Hand Surg. J. Br. Soc. Surg. Hand* **20**, 63–71 (1995).
 15. Michalopoulos, G. K. Liver regeneration. *J. Cell. Physiol.* **213**, 286–300 (2007).
 16. Butler, A. E. *et al.* Adaptive changes in pancreatic beta cell fractional area and beta cell turnover in human pregnancy. *Diabetologia* **53**, 2167–76 (2010).
 17. Epstein, W. L. & Maibach, H. I. Cell Renewal in Human Epidermis. *Arch. Dermatol.* **92**, 462–8 (1965).
 18. Agrawal, V. *et al.* Epimorphic regeneration approach to tissue replacement in adult mammals. *Proc. Natl. Acad. Sci.* **107**, 3351–5 (2010).
 19. Sánchez Alvarado, A. Regeneration in the metazoans: Why does it happen? *BioEssays* **22**, 578–90 (2000).
 20. Brockes, J. P. & Kumar, A. Comparative Aspects of Animal Regeneration. *Annu. Rev. Cell Dev. Biol.* **24**, 525–49 (2008).
 21. Bely, A. E. Evolutionary loss of animal regeneration: Pattern and process. *Integr. Comp. Biol.* **50**, 515–27 (2010).
 22. Goss, A. N. Intra-uterine healing of fetal rat oral mucosal, skin and cartilage wounds. *J. Oral Pathol. Med.* **6**, 35–43 (1977).
 23. Whitby, D. J. & Ferguson, M. W. J. The extracellular matrix of lip wounds in fetal, neonatal and adult mice. *Development* **112**, 651–68 (1991).
 24. Longaker, M. T. & Scott Adzick, N. The biology of fetal wound healing: A review. *Plast. Reconstr. Surg.* **87**, 788–98 (1991).
 25. Somasundaram, K. & Prathap, K. Intra-uterine healing of skin wounds in rabbit foetuses. *J. Pathol.* **100**, 81–6 (1970).
 26. Lorenz, H. P. *et al.* Scarless wound repair: a human fetal skin model. *Development* **114**, 253–9 (1992).
 27. Rowlatt, U. Intrauterine wound healing in a 20 week human fetus. *Virchows Arch. A Pathol. Anat. Histol.* **381**, 353–61 (1979).
 28. Seifert, A., Monaghan, J., Voss, R. & Maden, M. Skin regeneration in adult axolotls:

- A blueprint for scar-free healing in vertebrates. *PLoS One* **7**, e32875 (2012).
29. Bayat, A., McGrouther, D. A. & Ferguson, M. W. J. Skin scarring. *BMJ* **326**, 88–92 (2003).
 30. Larson, B. J., Longaker, M. T. & Lorenz, H. P. Scarless fetal wound healing: A basic science review. *Plast. Reconstr. Surg.* **126**, 1172–80 (2010).
 31. Longaker, M. T. *et al.* Adult skin wounds in the fetal environment heal with scar formation. *Ann. Surg.* **219**, 65–72 (1994).
 32. Garza-Garcia, A., Harris, R., Esposito, D., Gates, P. B. & Driscoll, P. C. Solution structure and phylogenetics of Prodl, a member of the three-finger protein superfamily implicated in salamander limb regeneration. *PLoS One* **4**, e7123 (2009).
 33. Stocum, D. L. & Cameron, J. A. Looking proximally and distally: 100 years of limb regeneration and beyond. *Dev. Dyn.* **240**, 943–68 (2011).
 34. Tanaka, E. M., Gann, A. A. F., Gates, P. B. & Brockes, J. P. Newt myotubes reenter the cell cycle by phosphorylation of the retinoblastoma protein. *J. Cell Biol.* **136**, 155–65 (1997).
 35. Huh, J. R., Guo, M. & Hay, B. A. Compensatory proliferation induced by cell death in the *Drosophila* wing disc requires activity of the apical cell death caspase dronc in a nonapoptotic role. *Curr. Biol.* **14**, 1262–6 (2004).
 36. Pajcini, K. V., Corbel, S. Y., Sage, J., Pomerantz, J. H. & Blau, H. M. Transient inactivation of Rb and ARF yields regenerative cells from postmitotic mammalian muscle. *Cell Stem Cell* **7**, 198–213 (2010).
 37. Levi, B. P. & Morrison, S. J. Stem cells use distinct self-renewal programs at different ages. *Cold Spring Harb. Symp. Quant. Biol.* **73**, 539–53 (2008).
 38. Kuhn, H., Dickinson-Anson, H. & Gage, F. Neurogenesis in the dentate gyrus of the adult rat: age-related decrease of neuronal progenitor proliferation. *J. Neurosci.* **16**, 2027–33 (1996).
 39. Shay, J. W. & Wright, W. E. Telomeres and telomerase in normal and cancer stem cells. *FEBS Lett.* **584**, 3819–25 (2010).
 40. Krtolica, A. Stem cell: Balancing aging and cancer. *Int. J. Biochem. Cell Biol.* **37**,

- 935–41 (2005).
41. Conboy, I. M. *et al.* Rejuvenation of aged progenitor cells by exposure to a young systemic environment. *Nature* **433**, 760–4 (2005).
 42. Alexson, T. O., Hitoshi, S., Coles, B. L., Bernstein, A. & Van Der Kooy, D. Notch signaling is required to maintain all neural stem cell populations - Irrespective of spatial or temporal niche. *Dev. Neurosci.* **28**, 34–48 (2006).
 43. Ruckh, J. M. *et al.* Rejuvenation of regeneration in the aging central nervous system. *Cell Stem Cell* **10**, 96–103 (2012).
 44. Brockes, J. F. & Kumar, A. Appendage regeneration in adult vertebrates and implications for regenerative medicine. *Science (80-.)*. **310**, 1919–1923 (2005).
 45. Shieh, S.-J. & Cheng, T.-C. Regeneration and repair of human digits and limbs: fact and fiction. *Regeneration* **2**, 149–68 (2015).
 46. Niewiarowski, P. H., Congdon, J. D., Dunham, A. E., Vitt, L. J. & Tinkle, D. W. Tales of lizard tails: effects of tail autotomy on subsequent survival and growth of free-ranging hatchling *Uta stansburiana*. *Can. J. Zool.* **75**, 542–8 (1997).
 47. Ballinger, R. E., Tinkle, D. W. & Murphy, J. B. Society for the Study of Amphibians and Reptiles On the Cost of Tail Regeneration to Body Growth in Lizards IN LIZARDS TO BODY GROWTH. *Society* **13**, 374–5 (2012).
 48. Maiorana, V. C. Tail autotomy, functional conflicts and their resolution by a salamander [15]. *Nature* **265**, 533–5 (1977).
 49. Dial, B. E. & Fitzpatrick, L. C. Lizard tail autotomy: Function and energetics of postautotomy tail movement in *Scincella lateralis*. *Science (80-.)*. **219**, 391–3 (1983).
 50. Smyth, M. Changes in the Fat Stores of the Skinks *Morethia boulengeri* and *Hemiergis perottii* (Lacertilia). *Aust. J. Zool.* **22**, 133–45 (1974).
 51. Maginnis, T. L. The costs of autotomy and regeneration in animals: A review and framework for future research. *Behav. Ecol.* **17**, 857–72 (2006).
 52. Okamoto, M. Simultaneous demonstration of lens regeneration from dorsal iris and tumour production from ventral iris in the same newt eye after carcinogen administration. *Differentiation* **61**, 285–92 (1997).

53. Tsonis, P. A. & Eguchi, G. Carcinogens on Regeneration: Effects of N-Methyl-N'-Nitro-N-Nitrosoguanidine and 4-Nitroquinoline-1-Oxide on Limb Regeneration in Adult Newts. *Differentiation* **20**, 52–60 (1981).
54. Tsonis, P. A. Effects of carcinogens on regenerating and non-regenerating limbs in amphibia (review). *Anticancer Res.* **3**, 195–202 (1983).
55. Yates, C. C., Hebda, P. & Wells, A. Skin Wound Healing and Scarring: Fetal Wounds and Regenerative Restitution. *Birth Defects Res. Part C - Embryo Today Rev.* **96**, 325–33 (2012).
56. Dvorak, H. F. Tumors: wounds that do not heal. Similarities between tumor stroma generation and wound healing. *N. Engl. J. Med.* **315**, 1650–9 (1986).
57. Schäfer, M. & Werner, S. Cancer as an overhealing wound: An old hypothesis revisited. *Nat. Rev. Mol. Cell Biol.* **9**, 628–38 (2008).
58. Allavena, P., Sica, A., Solinas, G., Porta, C. & Mantovani, A. The inflammatory micro-environment in tumor progression: The role of tumor-associated macrophages. *Crit. Rev. Oncol. Hematol.* **66**, 1–9 (2008).
59. Orimo, A. *et al.* Stromal fibroblasts present in invasive human breast carcinomas promote tumor growth and angiogenesis through elevated SDF-1/CXCL12 secretion. *Cell* **121**, 335–48 (2005).
60. Dolberg, D. S., Hollingsworth, R., Hertle, M. & Bissell, M. J. Wounding and its role in RSV-mediated tumor formation. *Science (80-.).* **230**, 676–8 (1985).
61. Pearson, B. J. & Sánchez Alvarado, A. Regeneration, stem cells, and the evolution of tumor suppression. *Cold Spring Harb. Symp. Quant. Biol.* **73**, 565–72 (2008).
62. Kierdorf, U., Kierdorf, H., Schultz, M. & Rolf, H. J. Histological structure of antlers in castrated male fallow deer (*Dama dama*). *Anat. Rec. - Part A Discov. Mol. Cell. Evol. Biol.* **281A**, 1352–62 (2004).
63. Decaroli, M. C. & Rochira, V. Aging and sex hormones in males. *Virulence* **8**, 545–70 (2017).
64. Oldham, S., Montagne, J., Radimerski, T., Thomas, G. & Hafen, E. Genetic and biochemical characterization of dTOR, the *Drosophila* homolog of the target of

- rapamycin. *Genes Dev.* **14**, 2689–94 (2000).
65. Shingleton, A. W. The regulation of organ size in *Drosophila*: Physiology, plasticity, patterning and physical force. *Organogenesis* **6**, 76–87 (2010).
 66. Swarup, S. & Verheyen, E. M. Wnt/wingless signaling in *Drosophila*. *Cold Spring Harb. Perspect. Biol.* **4**, a007930 (2012).
 67. Tanimoto, H., Itoh, S., Ten Dijke, P. & Tabata, T. Hedgehog creates a gradient of DPP activity in *Drosophila* wing imaginal discs. *Mol. Cell* **5**, 59–71 (2000).
 68. Fristrom, J. W., Fristrom, D. K., Fekete, E. & Kuniyuki, A. H. The mechanism of evagination of imaginal discs of *Drosophila melanogaster*. *Integr. Comp. Biol.* **17**, 671–684 (1977).
 69. Ursprung, H. & Hadorn, E. Weitere Untersuchungen über Musterbildung in Kombinatenscheiben aus teilweise dissoziierten Flügel-Imaginalscheiben von *Drosophila melanogaster*. *Dev. Biol.* (1962). doi:10.1016/0012-1606(62)90032-5
 70. Hadorn, E. & Buck, D. Über entwicklungsleistungen transplantierter teilstücke von flügel-imaginalscheiben von *Drosophila melanogaster*. *Rev Suisse Zool* **69**, 302–310 (1962).
 71. Haynie, J. L. & Bryant, P. J. Intercalary regeneration in imaginal wing disk of *Drosophila melanogaster*. *Nature* **259**, 659–62 (1976).
 72. Smith-Bolton, R. K., Worley, M. I., Kanda, H. & Hariharan, I. K. Regenerative Growth in *Drosophila* Imaginal Discs Is Regulated by Wingless and Myc. *Dev. Cell* **16**, 797–809 (2009).
 73. Herrera, S. C., Martín, R. & Morata, G. Tissue Homeostasis in the Wing Disc of *Drosophila melanogaster*: Immediate Response to Massive Damage during Development. *PLoS Genet.* **9**, e1003446 (2013).
 74. Hussey, R. G., Thompson, W. R. & Calhoun, E. T. The influence of X-rays on the development of *Drosophila* larvae. *Science (80-.)*. **66**, 65–6 (1927).
 75. Simpson, P., Berreur, P. & Berreur-Bonnenfant, J. The initiation of pupariation in *Drosophila*: dependence on growth of the imaginal discs. *J Embryol Exp Morphol* **57**, 155–65 (1980).

76. Halme, A., Cheng, M. & Hariharan, I. K. Retinoids Regulate a Developmental Checkpoint for Tissue Regeneration in *Drosophila*. *Curr. Biol.* **20**, 458–63 (2010).
77. Wichmann, A., Jaklevic, B. & Su, T. T. Ionizing radiation induces caspase-dependent but Chk2- and p53-independent cell death in *Drosophila melanogaster*. *Proc. Natl. Acad. Sci. U. S. A.* **103**, 9952–7 (2006).
78. Edwards, A. *et al.* Combinatorial effect of maytansinol and radiation in *Drosophila* and human cancer cells. *Dis. Model. Mech.* **4**, 496–503 (2011).
79. Reinhardt, C. A., Hodgkin, N. M. & Bryant, P. J. Wound healing in the imaginal discs of *Drosophila*: I. Scanning electron microscopy of normal and healing wing discs. *Dev. Biol.* **60**, 238–57 (1977).
80. Reinhardt, C. A. & Bryant, P. J. Wound healing in the imaginal discs of *Drosophila* II. Transmission electron microscopy of normal and healing wing discs. *J. Exp. Zool.* **216**, 45–61 (1981).
81. Bosch, M., Serras, F., Martín-Blanco, E. & Baguña, J. JNK signaling pathway required for wound healing in regenerating *Drosophila* wing imaginal discs. *Dev. Biol.* **280**, 73–86 (2005).
82. Wang, J. *et al.* A non-canonical MEK/ERK signaling pathway regulates autophagy via regulating Beclin 1. *J. Biol. Chem.* **284**, 21412–24 (2009).
83. Ríos-Barrera, L. D. & Riesgo-Escovar, J. R. Regulating cell morphogenesis: The *Drosophila* jun N-terminal kinase pathway. *Genesis* **51**, 147–62 (2013).
84. Kockel, L., Homsy, J. G. & Bohmann, D. *Drosophila* AP-1: Lessons from an invertebrate. *Oncogene* **20**, 2347–64 (2001).
85. Adachi-Yamada, T., Fujimura-Kamada, K., Nishida, Y. & Matsumoto, K. Distortion of proximodistal information causes JNK-dependent apoptosis in *Drosophila* wing. *Nature* **400**, 166–9 (1999).
86. Takatsu, Y. *et al.* TAK1 Participates in c-Jun N-Terminal Kinase Signaling during *Drosophila* Development. *Mol. Cell. Biol.* **20**, 3015–26 (2000).
87. Uhlirova, M., Jasper, H. & Bohmann, D. Non-cell-autonomous induction of tissue overgrowth by JNK/Ras cooperation in a *Drosophila* tumor model. *Proc. Natl. Acad.*

- Sci.* **102**, 13123–8 (2005).
88. Igaki, T., Pagliarini, R. A. & Xu, T. Loss of Cell Polarity Drives Tumor Growth and Invasion through JNK Activation in *Drosophila*. *Curr. Biol.* **16**, 1139–46 (2006).
 89. Uhlírova, M. & Bohmann, D. JNK- and Fos-regulated Mmp1 expression cooperates with Ras to induce invasive tumors in *Drosophila*. *EMBO J.* **25**, 5294–304 (2006).
 90. Maves, L. & Schubiger, G. Transdetermination in *Drosophila* imaginal discs: A model for understanding pluripotency and selector gene maintenance. *Curr. Opin. Genet. Dev.* **13**, 472–9 (2003).
 91. Herranz, H., Pérez, L., Martín, F. A. & Milán, M. A Wingless and Notch double-repression mechanism regulates G1-S transition in the *Drosophila* wing. *EMBO J.* **27**, 1633–45 (2008).
 92. Johnston, L. A., Prober, D. A., Edgar, B. A., Eisenman, R. N. & Gallant, P. *Drosophila myc* regulates cellular growth during development. *Cell* **98**, 779–90 (1999).
 93. Bryant, P. J. Regeneration and duplication in imaginal discs. *Ciba Found Symp* **0**, 71–73 (1975).
 94. Bryant, P. J. Pattern formation in the imaginal wing disc of *Drosophila melanogaster*: Fate map, regeneration and duplication. *J. Exp. Zool.* **193**, 49–77 (1975).
 95. Schubiger, G. Regeneration, duplication and transdetermination in fragments of the leg disc of *Drosophila melanogaster*. *Dev. Biol.* **26**, 277–95 (1971).
 96. Mattila, J., Omelyanchuk, L., Kytälä, S., Turunen, H. & Nokkala, S. Role of Jun N-terminal Kinase (JNK) signaling in the wound healing and regeneration of a *Drosophila melanogaster* wing imaginal disc. *Int. J. Dev. Biol.* **49**, 391–9 (2005).
 97. Jaszczak, J. S., Wolpe, J. B., Dao, A. Q. & Halme, A. Nitric oxide synthase regulates growth coordination during *Drosophila melanogaster* imaginal disc regeneration. *Genetics* **200**, 1219–28 (2015).
 98. Stieper, B. C., Kupershtok, M., Driscoll, M. V. & Shingleton, A. W. Imaginal discs regulate developmental timing in *Drosophila melanogaster*. *Dev. Biol.* **321**, 18–26 (2008).

99. Colombani, J., Andersen, D. S. & Léopol, P. Secreted peptide dilp8 coordinates *Drosophila* tissue growth with developmental timing. *Science (80-.)*. **336**, 582–5 (2012).
100. Garelli, A., Gontijo, A. M., Miguela, V., Caparros, E. & Dominguez, M. Imaginal discs secrete insulin-like peptide 8 to mediate plasticity of growth and maturation. *Science (80-.)*. **336**, 579–82 (2012).
101. Jaszczak, J. S., Wolpe, J. B., Bhandari, R., Jaszczak, R. G. & Halme, A. Growth coordination during *Drosophila melanogaster* imaginal disc regeneration is mediated by signaling through the relaxin receptor Lgr3 in the prothoracic gland. *Genetics* **204**, 703–9 (2016).
102. Yin, V. P. & Thummel, C. S. A balance between the diap1 death inhibitor and reaper and hid death inducers controls steroid-triggered cell death in *Drosophila*. *Proc. Natl. Acad. Sci.* **101**, 8022–7 (2004).
103. Brodsky, M. H. *et al.* *Drosophila* p53 binds a damage response element at the reaper locus. *Cell* **101**, 103–13 (2000).
104. Wells, B. S., Yoshida, E. & Johnston, L. A. Compensatory Proliferation in *Drosophila* Imaginal Discs Requires Dronc-Dependent p53 Activity. *Curr. Biol.* **16**, 1606–15 (2006).
105. Junttila, M. R. & Evan, G. I. P53 a Jack of all trades but master of none. *Nat. Rev. Cancer* **9**, 821–9 (2009).
106. Zhou, L., Song, Z., Tittel, J. & Steller, H. HAC-1, a *Drosophila* homolog of APAF-1 and CED-4, functions in developmental and radiation-induced apoptosis. *Mol. Cell* **4**, 745–55 (1999).
107. Nhan, T. Q., Liles, W. C. & Schwartz, S. M. Physiological functions of caspases beyond cell death. *Am. J. Pathol.* **169**, 729–37 (2006).
108. Kumar, S. Caspase function in programmed cell death. *Cell Death Differ.* **14**, 32–43 (2007).
109. Xu, D. The CARD-carrying caspase Dronc is essential for most, but not all, developmental cell death in *Drosophila*. *Development* **132**, 2125–34 (2005).

110. Rodriguez, A. *et al.* Dark is a Drosophila homologue of Apaf-1/CED-4 and functions in an evolutionarily conserved death pathway. *Nat. Cell Biol.* **1**, 272–9 (1999).
111. Kang, Y., Neuman, S. D. & Bashirullah, A. Tango7 regulates cortical activity of caspases during reaper-triggered changes in tissue elasticity. *Nat. Commun.* **8**, 603 (2017).
112. Lannan, E., Vandergaast, R. & Friesen, P. D. Baculovirus Caspase Inhibitors P49 and P35 Block Virus-Induced Apoptosis Downstream of Effector Caspase DrICE Activation in Drosophila melanogaster Cells. *J. Virol.* **81**, 9319–30 (2007).
113. Jabbour, A. M. *et al.* The p35 relative, p49, inhibits mammalian and Drosophila caspases including DRONC and protects against apoptosis. *Cell Death Differ.* **9**, 1311–20 (2002).
114. Leulier, F. *et al.* Systematic in vivo RNAi analysis of putative components of the Drosophila cell death machinery. *Cell Death Differ.* **13**, 1663–74 (2006).
115. He, B., Lu, N. & Zhou, Z. Cellular and nuclear degradation during apoptosis. *Curr. Opin. Cell Biol.* **21**, 900–12 (2009).
116. Hay, B. A., Wassarman, D. A. & Rubin, G. M. Drosophila homologs of baculovirus inhibitor of apoptosis proteins function to block cell death. *Cell* **83**, 1253–62 (1995).
117. Kaiser, W. J., Vucic, D. & Miller, L. K. The Drosophila inhibitor of apoptosis D-IAP1 suppresses cell death induced by the caspase drICE. *FEBS Lett.* **440**, 243–8 (1998).
118. Muro, I., Hay, B. A. & Clem, R. J. The Drosophila DIAP1 protein is required to prevent accumulation of a continuously generated, processed form of the apical caspase DRONC. *J. Biol. Chem.* **277**, 49644–50 (2002).
119. Huh, J. R. *et al.* The Drosophila inhibitor of apoptosis (IAP) DIAP2 is dispensable for cell survival, required for the innate immune response to Gram-negative bacterial infection, and can be negatively regulated by the Reaper/Hid/Grim family of IAP-binding apoptosis induce. *J. Biol. Chem.* **282**, 2056–68 (2007).
120. Arama, E., Bader, M., Rieckhof, G. E. & Steller, H. A ubiquitin ligase complex regulates caspase activation during sperm differentiation in Drosophila. *PLoS Biol.* **5**, e251 (2007).

121. Wilson, R. *et al.* The DIAP1 RING finger mediates ubiquitination of Dronc and is indispensable for regulating apoptosis. *Nat. Cell Biol.* **4**, 445–50 (2002).
122. Zhou, L. *et al.* Cooperative functions of the reaper and head involution defective genes in the programmed cell death of *Drosophila* central nervous system midline cells. *Proc. Natl. Acad. Sci.* **94**, 5131–6 (1997).
123. Wing, J. P., Zhou, L., Schwartz, L. M. & Nambu, J. R. Distinct cell killing properties of the *Drosophila* reaper, head involution defective, and grim genes. *Cell Death Differ.* **5**, 930–9 (1998).
124. Zachariou, A. *et al.* IAP-antagonists exhibit non-redundant modes of action through differential DIAP1 binding. *EMBO J.* **22**, 6642–52 (2003).
125. Shi, Y. A conserved tetrapeptide motif: potentiating apoptosis through IAP-binding. *Cell Death Differ.* **9**, 93–5 (2002).
126. Steller, H. Regulation of apoptosis in *Drosophila*. *Cell Death Differ.* **15**, 1132–8 (2008).
127. Sandu, C., Ryoo, H. D. & Steller, H. *Drosophila* IAP antagonists form multimeric complexes to promote cell death. *J. Cell Biol.* **190**, 1039–52 (2010).
128. Chera, S. *et al.* Apoptotic Cells Provide an Unexpected Source of Wnt3 Signaling to Drive Hydra Head Regeneration. *Dev. Cell* **17**, 279–289 (2009).
129. Martín, F. A., Pérez-Garijo, A. & Morata, G. Apoptosis in *Drosophila*: Compensatory proliferation and undead cells. *Int. J. Dev. Biol.* **53**, 1341–7 (2009).
130. Perez-Garijo, A. Caspase inhibition during apoptosis causes abnormal signalling and developmental aberrations in *Drosophila*. *Development* **131**, 5591–8 (2004).
131. Ryoo, H. D., Gorenc, T. & Steller, H. Apoptotic cells can induce compensatory cell proliferation through the JNK and the wingless signaling pathways. *Dev. Cell* **7**, 491–501 (2004).
132. Bergantinos, C., Corominas, M. & Serras, F. Cell death-induced regeneration in wing imaginal discs requires JNK signalling. *Development* **137**, 1169–79 (2010).
133. Morata, G., Shlevkov, E. & Pérez-Garijo, A. Mitogenic signaling from apoptotic cells in *Drosophila*. *Dev. Growth Differ.* **53**, 168–76 (2011).

134. Schubiger, M., Sustar, A. & Schubiger, G. Regeneration and transdetermination: The role of wingless and its regulation. *Dev. Biol.* **347**, 315–24 (2010).
135. Harris, R. E., Setiawan, L., Saul, J. & Hariharan, I. K. Localized epigenetic silencing of a damage-activated WNT enhancer limits regeneration in mature *Drosophila* imaginal discs. *Elife* **5**, e11588 (2016).
136. Fan, Y. & Bergmann, A. Apoptosis-induced compensatory proliferation. The Cell is dead. Long live the Cell! *Trends Cell Biol.* **18**, 467–473 (2008).
137. Garcia-Bellido, A. & Merriam, J. R. Parameters of the wing imaginal disc development of *Drosophila melanogaster*. *Dev. Biol.* **24**, 61–87 (1971).
138. Milán, M., Campuzano, S. & García-Bellido, A. Cell cycling and patterned cell proliferation in the *Drosophila* wing during metamorphosis. *Proc. Natl. Acad. Sci. U. S. A.* **93**, 11687–11692 (1996).
139. Hanahan, D. & Weinberg, R. A. Hallmarks of cancer: The next generation. *Cell* **144**, 646–74 (2011).
140. Hanahan, D. & Weinberg, R. A. The Hallmarks of Cancer Review University of California at San Francisco. *Cell* **100**, 57–70 (2000).
141. Adams, J. M. & Cory, S. The Bcl-2 apoptotic switch in cancer development and therapy. *Oncogene* **26**, 1324–37 (2007).
142. Ollmann, M. *et al.* *Drosophila* p53 is a structural and functional homolog of the tumor suppressor p53. *Cell* **101**, 91–101 (2000).
143. Grasso S, Menéndez-Gutiérrez M, Carrasco-García E, Mayor-López L, Tristante E, Rocamora-Reverte L, Gómez-Martínez A, García-Morales P, Ferragut J, S. M. and M.-L. I. Cell Death and Cancer, Novel Therapeutic Strategies. in *Apoptosis and Medicine* 67–111 (InTech Open, 2012). doi:10.5772/51285
144. Yip, K. W. & Reed, J. C. Bcl-2 family proteins and cancer. *Oncogene* **27**, 6398–406 (2008).
145. Tagawa, H. *et al.* Genome-wide array-based CGH for mantle cell lymphoma: Identification of homozygous deletions of the proapoptotic gene BIM. *Oncogene* **24**, 1348–58 (2005).

146. Pierce, A. M. *et al.* Increased E2F1 activity induces skin tumors in mice heterozygous and nullizygous for p53. *Proc. Natl. Acad. Sci.* **95**, 8858–63 (1998).
147. Garrison, S. P. *et al.* Selection against PUMA Gene Expression in Myc-Driven B-Cell Lymphomagenesis. *Mol. Cell. Biol.* **28**, 5391–402 (2008).
148. Michalak, E. M. *et al.* Puma and to a lesser extent Noxa are suppressors of Myc-induced lymphomagenesis. *Cell Death Differ.* **16**, 684–96 (2009).
149. Nijhout, H. F. & Williams, C. M. Control of moulting and metamorphosis in the tobacco hornworm, *Manduca sexta* (L.): Growth of the last-Instar larva and the decision to pupate. *J. Exp. Biol.* **61**, 481–91 (1974).
150. Yamanaka, N., Rewitz, K. F. & O'Connor, M. B. Ecdysone Control of Developmental Transitions: Lessons from *Drosophila* Research. *Annu. Rev. Entomol.* **58**, 497–516 (2013).
151. Shingleton, A. W., Mirth, C. K. & Bates, P. W. Developmental model of static allometry in holometabolous insects. *Proc. R. Soc. B Biol. Sci.* **275**, 1875–85 (2008).
152. Gibbens, Y. Y., Warren, J. T., Gilbert, L. I. & O'Connor, M. B. Neuroendocrine regulation of *Drosophila* metamorphosis requires TGF /Activin signaling. *Development* **138**, 2693–703 (2011).
153. McBrayer, Z. *et al.* Prothoracicotropic Hormone Regulates Developmental Timing and Body Size in *Drosophila*. *Dev. Cell* **13**, 857–71 (2007).
154. Rewitz, K. F., Yamanaka, N., Gilbert, L. I. & O'Connor, M. B. The insect neuropeptide PTTH activates receptor tyrosine kinase torso to initiate metamorphosis. *Science (80-.).* **326**, 1403–5 (2009).
155. Petryk, A. *et al.* Shade is the *Drosophila* P450 enzyme that mediates the hydroxylation of ecdysone to the steroid insect molting hormone 20-hydroxyecdysone. *Proc. Natl. Acad. Sci.* **100**, 13773–8 (2003).
156. Caldwell, P. E., Walkiewicz, M. & Stern, M. Ras activity in the *Drosophila* prothoracic gland regulates body size and developmental rate via ecdysone release. *Curr. Biol.* **15**, 1785–95 (2005).
157. Galloni, M. & Edgar, B. A. Cell-Autonomous and Non-Autonomous

- Growth-Defective Mutants of *Drosophila Melanogaster*. *Development* **126**, 2365–75 (1999).
158. Tennessen, J. M. & Thummel, C. S. Coordinating growth and maturation - Insights from drosophila. *Curr. Biol.* **21**, R750–7 (2011).
 159. Martin, J. F., Hersperger, E., Simcox, A. & Shearn, A. *minidiscs* encodes a putative amino acid transporter subunit required non-autonomously for imaginal cell proliferation. *Mech. Dev.* **92**, 155–67 (2000).
 160. Colombani, J. *et al.* A nutrient sensor mechanism controls *Drosophila* growth. *Cell* **114**, 739–49 (2003).
 161. Oldham, S. & Hafen, E. Insulin/IGF and target of rapamycin signaling: a TOR de force in growth control. *Trends Cell Biol.* **13**, 79–85 (2003).
 162. Puig, O., Marr, M. T., Ruhf, M. L. & Tjian, R. Control of cell number by *Drosophila* FOXO: Downstream and feedback regulation of the insulin receptor pathway. *Genes Dev.* **17**, 2006–20 (2003).
 163. Ikeya, T., Galic, M., Belawat, P., Nairz, K. & Hafen, E. Nutrient-dependent expression of insulin-like peptides from neuroendocrine cells in the CNS contributes to growth regulation in *Drosophila*. *Curr. Biol.* **12**, 1293–300 (2002).
 164. Géminard, C., Rulifson, E. J. & Léopold, P. Remote Control of Insulin Secretion by Fat Cells in *Drosophila*. *Cell Metab.* **10**, 199–207 (2009).
 165. Hoffmann, J. A. & Reichhart, J. M. *Drosophila* innate immunity: An evolutionary perspective. *Nat. Immunol.* **3**, 121–6 (2002).
 166. DiAngelo, J. R., Bland, M. L., Bambina, S., Cherry, S. & Birnbaum, M. J. The immune response attenuates growth and nutrient storage in *Drosophila* by reducing insulin signaling. *Proc. Natl. Acad. Sci.* **106**, 20853–8 (2009).
 167. Warburg, O., Posner, K. & Negelein, E. Ueber den Stoffwechsel der Tumoren. *Biochemische Zeitschrift (German)*. *Metab. Tumors* **152**, 319–44 (1924).
 168. Weinhouse, S., Warburg, O., Burk, D. & Schade, A. L. On respiratory impairment in cancer cells. *Science (80-.)*. **124**, 269–70 (1956).
 169. Warburg, O. On Origin of Cancer Cells. *Science (80-.)*. **123**, 309–14 (1956).

170. Deberardinis, R. J. & Cheng, T. Q's next: The diverse functions of glutamine in metabolism, cell biology and cancer. *Oncogene* **29**, 313–24 (2010).
171. Phan, L. M., Yeung, S.-C. J. & Lee, M.-H. Cancer metabolic reprogramming: importance, main features, and potentials for precise targeted anti-cancer therapies. *Cancer Biol. Med.* **11**, 1–19 (2014).
172. Miyamoto, Y., Hanna, D. L., Zhang, W., Baba, H. & Lenz, H. J. Molecular pathways: Cachexia signaling - A targeted approach to cancer treatment. *Clin. Cancer Res.* **22**, 3999–4004 (2016).
173. Fearon, K., Arends, J. & Baracos, V. Understanding the mechanisms and treatment options in cancer cachexia. *Nat. Rev. Clin. Oncol.* **10**, 90–9 (2013).
174. Tisdale, M. J. Cachexia in cancer patients. *Nat. Rev. Cancer* **2**, 862–71 (2002).
175. Fearon, K. C. H., Glass, D. J. & Guttridge, D. C. Cancer cachexia: Mediators, signaling, and metabolic pathways. *Cell Metab.* **16**, 153–66 (2012).
176. Kir, S. *et al.* Tumour-derived PTH-related protein triggers adipose tissue browning and cancer cachexia. *Nature* **513**, 100–4 (2014).
177. Penna, F. *et al.* Anti-cytokine strategies for the treatment of cancer-related anorexia and cachexia. *Expert Opin. Biol. Ther.* **10**, 1241–50 (2010).
178. Tisdale, M. J. Mechanisms of Cancer Cachexia. *Physiol. Rev.* **89**, 381–410 (2009).
179. Han, H. Q., Zhou, X., Mitch, W. E. & Goldberg, A. L. Myostatin/activin pathway antagonism: Molecular basis and therapeutic potential. *Int. J. Biochem. Cell Biol.* **45**, 2333–47 (2013).
180. Mueller, T. C., Bachmann, J., Prokopchuk, O., Friess, H. & Martignoni, M. E. Molecular pathways leading to loss of skeletal muscle mass in cancer cachexia - can findings from animal models be translated to humans? *BMC Cancer* **16**, 75 (2016).
181. Figueroa-Clarevega, A. & Bilder, D. Malignant drosophila tumors interrupt insulin signaling to induce cachexia-like wasting. *Dev. Cell* **33**, 47–56 (2015).
182. Sell, S. Cellular origin of cancer: Dedifferentiation or stem cell maturation arrest? *Environ. Health Perspect.* **101 Suppl**, 5–26 (1993).
183. Friedl, P. *et al.* Migration of Coordinated Cell Clusters in Mesenchymal and Epithelial

- Cancer Explants in Vitro. *Cancer Res.* **55**, 4557–60 (1995).
184. Bilder, D., Li, M. & Perrimon, N. Cooperative regulation of cell polarity and growth by *Drosophila* tumor suppressors. *Science (80-.)*. **289**, 113–6 (2000).
185. Menut, L. *et al.* A mosaic genetic screen for *Drosophila* neoplastic tumor suppressor genes based on defective pupation. *Genetics* **177**, 1667–77 (2007).
186. Hariharan, I. K. & Bilder, D. Regulation of Imaginal Disc Growth by Tumor-Suppressor Genes in *Drosophila*. *Annu. Rev. Genet.* **40**, 335–61 (2006).
187. Quijano, L. M., Lynch, K. M., Allan, C. H., Badylak, S. F. & Ahsan, T. Looking Ahead to Engineering Epimorphic Regeneration of a Human Digit or Limb. *Tissue Eng. Part B Rev.* **22**, 251–62 (2016).
188. Simkin, J. & Seifert, A. W. Concise Review: Translating Regenerative Biology into Clinically Relevant Therapies: Are We on the Right Path? *Stem Cells Transl. Med.* **7**, 220–31 (2018).
189. Siegrist, S. E., Haque, N. S., Chen, C. H., Hay, B. A. & Hariharan, I. K. Inactivation of Both *foxo* and *reaper* Promotes Long-Term Adult Neurogenesis in *Drosophila*. *Curr. Biol.* **20**, 643–8 (2010).
190. Lee, G. *et al.* Essential role of *grim*-led programmed cell death for the establishment of corazonin-producing peptidergic nervous system during embryogenesis and metamorphosis in *Drosophila melanogaster*. *Biol. Open* **2**, 283–94 (2013).
191. Church, R. B. & Robertson, F. W. A biochemical study of the growth of *Drosophila melanogaster*. *J. Exp. Zool.* **162**, 337–51 (1966).
192. Brogiolo, W. *et al.* An evolutionarily conserved function of the *drosophila* insulin receptor and insulin-like peptides in growth control. *Curr. Biol.* **11**, 213–21 (2001).
193. Testa, N. D., Ghosh, S. M. & Shingleton, A. W. Sex-Specific Weight Loss Mediates Sexual Size Dimorphism in *Drosophila melanogaster*. *PLoS One* **8**, e58936 (2013).
194. Lucchesi, J. C. & Kuroda, M. I. Dosage compensation in *drosophila*. *Cold Spring Harb. Perspect. Biol.* **7** (2015).
195. Lu, H. & Bilder, D. Endocytic control of epithelial polarity and proliferation in *Drosophila*. *Nat. Cell Biol.* **7**, 1232–9 (2005).

196. McEwen, D. G. & Peifer, M. Puckered, a Drosophila MAPK phosphatase, ensures cell viability by antagonizing JNK-induced apoptosis. *Development* **132**, 3935–46 (2005).
197. Kolahgar, G., Bardet, P.-L., Langton, P. F., Alexandre, C. & Vincent, J.-P. Apical deficiency triggers JNK-dependent apoptosis in the embryonic epidermis of Drosophila. *Development* **138**, 3021–31 (2011).
198. Gowda, P. S., Zhou, F., Chadwell, L. V. & McEwen, D. G. p53 binding prevents phosphatase-mediated inactivation of diphosphorylated c-Jun N-terminal kinase. *J. Biol. Chem.* **287**, 17554–67 (2012).
199. Tseng, A. S., Adams, D. S., Qiu, D., Koustubhan, P. & Levin, M. Apoptosis is required during early stages of tail regeneration in *Xenopus laevis*. *Dev. Biol.* **301**, 62–9 (2007).
200. Perez-Garijo, A., Shlevkov, E. & Morata, G. The role of Dpp and Wg in compensatory proliferation and in the formation of hyperplastic overgrowths caused by apoptotic cells in the Drosophila wing disc. *Development* **136**, 1169–77 (2009).
201. Chen, H., Liu, H. & Qing, G. Targeting oncogenic Myc as a strategy for cancer treatment. *Signal Transduct. Target. Ther.* **3**, (2018).
202. Kaplan, D. D., Zimmermann, G., Suyama, K., Meyer, T. & Scott, M. P. A nucleostemin family GTPase, NS3, acts in serotonergic neurons to regulate insulin signaling and control body size. *Genes Dev.* **22**, 1877–93 (2008).
203. Vitt, L. J., Congdon, J. D. & Dickson, N. A. Adaptive Strategies and Energetics of Tail Autonomy in Lizards. *Ecology* **58**, 326–37 (1977).
204. Britton, J. S., Lockwood, W. K., Li, L., Cohen, S. M. & Edgar, B. A. Drosophila's Insulin/PI3-Kinase Pathway Coordinates Cellular Metabolism with Nutritional Conditions. *Dev. Cell* **2**, 239–49 (2002).
205. Pinal, N., Martín, M., Medina, I. & Morata, G. Short-term activation of the Jun N-terminal kinase pathway in apoptosis-deficient cells of Drosophila induces tumorigenesis. *Nat. Commun.* **9**, 1–10 (2018).
206. Agata, K. & Inoue T. Survey of the differences between regenerative and non-regenerative animals. *Dev Growth Differ.* **54**, 143-52 (2012).

207. Simon, A., Hollander, G., McMichael, A. Evolution of the immune system in humans from infancy to old age. *Proc. R. Soc. B.* **282**, 20143085. (2015).
208. Couso, J.P., Martinez Arias, A. Notch is required for wingless signaling in the epidermis of *Drosophila*. *Cell.* **79**, 259-72 (1994).
209. Ring, J.M., Martinez Arias, A. puckered, A gene involved in position-specific cell differentiation in the dorsal epidermis of the *Drosophila* larva. *Dev Suppl.* **1993**, 251-259 (1993).
210. Chatterjee, N. & Bohmann, D. A versatile PhiC31 based reporter system for measuring AP-1 and Nrf2 signaling in *Drosophila* and in tissue culture. *PLoS ONE.* **7**, e34063 (2012).
211. Venken, K.J., Schulze K.L., Haelterman N.A., Pan H., He Y., Evans-Holm M., Carlson J.W., Levis R.W., Spradling A.C., Hoskins R.A., Bellen H.J. MiMIC: a highly versatile transposon insertion resource for engineering *Drosophila melanogaster* genes. *Nat. Methods.* **8**, 737-743 (2011)